Chapter 1

INTRODUCTION

"Any sufficiently advanced technology is indistinguishable from magic."
Arthur C. Clarke: The lost world of 2001

1.1 Dissertation Overview

Cellular mobile radio, the magic technology that enables everyone to communicate everywhere with anybody, has created an entire industry in mobile telecommunication, an industry that is rapidly growing and that has become a backbone for business success, efficiency and a part of the modern lifestyle all over the world.

Although mobile radio has been used for almost 80 years, mobile telephone services did not appear in a useful form until the early 1960s. The convenience of these early mobile phone systems, were severely limited, and their maximum capacity was tiny by today's standards. In the 1980's, all the systems were popular and grew at rates tempered only by local regularity anomalies, commercial considerations, and available radio spectrum.

Cellular radio is a fast-changing field of mobile communication. The whole concept of mobile communication is changing so rapidly, that it is hardly possible to keep pace with the changes. The early 1980's saw the advent of analog systems that had an uncertain

future. Subscriber growth in this area has been phenomenal, however, and as a result low capacity cellular systems are being replaced by digital systems throughout the world.

The development in cellular technology over the past decade and the success of GSM networks around the world has created the need for better, cheaper and customer-focused services. The challenges of the future are going to be addressed by the introduction of the third generation UMTS systems. A key feature in the development of UMTS technology to achieve the desired performance is by introducing smart antenna systems.

A smart antenna model is presented here and analysed for the advantages it has in reducing the effect of fading due to multipath propagation. A detailed analytical analysis of the model is presented to show the improvement in the overall system performance.

An overview of some important concepts is explained below as an effort towards establishing the basis for the smart antenna model presented here for WCDMA cellular systems. Figure 1.1 shows the area of coverage with regards to the different technologies.

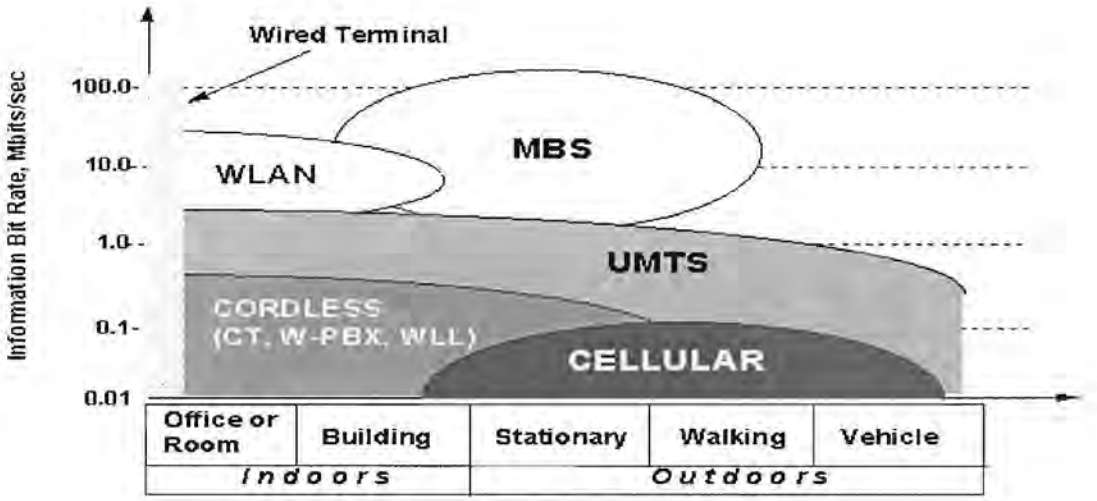

Figure 1.1: Coverage of wired and wireless technologies in different scenarios

1.2 WCDMA and UMTS

In the past, many systems in mobile communication have been adopted, of which CDMA (Code Division Multiple Access) is the most popular. The development of the Code Division Multiple Access (CDMA) scheme is mainly for capacity reasons. Wide-band code-division multiple-access (WCDMA) has, been adapted as the 3G standard, and also

been chosen as the basic radio-access technology for UMTS/IMT-2000 in both Europe and Japan [1].

1.2.1 WCDMA

Development of mobile communication technology started in mid 19th century. During 1960-70 the technology developed rapidly and the mobile era started. To understand the theory of mobile communication one needs to understand the cellular concepts. Concepts like *frequency reuse, cell splitting* and *types of cells* are well explained in the literature [2, 3]. Multiplexing is a very important aspect of any telecommunication system and so it is in cellular systems. There are three basic multiple access schemes used in cellular mobile communications, namely Frequency division multiple access (FDMA), time division multiple access (TDMA), and code division multiple access (CDMA). Cellular CDMA is uniquely designed to work in cellular systems. The primary purpose of using CDMA is for high capacity. CDMA has many other advantages over FDMA and TDMA as pointed out in the literature [4, 5, and 6].

Frequency Division Multiple Access assigns individual channels to individual users. Each user is allocated a unique frequency band or channel. These channels are assigned on demand to users who request service. During the period of the call, no other user can share the same frequency band.

Time Division Multiple Access systems divide the radio spectrum into time-slots, and in each slot one user is allowed to either transmit or receive. TDMA shares a single carrier frequency with several users, where each user makes use of one-time slot. Figure 1.2 shows the difference between FDMA/TDMA and CDMA.

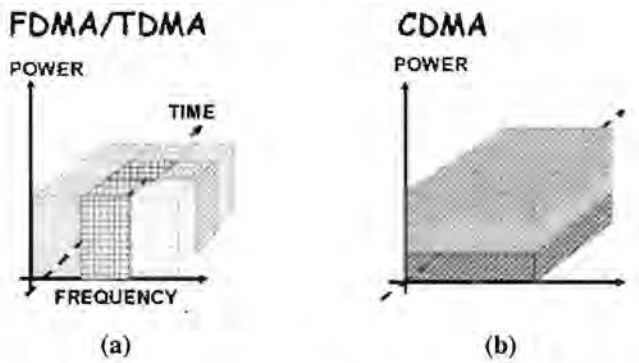

Figure 1.2: (a) shows FDMA/TDMA concept and (b) CDMA concept.

CDMA uses a form of direct sequence, which is, in essence, multiplication of a more conventional communication waveform by a pseudo-noise (PN) sequence in the transmitter, as shown in Figure 1.3.

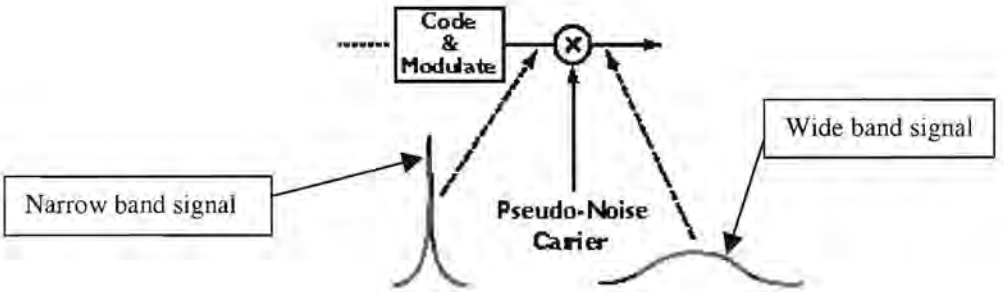

Figure 1.3: CDMA Transmitter.

In reality spreading takes place prior to any modulation, entirely in the binary domain, and the transmitted signals are carefully band-limited. A second multiplication by a replica of the same sequence in the receiver recovers the original signal as shown in Figure 1.4.

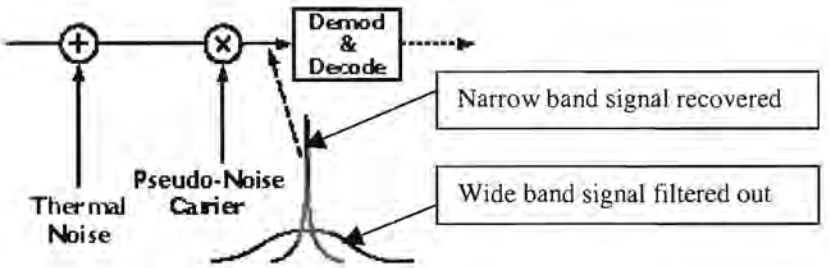

Figure 1.4: CDMA Receiver.

The noise and interference, being uncorrelated with the PN sequence, become noise-like and increase in bandwidth after despreading when they reach the detector. The signal-to-noise ratio can be enhanced, by narrowband filtering that rejects most of the narrow band interference power [7].

The European Telecommunication Standards Institute (ETSI) has decided to adopt W-CDMA and Time-Division CDMA (TD-CDMA) as the basis for the implementation of UMTS. ETSI fully supports the concept of smart antenna and Space Division Multiple Access (SDMA) technique to increase the capacity of third generation mobile systems.

Smart antenna techniques will be implemented on UMTS systems to *increase cell coverage area, reduction of interference* and *extend system traffic capacity* [8, 9]. A detailed description of the physical layer of ETSI WCDMA has been given in [1], together with an overview of the structure of the higher layers of WCDMA radio interface (layers 2 and 3), and WCDMA performance results from ETSI evaluation of UMTS radio-interface.

1.2.2 UMTS

The world of communications is evolving at an exciting pace, driven by European successes such as GSM, and global phenomena such as the Internet. Leading-edge technologies and pro-competitive policies are empowering citizens to an extent hitherto reserved to the realm of science fiction. Figure 1.5 shows the concept of universal coverage presented by UMTS technology.

UMTS marks a major step forward in mobile telecommunications, as it contains a service creation virtual home environment (VHE) which allows UMTS operators and other entities to rapidly create entirely new services. The VHE will include high level tools for service design and testing, so that both operators and other service entities can introduce new services with speed, confidence, and know that they will function independent of network, access, or terminal.

The flexibility introduced by VHE not only increases the range of services that can be offered to subscribers and users, but also allows them to be tailored to different user types and market sectors, even down to an individual user. The personal profiles can be extended beyond *"any one, any time, any place"* so that the services are consistent but also able to adapt to the users' circumstances as well as the capabilities of their terminals and access networks.

A few key words need to be explained in as simple terms as possible for the end user to be able to comprehend and understand the so much talked about magic technology.

- What is UMTS?
    1. UMTS stands for Universal Mobile Communication System
    2. UMTS is a part of International Telecommunications Union's 'IMT-2000' vision of a global family of 'third generation' (3G) mobile communication systems.

3. UMTS will play a key role in creating the future mass market for high-quality wireless multimedia communications that will approach 2 billion users worldwide by the year 2010.

- Why UMTS?
  1. UMTS will enable tomorrow's wireless Information Society, delivering high-value broadband information, commerce and entertainment services to mobile users via fixed, wireless and satellite networks
  2. UMTS will speed convergence between telecommunications, IT, media and content industries to deliver new services and create fresh revenue-generating opportunities
  3. UMTS will deliver low-cost, high-capacity mobile communications offering data rates up to 2Mbit/sec with global roaming and other advanced capabilities.
- When UMTS?
  1. UMTS services will launch commercially from 2002 onwards.
  2. UMTS licenses have already been awarded in several European countries.
  3. UMTS experimental systems are now in field trials with leading vendors worldwide
- How UMTS?
  1. UMTS builds on today's significant investments in second generation mobile systems.
  2. UMTS has the support of several hundred network operators, manufacturers and equipment vendors worldwide.

UMTS is a significant opportunity for manufacturers, operators, regulators and content providers, both as a communications system in itself, as well as a part of the greater Information Society. The vision of UMTS is of a customer-focused system, where customers include both network operators and end users. The challenge to the communications industry is to integrate the technologies needed for UMTS in a way that supports this goal and thereby transforms the vision into reality [10, 11].

1.2.3 UMTS for Africa

Much has been said of the African Renaissance, the economic revolution that will see Africa take its rightful place as a prosperous and thriving force on the world stage. The

African Region stands at a crossroad. The political and social will for change is manifest, but must necessarily be translated into action if the Region is to catch up with its First World partners, rather than falling further behind.

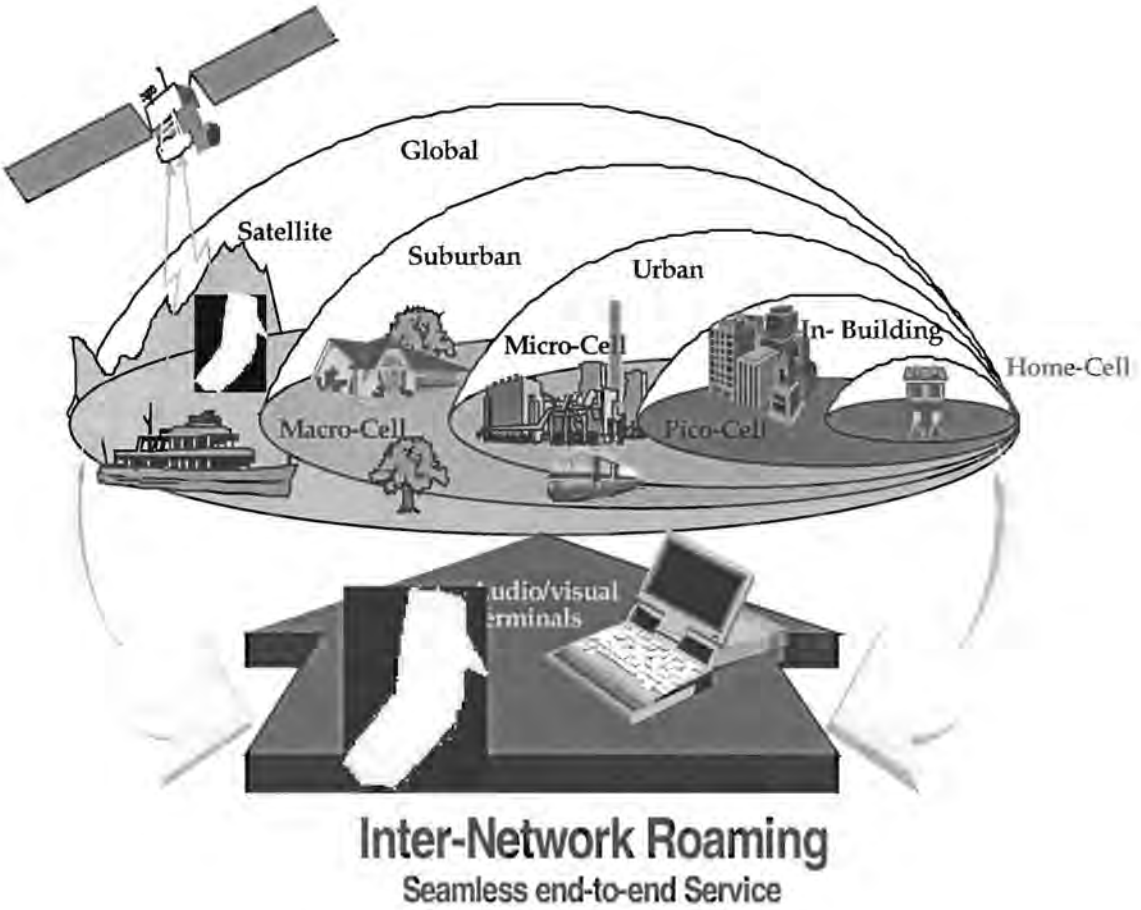

Figure 1.5: UMTS coverage is universal [10].

GSM has a fundamental role to play in ensuring that the African Renaissance becomes a reality. In South Africa, the fast roll-out of cellular technology brought telecommunications to many areas for the first time ever and prepaid services are now opening up the market to include many customers, previously excluded from connection in areas where access to traditional fixed services is still many years away.

In some African countries GSM networks will become the *de facto* national telecommunications network, with world class services taking the place of no, or largely ineffective, fixed services. It will become increasingly evident in the next few years that GSM will be the only telecommunications service available in much of Africa.

3G has the potential to provide high bandwidth and all its associated service opportunities to areas in the path of the GSM roll-out where there is at present no telecommunications at all, from nothing to the information age and beyond.

In the African Region, and in other parts of the world, a clear and economical evolutionary strategy for GSM into 3G is not a nicety, but a socio-economic imperative. The continued and profound development of GSM and a cost-effective evolutionary concept for the introduction of UMTS is critical to ensure that Africa is able to build upon existing investments and seize the opportunity presented by this new technology [12].

1.2.4 The path to 4G

4G is a collection of ideas to enhance existing wireless systems such as adaptive antennas, software defined radio Base Stations and terminals while simultaneously improving spectrum efficiency. There is no common architecture/standard defined today. It will be an extension of mobile networks to Wireless Local Area Networks (WLANs), Wireless Local Loop (WLL) and hybrid-systems. 4G is scheduled to be introduced in 2010 or later. None of the 4G radio access characteristics will provide Public Land Mobile Network (PLMN) capability (Hot-spot for packet access with 50 to 100 Mbps). It will be used for Web browsing, video conferencing, digital radio broadcasting, with the use of PC type of terminals with high memory & hard disk and very intelligent applications software.

4G will be very different from 3G and will not provide what 3G already does, e.g. provide wide area coverage with seamless connectivity, designed for anytime Person to Person communication, for mass market (but for high-speed/high-volume data for business users). 4G will be an evolution of 3G UMTS and designed for handset type terminals.

1.3 Smart Antenna Aspects

The field of *smart antennas* has matured significantly over the past decade. In recent years this technology seems to provide promising results for the wireless industry. Smart antenna systems utilise more than one antenna element to optimally transmit or receive signals to or from users by incorporating both temporal and spatial signal processing techniques in the transceiver.

All antenna array systems and techniques, including antenna sectorization (spatial signal processing), diversity combining (spatial & temporal signal processing) and beam forming (spatial and temporal signal processing) can be considered to be smart antennas [7].

Smart antennas or adaptive antennas can be placed in any environment and automatically configured to the dynamic spatial and temporal conditions of the wireless surrounding, thus offering tremendous flexibility to the wireless service provider who must provide coverage and quality of service to its rapidly growing customer base.

The base station will process the signals using algorithms for smart antennas, including estimation of direction of arrival, beam forming and beam steering in multipath channels for narrow and wideband signals, tracking of user transmitting desired signal, estimation and cancellation of co-channel interference etc.

A number of smart antenna techniques, namely beamforming, diversity, sectorization, and switched beam systems can be used to mitigate channel effects. These techniques can prove very useful to mobile CDMA systems that have high interference due to the fact that users transmit on the same frequency. Diversity combining is of cardinal importance and part and parcel of smart antenna techniques. Different forms of diversity and combining methods are discussed in Chapter 2, and in Appendix A.

1.3.1 Antenna Arrays and Configurations

A number of techniques can be used to filter the signal at the base station. Different antenna array geometries, from very complex to simple arrangements of antenna elements, can be used to process the signal. A few of the adaptive antenna arrays used for smart antenna applications are *uniform array, broadside array, end-fire array, phased array, planar array*, etc. In Figure 1.6 some common antenna geometries are shown. Many references can be found in the literature on array geometeries and antenna array systems, e.g., as given in [13] where different antenna geometries have been considered.

An adaptive array consists of an array of spatially distributed radiating elements, with each element in the array receiving highly correlated replica of the original signal. The outputs of each element are adaptively weighted and combined with the other outputs to extract a specific signal from the superposition of the signals received.

1.3.2 Factors influencing antenna performance

There are three main factors affecting antenna performance that can be identified, namely the propagation path of the signal, the distribution of subscribers, and the quality of service required by the subscriber. The propagation path model needs to take into account the following:

- Path loss
- Shadowing
- Losses due to multipath components and
- Losses due to scattering

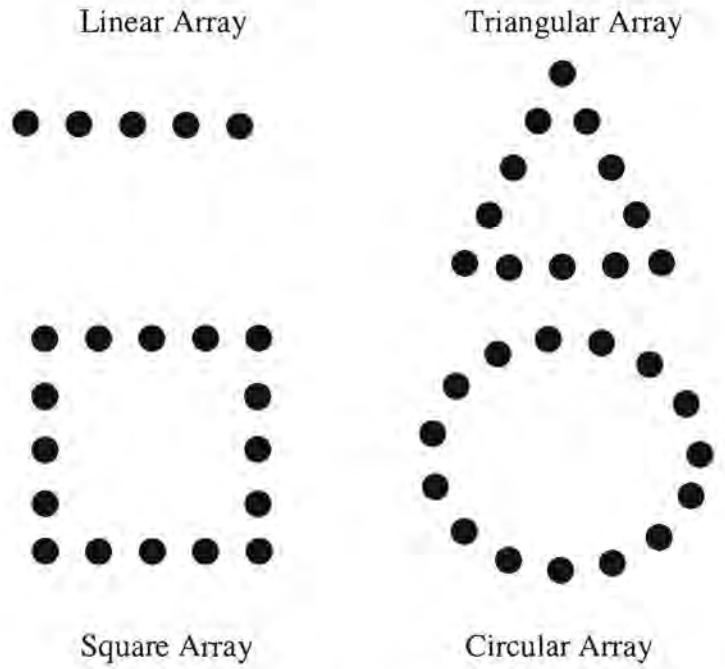

Figure 1.6: Some common array geometries.

1.4 Problem Definition

The aim of this dissertation is to develop an analytical base for the analysis of a WCDMA system incorporating smart antenna techniques by modelling the spatial/temporal channel and MRC receiver with negatively correlated signals.

The problem can be subdivided in to three main parts, namely, the channel model (Spatial/Temporal), the diversity receiver (Maximal Ratio Combiner) and the performance evaluation model (BER and Probability of Outage) as discussed below.

1.4.1 Channel Model

The proposed spatial/temporal channel can be further subdivided in to the *spatial* and *temporal* parts, which requires modelling the following:

- To choose an accurate SPATIAL model and modify it to fit our system model. This requires modelling the *user* distribution and the *scatterer* distribution. A spatial model calculated in [8] is chosen and will be modified for a more general case scenario.
- To develop a TEMPORAL model as calculated in [8], and combine it with the SPATIAL models to produce the system channel model. The TEMPORAL model is developed using the NAKAGAMI-*m* distribution to model the multipath of the signals in a correlated fading environment.
- To integrate the two models, SPATIAL and TEMPORAL, to produce the system channel model, two models namely Exponential and Gaussian presented in [8] will be used to model signals in both Line Of Sight and Non Line Of Sight conditions.

1.4.2 Maximal Ratio Combiner

The second part of the problem is to model the diversity receiver. A Maximal Ratio Combiner receiver given in [36] will be used to calculate the following sub sections of the receiver:

- To decide on the best antenna geometry and the number of elements in the array.
- To develop a mathematical model to combine the faded signals which are received at the antenna using Maximal Ratio Combining.
- To calculate a correlation model that accurately represents the correlation between signals at the antenna.
- To extend the pdf of the MRC receiver calculated in [36] for *negatively correlated* signals with correlation coefficient (ρ) ranging from -1 and 1.

1.4.3 System Model Evaluation

Finally the two models mentioned above, namely the channel model and the MRC receiver model, would be combined to produce the system model. This proposed system model will be evaluated using BER and probability of Outage predictions to calculate improvement in BER and Outage due to signals with negative correlation coefficient.

1.5 Contributions

The work in this dissertation presents a unique set of results in the field of smart antenna systems. It provides new results especially for system models that incorporate negatively correlated signals. The results show that by extending the system to negative values of correlation coefficient ρ, better system performance can be obtained. This work was consolidated into the following:

- **Conference**
  1) A. N. Pandey and L. P. Linde, "Performance of Maximal-Ratio Combining in WCDMA Cellular Systems with Spatial/Temporal Channel Model", *World Multiconference on Systemics, Cybernetics and Informatics, July 22-25, 2001, pp 281-286, Orlando, Florida* [69].
- **Journals**

The following papers have been submitted to the South African Institute of Electrical Engineers for possible publication.

1. A. N. Pandey and L. P. Linde, " Analytical results on Maximal-Ratio Combining with negatively correlated Spatial/Temporal Channel", *submitted to the Transaction of the SAIEE.*
2. A. N. Pandey and L. P. Linde, "Probability of Outage for WCDMA systems with Maximal-Ratio Combining in a negatively correlated spatial/temporal Channel", *submitted to the Transaction of the SAIEE.*

1.6 Structure of the dissertation

The dissertation is organized into eight Chapters, Chapter 1 introduction, Chapter 2 literature survey, Chapters 3-5 the sub system models, Chapter 6 proposed system model, Chapter 7 performance evaluation and Chapter 8 conclusion as shown in Figure 1.7. A summary of the proposed Spatial/Temporal channel model with Maximal-Ratio Combining for negatively correlated signals is presented in Figure 1.8.

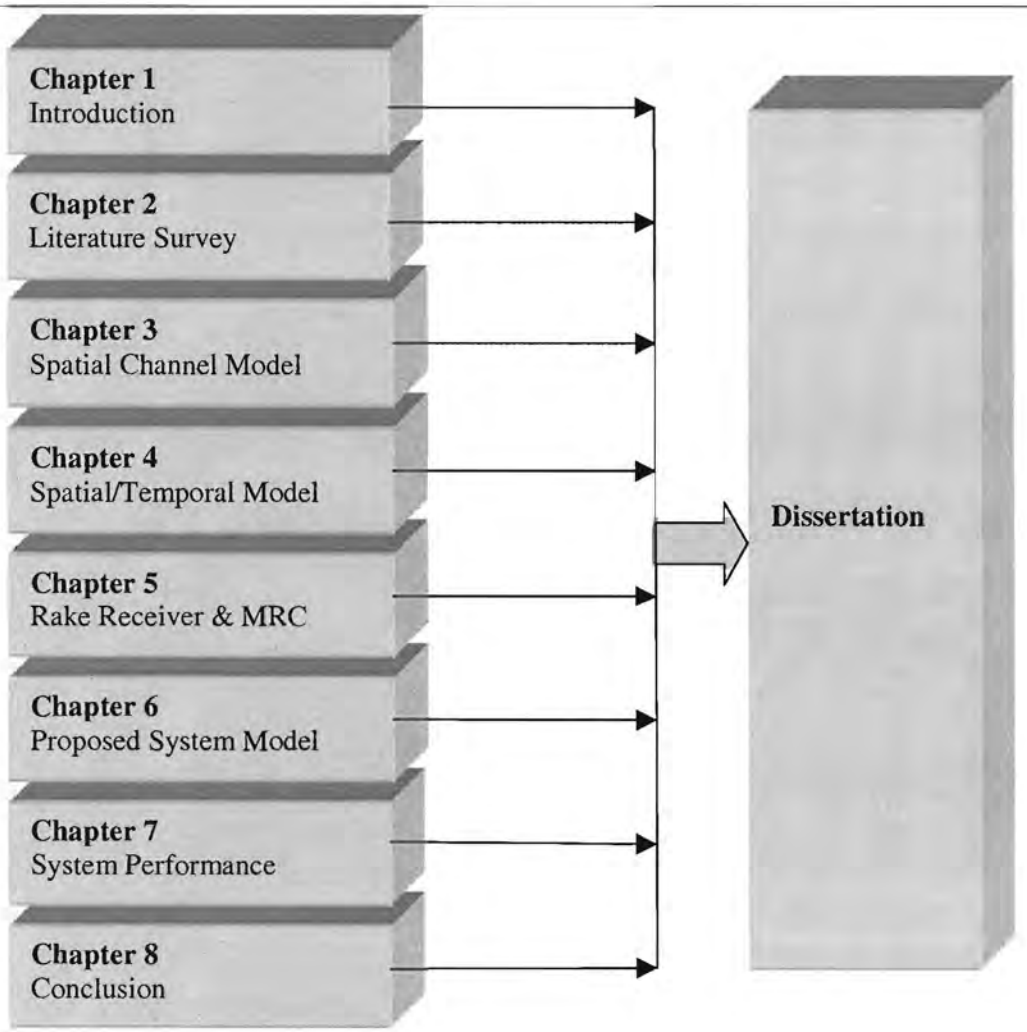

Figure 1.7: Dissertation summary.

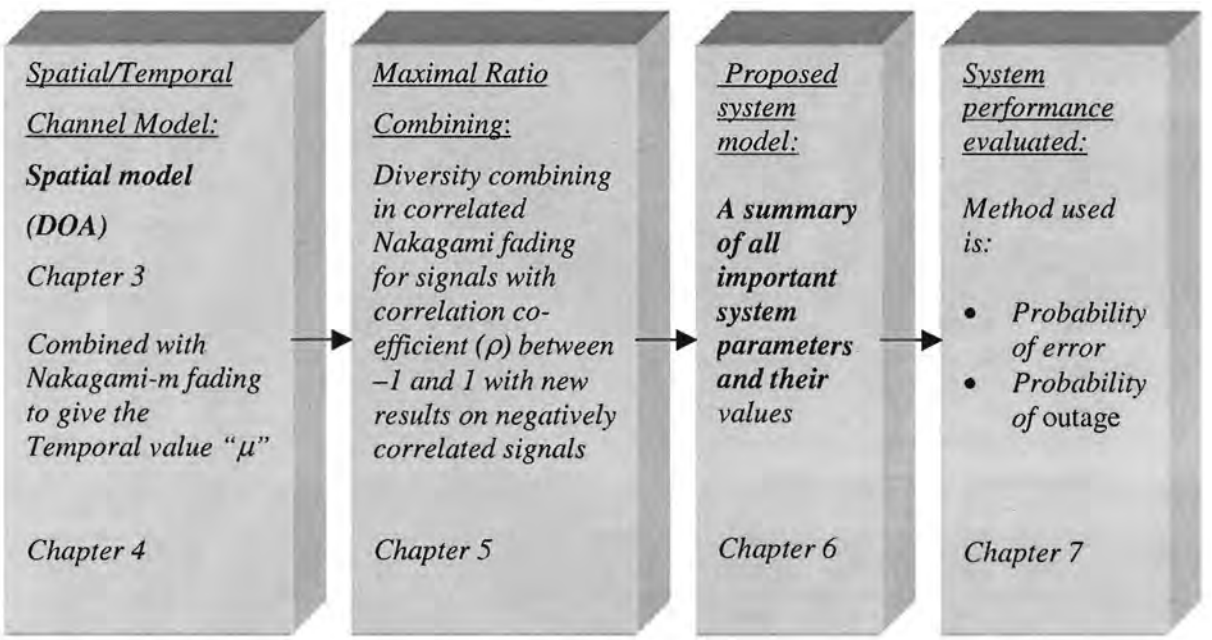

Figure 1.8: Summary of the proposed system model.

Chapter 2

LITERATURE SURVEY

2.1 Overview

The analysis of smart antenna systems is based on its adaptive nature and ability to filter both narrow and wide band signals. It uses different array configurations with weights on each branch. The weighted signal is then combined and processed using different algorithms to filter the desired signal. A number of references can be found in the literature that deals with these aspects [e.g. 14, 15, 16, and 17].

Space-time analysis of smart antennas can be categorised into four main techniques, namely, beamforming, diversity, sectorization, and switched beam. Beamforming, sectorization, and switched beam techniques are explained in detail in [26]. In this dissertation the main emphasis will be on diversity; however, beamforming will be briefly discussed due to its importance with regards to correlated signals. Figure 2.1 shows the classification of smart antenna techniques.

All the above-mentioned smart antenna techniques are applicable particularly to WCDMA mobile systems where interference is more pronounced due to the fact that users transmit on the same frequency with unique spreading codes. The aim of employing smart antenna techniques to any wireless system is to achieve the following:

- high throughput
- low average BER
- Smallest average delay possible.

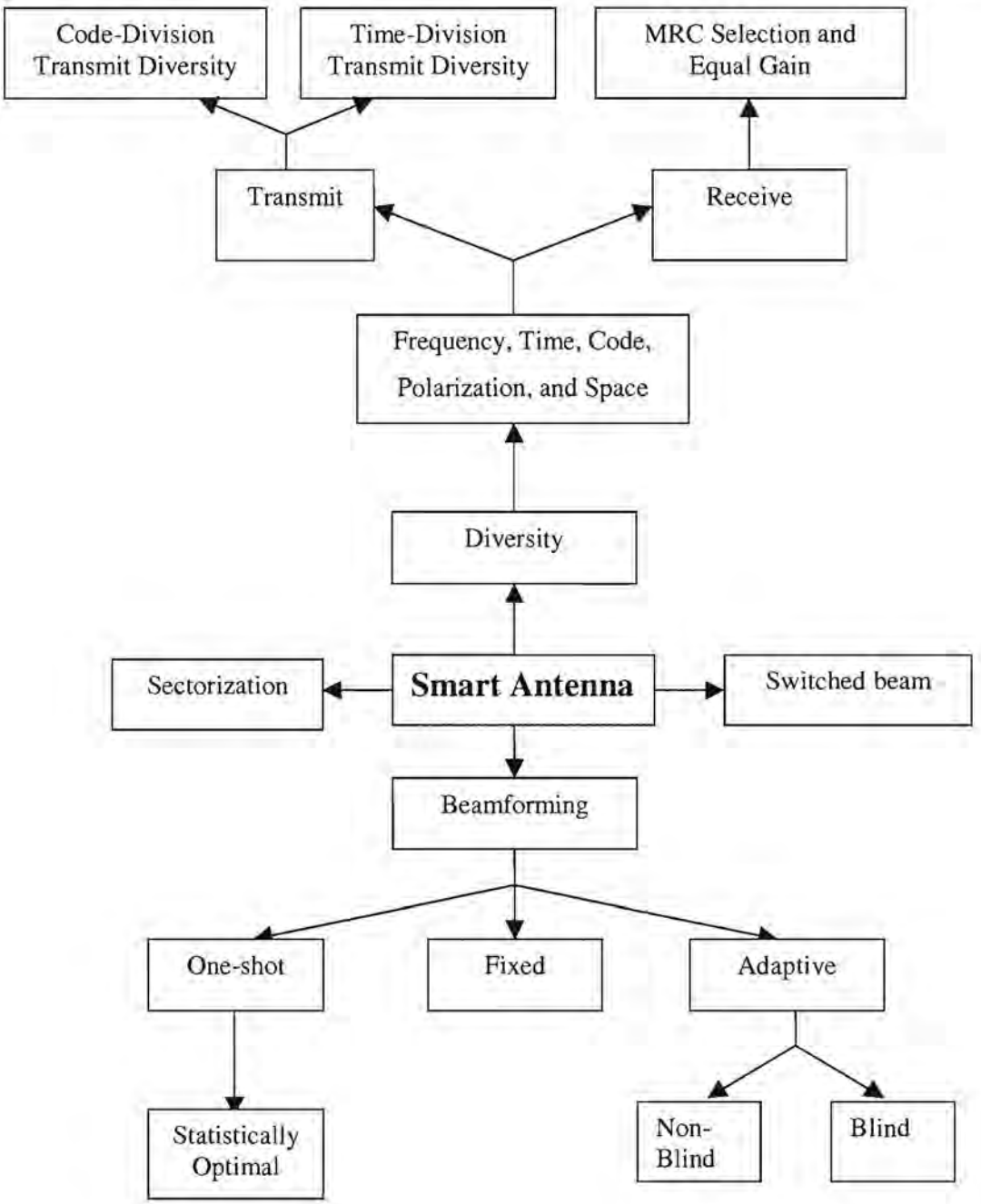

Figure 2.1: Classification of smart antenna techniques [26].

Diversity requires a number of signal transmission paths, called diversity branches (that carry the same information but have, ideally, uncorrelated multipath fading), and a circuit to combine the received signals or to select one signal from all the received signals. This definition of diversity differs from beamforming where it is normally assumed that the signals arriving at the antenna array are perfectly correlated. Whenever the signals on the various antenna elements are not perfectly correlated, the beamforming pattern is influenced in a detrimental way. At some point, due to a lack of correlation, the beam

pattern will revert back to an Omni-directional pattern. Lack of correlation is normally induced by the environment through which the received signal is propagated and also due to the spacing of the antenna elements. Whenever the correlation ρ_{ij} (i and j represent any two branches on the antenna), between branch "*i*" *and* "*j*", is less than perfect, that is $\rho_{ij} < 1$, there will be some diversity gain present in the system. Normally for $\rho_{ij} < 0.5$ diversity is considered and for $\rho_{ij} > 0.5$ beamforming is considered. In situations where $\rho_{ij} < 0$ and the correlation coefficient between the branches *i and j* is negative, it is relatively easier to identify the wanted signal and hence improve system performance. In Chapter 5 negatively correlated branches are analysed in detail.

2.2 Beamforming

The early concepts underlying digital beamforming (DBF) were first developed for application in sonar and radar systems. DBF represents a quantum step in antenna performance and complexity. It is based on well-established theoretical concepts which are now becoming practically exploitable, largely as a result of recent major advances in areas such as *monolithic microwave integrated circuit* (MMIC) technology and *digital signal processing* (DSP) technology. DBF technology has reached a sufficient level of maturity that it can be applied to communications for improving system performance.

DBF is a marriage between antenna technology and digital technology. A generic DBF antenna system in Figure 2.2 consists of three major components: the antenna array, the digital transceivers, and the digital signal processor. An analog beamformer on the other hand first combines all K signals received to a single signal as shown in Figure 2.3.

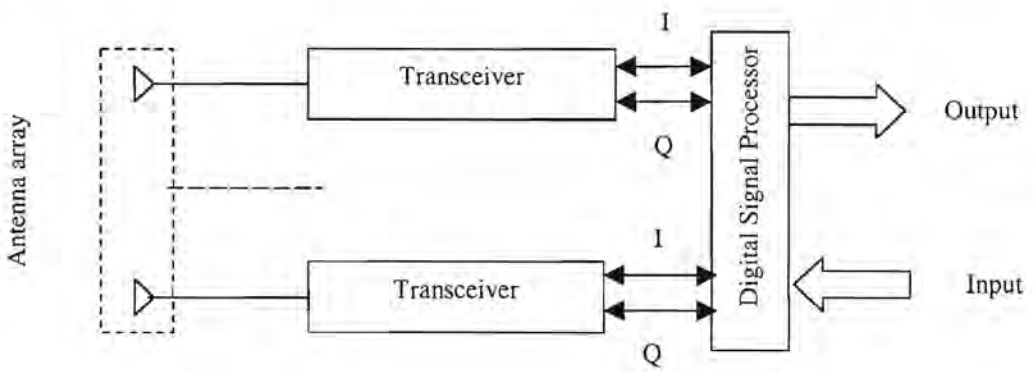

Figure 2.2: A generic DBF antenna system.

Digital beamforming is based on capturing the radio frequency (RF) signals at each of the antenna elements and converting them into two streams of binary baseband signals (i.e., in phase (I) and quadrature-phase (Q) channels).

Beamforming is carried out, by weighting the digital signals, thereby adjusting their amplitudes and phases, such that when added together they form the desired beam.

The main advantage to be gained from DBF is greatly added flexibility without any observed degradation in signal-to-noise ratio (SNR). In many ways it can be considered to be the ultimate antenna, in that all of the information arriving at the antenna face is captured in the digital streams that flow from this face. Since the beamforming instructions are driven by software routines, there is wide-ranging flexibility in the types of beams that can be produced, including scanned beams, multiple beams, shaped beams, and beams with steered nulls.

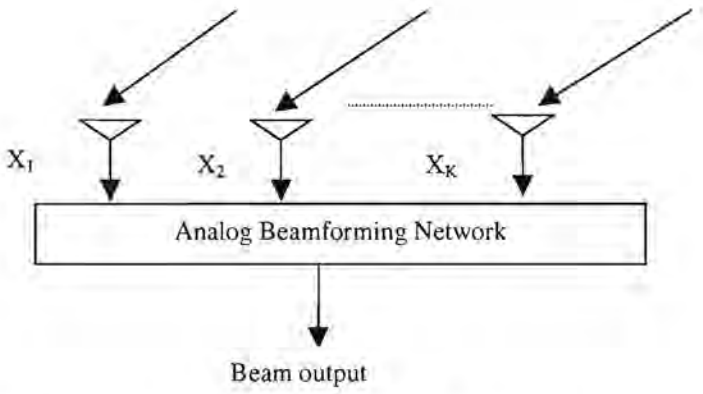

Figure 2.3: An analog beamformer reduces the signal dimensionality from K to1.

When we combine the RF signal with digital processing the output beam has a higher level of information with wide ranging flexibility. We find that digital beamforming allows for a number of attractive features beyond the capabilities of conventional phased arrays:

1. A large number of independently steered high-gain beams can be formed without any resulting degradation in signal-to-noise ratio.
2. All of the information arriving at the antenna array is accessible to the signal processors so that system performance can be optimised.
3. Beams can be assigned to individual users, thereby assuring that all links operate with maximum gain.

4. Adaptive beamforming can be easily implemented to improve the system capacity by suppressing cochannel interference.
5. DBF systems are capable of carrying out real-time antenna system calibration in the digital domain.
6. Digital beamforming has the potential for providing a major advantage when used in satellite communications as the antenna array can easily adapt to the changes in the signals received.

Adaptive beamforming technology is also referred to as smart antenna technology in some literature. The use of the term "smart" reflects the antenna's ability to intelligently adapt to the environment in which it operates.

The purpose of an adaptive beamformer is to adjust the weights of a linear array processor in real time to respond to a signal coming from a desired direction while discriminating against noise from other directions [18].

An adaptive multi-beam antenna uses 12 or 24 narrow beams; each with fixed pointing directions. Selection combining is used to switch the strongest two directional beams for a given subscriber at the base station's main and diversity receivers. Multibeam antenna performance is measured using experimental field tests from existing cellular sites located in heavy urban and light urban environments. The paper examines only reverse link improvements on the base station receive path; however, similar concepts can be used to provide improvements to the forward link base station transmit path as well.

Based on experimental observations in heavy urban environment, the relative power difference between the strongest and weakest beams is approximately 3 dB lower than for a light urban environment. A calculation of the probability of beam separation shows that, with a high probability, the first and second strongest beams will be located in physically adjacent antenna beams. The gain improvement obtainable from a multibeam antenna relative to a dual-diversity sector configuration has been examined in [19]. Experimental results in heavy and light urban environments show that linear average gain improvements of approximately 2.9 and 5.2 dB can be achieved with 12 and 24 beam antennas respectively.

The traditional beamforming approach requires knowledge of the direction of arrival of the signal, which is not always easy to calculate. Applying subspace methods, blind adaptive beamforming methods have been proposed to solve the problem [19]. One simple alternative to adaptive antennas is the switched multibeam antenna system, in which several narrow beams are used to cover the entire base station footprint [20]. A number of references can be found in the literature dealing with different ways, in which beamforming can provide improvement in the performance of cellular mobile communications [21, 22, 23, and 24].

2.3 Antenna Diversity

The principles of diversity combining have been known to the radio art for decades, with the first experiments reported as far back as in 1927. The diversity method requires that a number of transmission paths be available, all carrying the same message but having independent fading statistics. The mean signal strengths of the paths should also be approximately the same. Proper combination of the signals from these transmission paths yields a resultant with greatly reduced severity of fading and correspondingly improved reliability of transmission. In the early experiments the independent paths were realised by transmitting from a single antenna to a number of receiving antennas. The distance between the receiving antennas was made large enough to ensure independent fading. This arrangement is called space-diversity reception. Antenna diversity or space diversity can be applied at both the receiver and the transmitter.

The simplest technique to maintain acceptable channel capacity is to increase the transmitted power. However, in doing so, the overall spectrum efficiency is reduced and all other schemes consume extra spectrum to improve the channel capacity. On the other hand, antenna diversity improves the channel capacity at the expense of adding extra equipment (antenna, combiner) to the receive end of the link (no extra spectrum is required) [25]. It is important to note that although diversity systems can be implemented at the transmitter and/or the receiver, our main emphasis here is on receive diversity which will be considered in detail.

A number of transmit diversity techniques are described in literature [26] and have been found to be very useful in TDMA and CDMA. Two promising transmit diversity techniques well suited to CDMA are, Code-division transmit diversity (CDTD) and Time-

division transmit diversity (TDTD). A simple transmit technique was proposed in [27] which improves the signal quality at the receiver using one receive antenna by simple processing across two transmit antennas on the transmitter. The obtained diversity order is equivalent to applying maximal-ratio receiver combining (MRRC) with two antennas at the receiver. The best diversity gains can be achieved with uncorrelated diversity channels. However, diversity channels are correlated because of non-ideal space, time, or frequency separation. A good analytical method based on fading outage for fading distributions for selection combining (SC) and maximal–ratio combining (MRC) has been developed in [28] as an alternative to the complicated analysis required for correlated channels. This technique differs with the proposed model in this dissertation in that we extend our analysis to uncorrelated signals with negative correlation coefficient. A beamspace adaptive diversity combiner has been proposed in [29] for sectorised signal reception, to combat multipath fading and cochannel interference. In sectorized signal reception, the entire field of view of the receiver is divided into several angular sectors with each sector responsible for a distinct set of users. The method offers great improvement in the system performance. There are several techniques for obtaining diversity dimensions, which are discussed in Appendix A-1. Space diversity forms part of the proposed system model and will be discussed here.

2.3.1 Space Diversity

This has been the most common form of diversity employed in mobile radio base stations and is in wide use in a variety of present-day microwave systems. It is relatively simple to implement and does not require additional frequency spectrum. The basic requirement is that the spacing of the antennas in the receiving or transmitting array be chosen so that the individual signals are uncorrelated. A spacing of $\lambda/2$ between the branches should be sufficient to get uncorrelated signals. A diversity antenna can have M branches in its array. Each branch of the antenna array provides an independent signal to an M branch combiner, which then operates on the assemblage of signals to produce the most favourable result. A number of techniques are available to perform the combining process, as elaborated in Appendix A-2.

The diversity array can be located either at the mobile unit, the base station, or both, depending on the particular combining technique used and the degree of enhancement required. In principle, there is no limitation on M, the number of array elements, but the

amount of improvement in the fading characteristics realised by adding one more element decreases as M grows larger. A space diversity channel model for multipath propagation that compares the correlation of the main and space diversity is presented in [30]. In [31] a hybrid diversity scheme between space and path diversity noted a high channel capacity. Antenna diversity can be achieved by using a number of diversity techniques, namely polarisation, angle, frequency, path and time as explained in Appendix A-1.

2.3.2 Diversity Combining

Diversity combining is different from antenna array processing and beamforming in that it combines signals at baseband or at IF to increase the signal level without affecting the individual antenna patterns. Beamforming techniques, on the other hand, exploit the differential phase between different antennas normally at RF level to modify the antenna pattern of the whole array. In this arrangement, once the signals are combined, the whole array has a single antenna pattern.

With diversity systems, we can therefore utilise the fact that the signals arrive at different rates. A system employing a diversity combiner uses signals induced on various antennas placed a few wave-lengths apart at different locations and combine these signals in one of the many ways, as described below. A number of techniques have been noted in the literature to capitalise on the uncorrelated fading exhibited by separate antennas in a space-diversity array. The generic combining techniques can be divided into five categories, of which four are discussed in Appendix A-2. Figure 2.4 shows a generalised block diagram for space diversity combining.

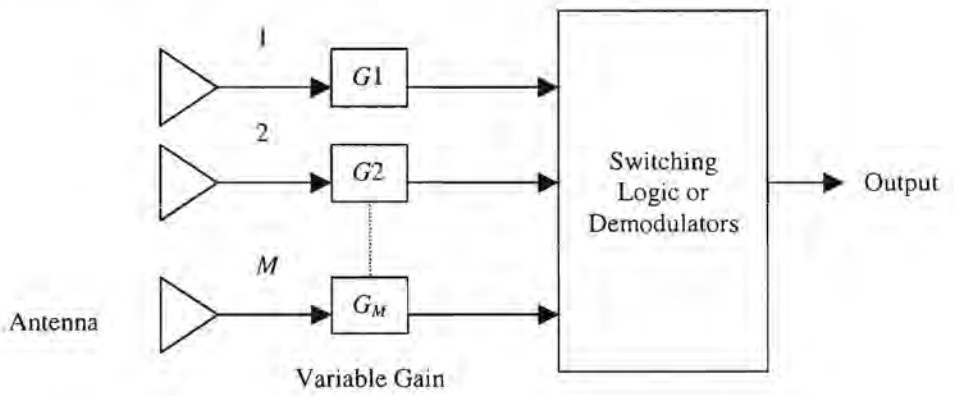

Figure 2.4: Generalised block diagram for space diversity combining.

2.3.3 Maximal Ratio Combining

Different combining methods have been discussed and compared in Appendix A-2. Maximum (or maximal) ratio combining is a method of choosing the branch weights so that the SNR at the output is maximised. Figure 2.5 shows a maximal ratio combiner where the optimum weighting w_i for branch i, is a ratio of the complex channel coefficient and the noise power on any branch M.

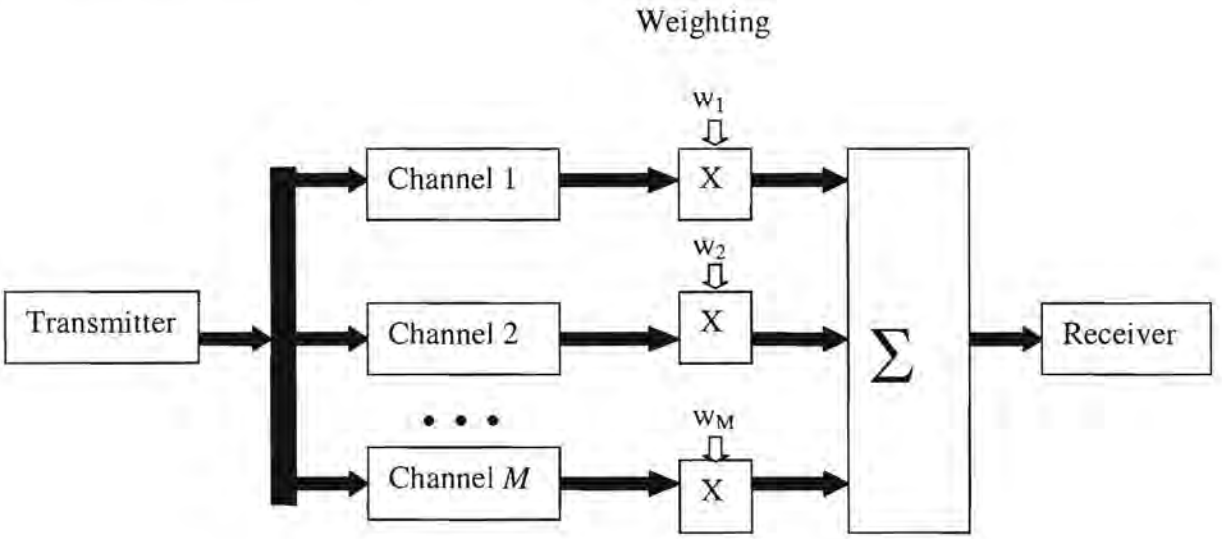

Figure 2.5: Maximum ratio combiner.

The SNR at the output of a maximum ratio combiner is given by the sum of the SNRs of the individual branches and is discussed in detail in Chapter 5. The best possible use is made of the signal energy and the noise energy is minimised as far as possible.

Maximal ratio combining (MRC) is important in diversity systems (e.g. RAKE receivers) both from a practical standpoint, and from a theoretical standoff since it represents a theoretically optimal combiner [32, 33]. Several applications and proposed implementations of MRC exist in the literature, especially to combat multipath fading [34, 35, 36, 37, 38, 39, 40, 41]. MRC over correlated Nakagami fading has received a lot of attention in the literature for its accuracy in modelling fading channels [34, 36, 38, 41, 42].

As shown in Figure 2.5, the weighting of the signals is an important part of MRC. In [32] an effort is made to calculate the effect of errors due to weighting on the probability of error. Several approaches have been used in the literature to calculate the probability density function (pdf) for the MR combiner. However, a pdf developed in [36] is used as a

basis for correlated fading systems. A pdf of MRC in negatively correlated Nakagami fading is calculated in [26]. This pdf is fully analysed, discussed in Chapter 5 and is integrated into the system model proposed in Chapter 6. Two MRC techniques have been proposed in [43] for antenna arrays and their performance evaluated. The performance of the two techniques, namely full spectrum combining (FSC) and complex symbol combining (CSC) in both degradation and loss are approximately equal at low values of symbol SNR, but diverge at high SNR values. Both FSC and CSC require that signals at the individual antenna be retransmitted (over a band-limited channel) to a central location for combining. The loss in signal energy due to transmission is higher with FSC than with CSC, because FSC retransmits the IF signal that occupies a much wider bandwidth than the complex baseband symbols that are retransmitted in CSC. Demodulation losses for FSC are less than in CSC, because all FSC synchronisation loops benefit from the combining gain. They have found that when the subcarrier and symbol loop losses are not negligible, FSC outperforms CSC. Alternatively, when the subcarrier and symbol losses are negligible, CSC can outperform FSC.

In mobile radio systems the signals at the mobile station become decorrelated as the antenna separation (or frequency separation) increases, giving rise to diversity. In space diversity systems, an antenna separation of 30 to 50 wavelengths is typically required to obtain a correlation coefficient strictly between zero and one [36]. The correlation coefficient is an important factor when calculating the pdf of MRC. It is shown in [36] that as the correlation coefficient approaches zero, the MRC performs better. It is also important to note that although the power correlation coefficient for fading signals cannot be negative, negative correlation has been reported between fading envelopes [33, 35, 44].

For diversity systems, signals with *negative correlation* coefficient can provide better diversity gain than those with zero correlation. The pdf of MRC in [36], which is valid for ρ (correlation coefficient) between 0 & 1, was extended for *negative* values of ρ in [26]. In this dissertation the extended pdf (negative ρ) for MRC developed in [26] is fully analysed, calculated, developed and simulated for different values of ρ between –1 & 1 see Chapter 5. This pdf is then integrated into the proposed system model in Chapter 6.

A very important factor besides *diversity* and *beamforming* that can improve the performance of a CDMA system employing smart antenna technique is the need for *power control*. Power control is an effective way to improve system performance in a WCDMA

system. It has been shown that perfect transmitter power control can provide up to 20 times the increase in capacity, compared with conventional FDMA mobile systems. Several power control schemes exist in the literature that attempt to eliminate the near-far and shadowing effects due to fast multipath fading process [46, 47].

Multi-user interference in CDMA is a serious problem, because all users are contending for the same bandwidth at the same time. Therefore a strong signal received from a near-in mobile unit will mask the weak signal from a far-end mobile unit at the cell site. To reduce this near-far ratio interference, a power control scheme should be applied on the reverse link. As a result, the signal received at the cell site from all the mobile units within a cell remains at the same level [5, 45].

2.4 Survey of generic Channel Models

The mobile radio channel places fundamental limitations on the performance of wireless communication systems. The transmission path between the transmitter and the receiver can vary from simple line-of-sight to one that is severely obstructed by buildings, mountains and foliage. Radio channels are extremely random and unpredictable in the fading of signal levels. Modelling the radio channels in a cellular mobile system is a difficult task, and is typically done in a statistical fashion [2]. Constructing a channel model for the evaluation of a CDMA system with smart antenna principles requires modelling and combining of teletraffic aspects, as well as spatial and temporal variables.

A spatial model constructed in Chapter 3 is combined with the temporal channel parameters in Chapter 4 to produce a complete model for our analysis of the system model proposed in Chapter 6. Table 2.1 [8] shows a summary of channel models that can be used for the analysis of mobile cellular systems. To understand the concepts related to channel models and their effect on our channel, two concepts, namely *Temporal* and *Spatial* will be studied here.

2.4.1 Temporal Parameters

The mechanisms behind electromagnetic wave propagation are diverse, but their behaviours can generally be summarised as reflection, diffraction, and scattering. Most cellular radio systems operate in urban areas where there is no direct line-of-sight path

Chapter 3

SPATIAL CHANNEL MODEL

3.1 Introduction

A proper knowledge of the channel parameters is of the utmost importance when developing an accurate channel model. An accurate channel model is vital in the analysis of WCDMA systems to improve the performance of future 3G mobile communications technologies. This mainly helps to reduce the interference considerably, as the users increase in a CDMA system.

Direction of arrival (DOA) is an important aspect of channel model and needs to be accurately calculated. A number of DOA techniques for spatial models have been analysed in the literature and also considered in Chapter 2. Other methods to evaluate array-based DOA or the steering vector include classical methods such as the MUSIC and ESPRIT-algorithms. However, in a CDMA system, such as the UMTS system with large number of users, the mentioned DOA techniques are not always applicable due to their limitations.

3.2 Direction of arrival (DOA) Techniques

Conventional methods for Direction-Of-Arrival estimation are based on the concept of beamforming and null-steering and do not exploit the nature of the method of the received signal vector, or the statistical model of the signal and noise.

3.2.1 The MUSIC Algorithm

Although much of the arrival direction distribution of radio waves in the multipath environment is still unknown, recent research indicates that radio waves originating from a single source are scattered and reflected in such a way that they tend to arrive at a distant point in clusters. It is assumed that the first cluster to arrive has the larger magnitude and is attributed to the direct ray as well as reflections near the antenna. The other clusters are composed of reflected rays, which travel longer and cause more attenuation in their paths.

Numerous methods to estimate AOA exist. Parametric methods which employ eigenanalysis of the data correlation matrix provide very accurate estimation of arrival angles and far higher resolution compared to other methods such as the Fourier transform. One such method is the MUltiple Signal Identification and Classification (MUSIC) algorithm.

The MUSIC algorithm proposed by Schmidt in 1979 is a high resolution multiple signal classification technique based on exploiting the eigenstructure of the input covariance matrix. MUSIC is a signal parameter estimation algorithm that provides information about the number of incident signals, Direction-Of-Arrival (DOA) of individual signals, strengths and cross correlation between incident signals, noise power, etc [58].

The music algorithm is an eigenanalysis direction finding method, which has demonstrated superior performance in terms of accuracy and resolution over other parametric methods, such as maximum likelihood and maximum entropy. MUSIC is not restricted to the geometry of the array but merely requires knowledge of it. It requires a multi element antenna array in order to form a correlation matrix using data received by the array. The requirement of multi element antenna is a major obstacle when applying MUSIC to estimate AOA at a land vehicle: it is impractical, costly and not aesthetically pleasing.

The ability to accurately resolve AOA of a number of coherent arrivals, using MUSIC, has been extensively analysed in [82]. The analysis was based on using four techniques to clearly identify the LOS cluster and provide accurate AOA estimation in the order of 5^0. It was also shown that MUSIC is able to resolve AOA of the single most powerful arrival in a cluster with an accuracy of better than 4^0. This is done by first identifying the LOS cluster and estimating its AOA using techniques 1-3 described in [82]. Spatial filtering is

then done using technique 4 also described in [82] to remove all other clusters, which gives a more accurate estimation of LOS angle of arrival.

3.2.2 The ESPRIT Algorithm

The Estimation of Signal Parameters via the Rotational Invariance Technique (ESPRIT) algorithm is another subspace-based DOA estimation technique developed by Roy [112]. ESPRIT dramatically reduced the computational and storage requirement of MUSIC and does not involve an exhaustive search through all possible steering vectors to estimate the Direction-of-arrival. ESPRIT derives its advantages by requiring that the sensor array have a structure that can be decomposed into two equal-sized identical subarrays with the corresponding elements of the two subarrays displaced from each other by a fixed translation (not rotational) distance [58].

An attempt to find simple yet robust techniques that may enable high–resolution DOA estimation of wideband sources without the need for constructing a complex spatio-temporal model has been made in [83]. The goal here was to obtain a *spatial-only* model for the array data, assuming all the sources to have a flat power spectrum over their region of spectral support. The work in [83] presents two formulations for DOA, a *multidimensional formulation* and *a single dimensional formulation*. The results were compared with other DOA techniques especially MUSIC and it was demonstrated that the methods proposed are not sensitive to the assumption of a flat power spectrum. The multidimensional search method works quite well even for the case of coherent sources.

3.3 Spatial Model

Constructing a channel model requires a good knowledge of spatial parameters. The spatial model in [65] is chosen here and the pdf for AOA will be calculated. This result will later be integrated into the system model.

The choice of a model is based on the universal nature of the model, its versatility, accuracy and simplicity to implement the model developed to be able to locate a reference user in terms of the angle, and express the location of the reference user relative to other users. It should take some of the mechanism that will generate multipath signals into account and should be able to accurately estimate what the angular distribution of signals

at the base station will be. The model is divided in two parts, the user distribution and the scatterer distribution. The two pdfs thus generated in the sections below are then convoluted to arrive at a final pdf of AOA.

3.3.1 User Distribution Model

One important component of the *spatial* model is the user distribution around the base station, which can correctly estimate the traffic demand in various areas. A real life scenario has been considered in [68]. Based on real-world scenarios, it is clear that making an assumption of a uniform distribution of users in a cell, under a number of circumstances, may not be correct. The above rationale is further confirmed in the literature by the fact that the geographical and demogaphical factors significantly influence all aspects of a cellular network.

The most accurate model with the description of user location would be gained through practical measurements at each site of interest, this however, is not practical. In order to define accurate pdf for user distribution, it is assumed that the cellular multiple access system is constituted by a number of non-overlapping hexagonal cells, each cell of radius R_c. Each cell has a base station located at its centre, with mobile users distributed throughout the cell. The position of a mobile user in the cellular structure (reference and adjacent cells) is fully defined by its distance r from the reference base station, and its angle, θ_0, measured from some reference, both of which can be considered to be random variables as shown in Figure 3.1.

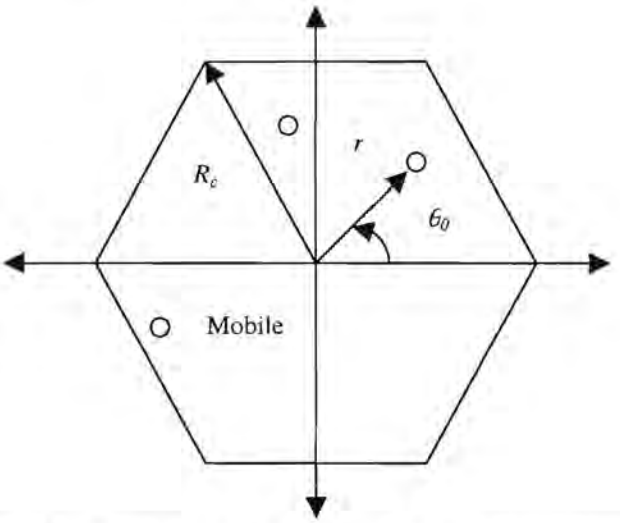

Figure 3.1: Modelling the location of users in a cellular system.

The pdf of the angular distribution of users in a cellular network can be expressed as [68]

$$P\Theta_0(\theta_0)=\frac{1}{A_{norm}}\left[1+\sum_{l=1}^{N_{peak}}\gamma_l\left[rect\left(\frac{\omega_l\theta_0}{\pi}-\alpha_l\right)+rect\left(\frac{\omega_l\theta_0}{\pi}-\alpha_l-2\pi\right)\right]\cos^2(\omega_l\theta_0-\alpha_l)\right] \tag{3.1}$$

$$0\le\theta_0\le 2\pi$$

where A_{norm} is a normalising factor to ensure that

$$\int_0^{2\pi} P\Theta_0(\beta\theta_0)d\theta_0 = 1$$

and N_{peak} is the number of peaks in the pdf. This factor (N_{peak}) is a measure of the angular clustering of mobiles in a cell. Clearly N_{peak} = 0 in (3.1), denotes a uniform angular subscriber distribution. In our analysis N_{peak} is chosen to be equal to zero, to represent a uniform user distribution as a more general result, as opposed to considering clusters of users. The *rect(x)* is defined as;

$$rect(x)=\begin{cases}1 & |x|<\frac{1}{2}\\ 0 & |x|>\frac{1}{2}\end{cases} \tag{3.2}$$

with ω_l an integer controlling the width of peak l. Typical values of ω_l will be chosen to give angular peaks of different maximum and minimum widths. For instance, if ω_l =10 is the width of the peak l in the pdf, then the angular distribution of mobiles will be 18^0. The angular location of the peak l is given by α_l, whilst the relative size of peak is determined by γ_l (typical values are between 0 and 100).

As an example, in [68] a situation shown in Figure 3.2 was considered. It is an intersection of two major roads and the base station situated at the crossing. It can be seen clearly that a larger portion of the traffic is on the roads compared to the total coverage area of the cell. The probability of receiving signals with angles of incidence of approximately 0^0, 90^0, 180^0, 270^0 rad is substantially higher, as the concentration of mobiles in these specific directions is higher. The pdf of location of mobiles for this scenario is shown in Figure 3.3 where the angular width of the street is taken to be 10^0.

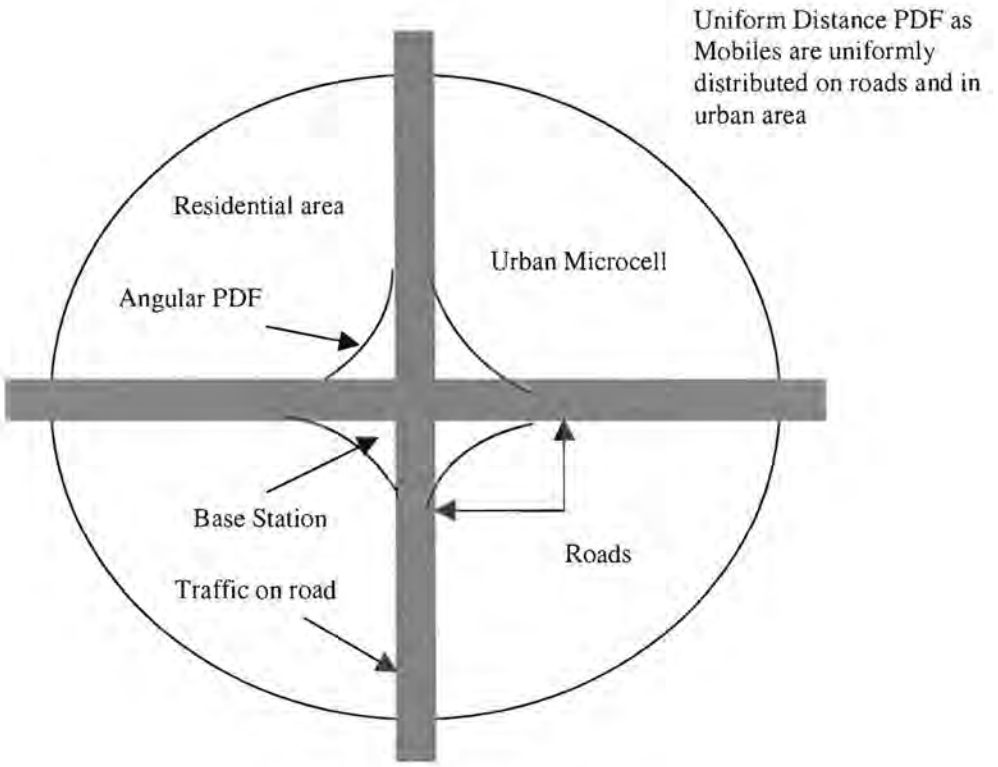

Figure 3.2: Qualitative description of the PDF of user distribution in a typical urban micro cellular scenario [68].

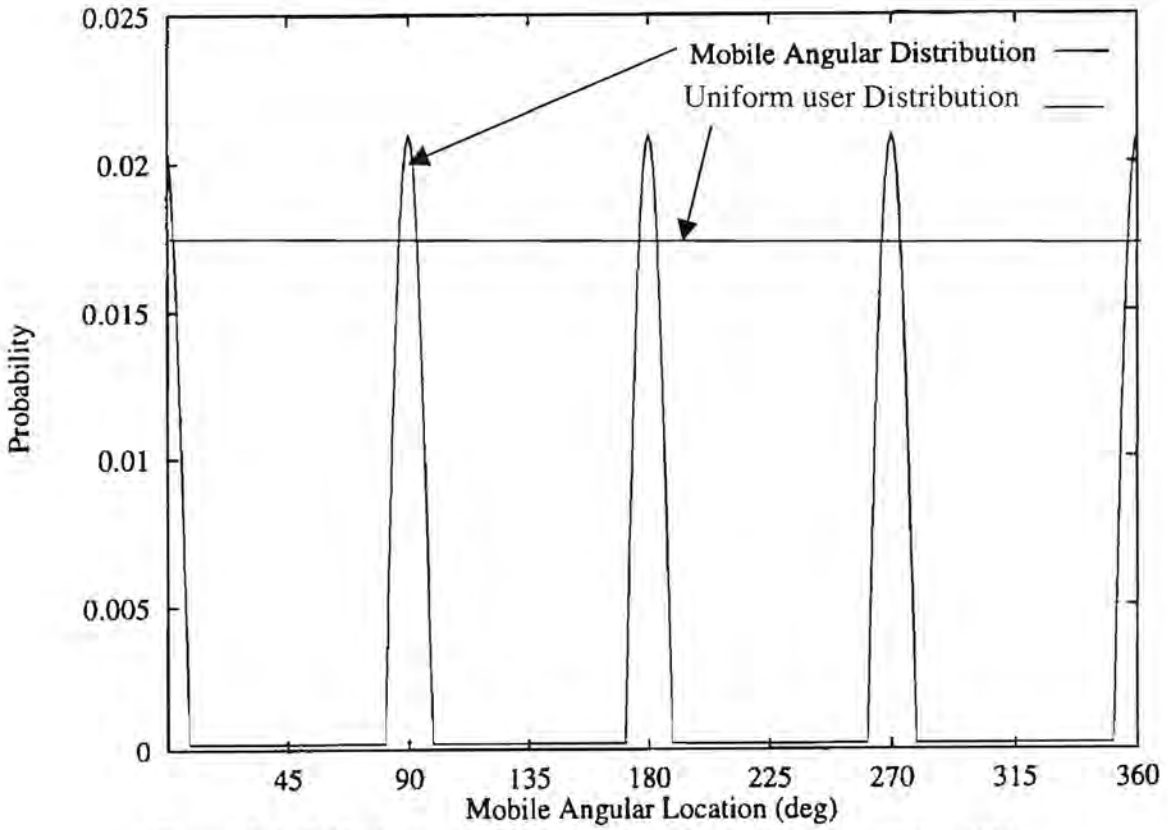

Figure 3.3: Pdf of angular and uniform distribution of mobiles [68].

The distance distribution of mobiles can be described by inserting variable transformation (3.3) in Equation (3.1). However, a uniform distance distribution is often a good approximation to make as seen in Figure 3.2.

$$r = \theta_0 \frac{3R_C}{2\pi} \qquad (3.3)$$

Uniform user distribution of mobiles is assumed here for the purpose of analysis. The assumption is well suited for both urban and suburban cases. The pdf is plotted in Figure 3.3 and can be compared with the plot for angular distribution of mobiles obtained from [68]. The uniform user distribution model is used with the scatterer model in the next section to calculate a final pdf of AOA (spatial parameter) for the proposed channel model.

3.3.2 Scatterer Distribution Model

The effect of scattering elements is of valuable importance when modelling the direction of arrival for signals associated with this user. The distribution of scattering elements around the mobile is not a fixed scenario and different approaches to model the scattering environment exist in the literature. Several approaches to the description of the scattering areas surrounding mobiles, base station or stand-alone objects exist that may cause reflection. Scattering elements can be described either as a ring of scatterers around the mobile or a disc of scatterers around the mobile as shown in Figure 3.4a & 3.4b respectively.

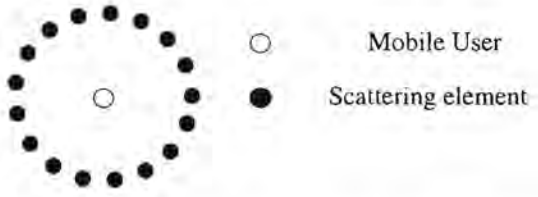

(a) Ring of Scattering Element

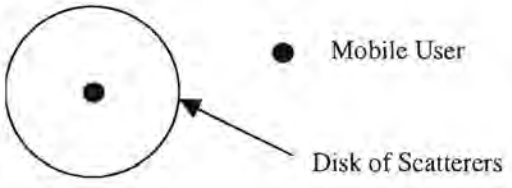

(b) Disc of scattering elements.

Figure 3.4: Modelling of scattering elements as (a) a ring of scatterers or (b) a continuous disc of scatterers.

However, it is shown in the literature that a Gaussian bell shape can best describe scattering elements. This model was chosen as the scatterer model in [65]. The Gaussian scattering model is shown in Figure 3.5. It is assumed that the majority of the scattering points, are clustered together and situated close to the mobile, with the density of the scattering points decreasing as the distance from the mobile is increased. This assumption is a good approximation of the physical reality in a micro cellular environment of scattering elements. The assumption however is not valid in case of a hilly terrain and indoor environment. In such cases the assumption of a ring of scattering elements may be more accurate.

The distribution described above is required to calculate the angular distribution of signals at the base station, this result is then used in the channel model. The model is calculated by considering the general case of mobile M separated from the base station B by an arbitrary distance D, as shown in Figure 3.5. The base station employs a directional antenna with beam width $2\alpha_b$ to illuminate the mobile, as well as a portion of the scatterers around the mobile. In this case, the density of the scattering elements at a distance r_b and angle θ_b from the mobile, can be described by the bivariate Gaussian distribution (3.4) [65].

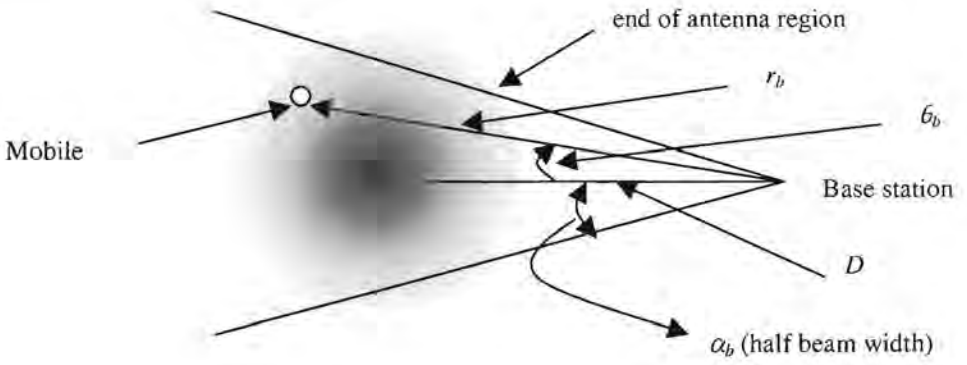

Figure 3.5: Gaussian bell shape model of scattering elements.

$$P_{scat}(r_b, \theta_b) = \frac{1}{2\pi\sigma^2} e^{\frac{(-r_b^2 + D^2 - 2 r_b D \cos\theta_b)}{2\sigma^2}} \qquad (3.4)$$

where θ_b is measured from the horizontal in Figure 3.5.

If the beam width of the antenna structure is known, the pdf of the AOA of the signal at the base station can be determined. It is assumed here that the scattering elements are

uniformly distributed and the antenna beam illuminates all scatterers in the cell. The cumulative distribution, or the addition of more scattering elements as a function of angle, can be expressed as

$$W_{\theta_b} = \int_{-\alpha}^{\alpha} \int_{0}^{\infty} P_{scat}(r_b, \theta_b) dr_b d\theta_b \qquad (3.5)$$

The probability of receiving a signal with a certain AOA is directly related to the density of scatterers in the specific direction or the derivative of (3.5) with respect to θ_b. Then:

$$P\Theta_b(\theta_b) = \frac{d}{d\theta_b} W_{\theta_b} = \int_0^{\infty} P_{scat}(r_b, \theta_b) dr_b$$
$$= \int_0^{\infty} \frac{A}{2\pi\sigma^2} e^{\frac{(-r_b^2 + D^2 - 2r_b D\cos\theta_b)}{2\sigma^2}} dr_b \qquad (3.6)$$

where A is a normalising constant such that

$$\int_0^{2\pi} P\Theta_b(\theta_b) d\theta_b = 1 \qquad (3.7)$$

By algebraic manipulations (3.6) can be simplified to

$$P\Theta_b(\theta_b) = \frac{A}{2\sqrt{2\pi}\sigma} e^{D^2(\cos^2\theta_b - 1)/2\sigma^2} erfc\left(\frac{-D\cos\theta_b}{\sqrt{2}\sigma}\right)$$
$$-\alpha_b \le \theta_b \le \alpha_b \qquad (3.8)$$

erfc (x) in (3.8) represents the complementary error function defined in Appendix C-2.

Equation (3.8) represents the post-antenna pdf of the AOA. It should be noted that the pre-antenna pdf of the AOA seen at the base station can be seen as a special case of (3.8) when $\alpha_b = 180^0$.

In order to calculate the pdf from (3.8), we need a value for the standard deviation of local scattering elements (σ). It is very difficult to propose a model for calculating accurate values of σ as it is dependent on the physical cell geometry. However, a general rule of thumb for first order approximation for σ was proposed in [8] and is shown in Table 3.1.

Table 3.1: Cell radii and standard deviation for macro and micro cells.

	Cell Radius (R_c)	Standard Deviation (σ)
LOS Micro cell	0.4 - 2 km	0.2R
N-LOS Micro cell	0.4 – 2 km	0.34R
Macro cell	2 – 20 km	0.1R

The Pdf of the AOA of signals in a scattering environment was calculated using (3.8) for values of D, α_b and R from Table 3.2 and plotted in Figure 3.6 & Figure 3.7.

Table 3.2: Typical values of $2\alpha_b$, D, and σ for the calculation of AOA.

	$2\alpha_b$	D	σ
LOS Micro cell	10^0	1000m	200m
N-LOS Micro cell	10^0	1000m	340m
Macro cell	10^0	10000m	1000m

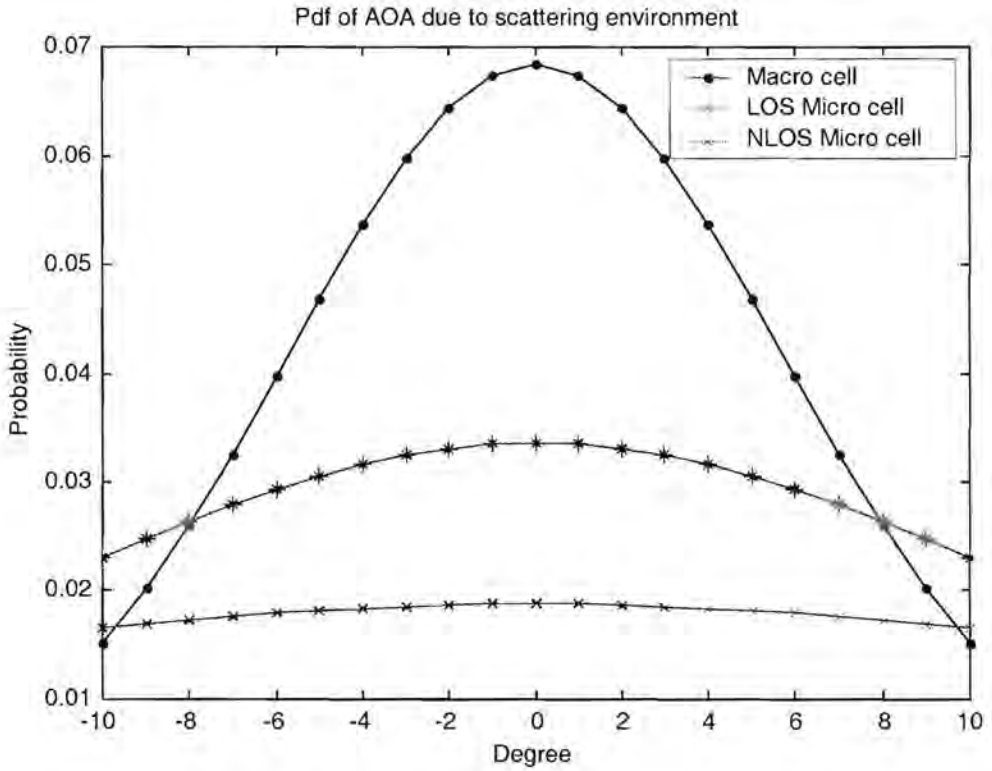

Figure 3.6: Pdf of AOA for Macro cell, LOS Micro cell, and NLOS Micro cell in local scattering environment [65].

Our analysis here will be restricted to LOS and NLOS micro cellular environment only, as shown in Figure 3.7.

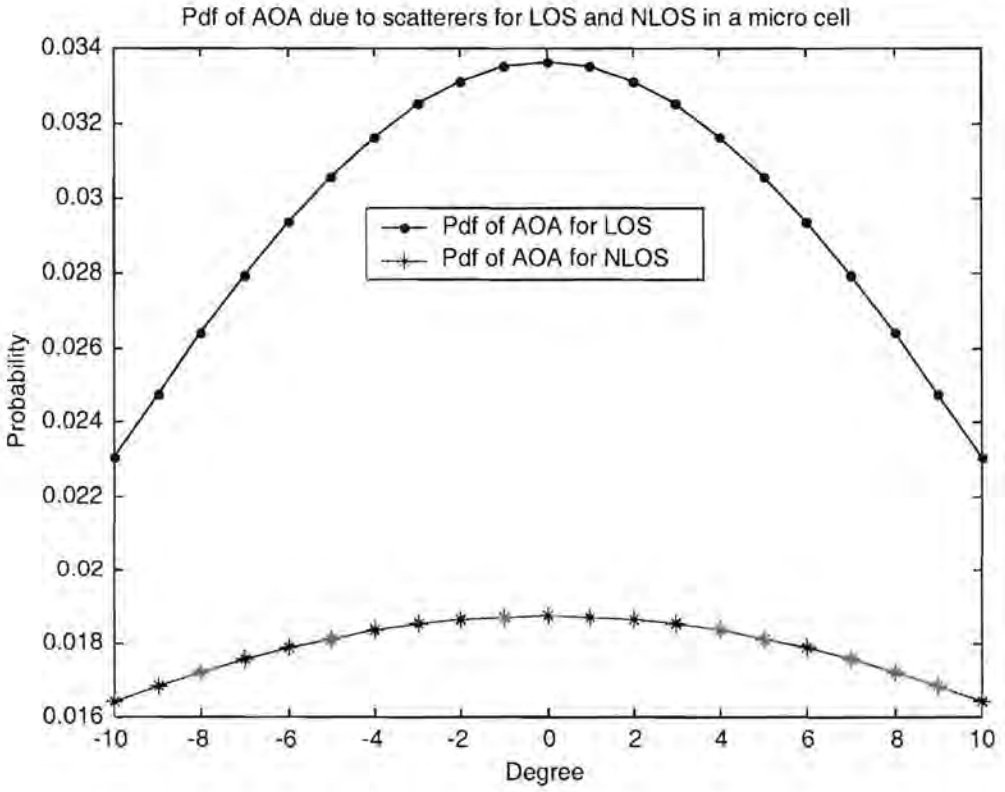

Figure 3.7: Pdf of AOA in scattering environment for LOS and NLOS micro cell.

3.3.3 DOA pdf for all user with local Scatterers

An accurate model of DOA will ideally comprise of both the user distribution model described in Section 3.3.1 and the scatterer distribution model described in Section 3.3.2. If no scattering around the mobile is assumed, then the pdf of the AOA at the base station would be exactly equal to the pdf of the mobile location in Section 3.3.1. However this is never true in real life scenarios. The final pdf of AOA at the base station is calculated by combining the two models (the user distribution & the scatterer distribution), as shown in (3.9).

$$P_{\Theta}(\theta) = P_{\Theta_a}(\theta_a) * P_{\Theta_b}(\theta_b) \qquad (3.9)$$

where * denotes convolution.

Figure 3.7 shows the pdf of the AOA at the base station with user distribution and scatterer distribution information. It can be seen clearly and concluded that the AOA is not a uniform distribution as it is often generally assumed. The results of the DOA model considered here are compared with the DOA obtained in the literature and are presented in Table 3.3.

Table 3.3: Comparison of angular spread of DOA at the base station calculated with the model presented here and the rule of thumb in [8].

Environment	Our value [96]	Value Lit. [8]	Other values [8]
LOS Micro cell	126^0	95^0	120^0
NLOS Micro cell	200^0	160^0	120^0

It is clear from these results that our angular spread is higher than the one proposed in the literature. This is as a result of our assumption that users are uniformly distributed. This is, however, not always true in a suburban area but can be a good assumption in a dense urban environment. The idea here is that the model caters for any kind of distribution, although our result is more general.

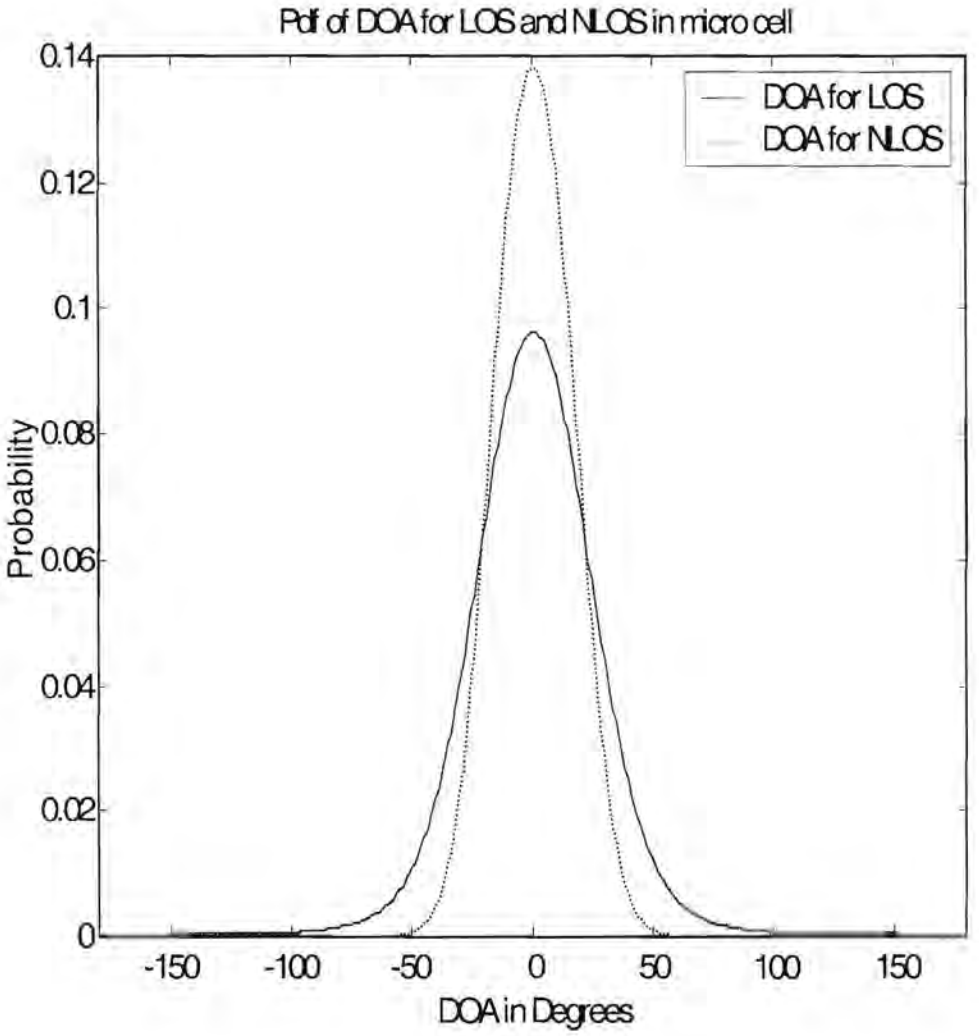

Figure 3.8: Pdf for DOA of signals at the base station with user location and local scatterer information in LOS and NLOS, macro cellular environments.

3.4 Conclusion

In this Chapter a *spatial* model has been established that has two main parts, namely, the *user* distribution and the scatterer distribution. A uniform user distribution is assumed around the base station, whereas a Gaussian bell shape distribution of scatterers is assumed. The pdfs thus calculated are then convolved to arrive at the final pdf of DOA at the base station with user distribution and local scatterer distribution information. As can be seen in Figure 3.8 and Table 3.3, the angular spread of DOA of signals arriving at the base station is 126^0 for LOS and 200^0 NLOS. In Figure 3.8 we also see that the probability of LOS signals is higher than the probability of NLOS signals for $\alpha_b < 10^0$ ($-10^0 < \theta_b < 10^0$). This DOA model is combined with the *temporal* model presented in Chapter 4 to yield the system channel model used in Chapter 6 & 7 to evaluate system performance.

Chapter 4

SPATIAL/TEMPORAL CHANNEL MODEL

4.1 Channel Model

A channel model as discussed in Chapter 2 comprises of two main parts, the *spatial* and the *temporal*. We have discussed the spatial aspect in Chapter 3, from developing the concepts and the mathematical base describing it to calculating the pdf of DOA. This chapter discusses the important concepts relating to temporal aspect, develop the analytical base, and calculate the model parameters. Temporal parameter is significantly influenced by the geography and the terrain of an area similar to the spatial parameter discussed in Chapter 3. This in turn influences the modelling of the envelopes of the fading signal. Finally the complete channel model is realised by combining the spatial model with the temporal model.

4.2 Temporal Fading Model

A typical fading channel can be modelled as a *Rayleigh*, *Rician* or a *Nakagami-m* distribution. The choice of the model depends on the operating environment of the communication system, with Rayleigh distributions commonly used for N-LOS and Rician distribution used for LOS propagation environments over small geographical areas with short term fading. Whereas log-normal distribution is used when much wider geographical

areas are involved with a characteristic long term fading component. An alternative to these fading distributions is the Nakagami m distribution, defined in (2.1).

Equation (2.1) can model a variety of fading environments including those modelled by the Rayleigh and the one-sided exponential distribution. The log-normal and Rician may be closely approximated by the Nakagami distribution in some ranges of mean signal values. It can also be used to model the Rician distribution with sufficient accuracy by calculating the values of m from (2.2) as defined in Chapter 2.

Furthermore, the Nakagami distribution is more flexible and can model experimental data more accurately for many physical propagation channels. It can also be used to accurately describe the fading behaviour of multipath signals, taking into account the varying physical scattering processes. In our analysis *Nakagami-m* distribution is used to model the fading due to multipath propagation, as will be discussed in Chapter 5.

The fading process on each of the received multipath signals can be modelled by incorporating information on the DOA of the multipath signals at the base station. Utilising the properties of the Nakagami distribution, varying degrees of fading can be approximated by the correct choice of the m parameter. In all cases considered here, the cumulative distribution function (cdf) of the κ (Rice factor) parameter measured over the three strongest paths received, is close to the cdf of a Gaussian pdf, or two-sided exponential distribution [8]. Based on these two alternative models, the *Exponential fading model* and the *Gaussian fading model* may be used to created a relationship between the fading experienced by multipath signals, embodied by the m-parameter, and the DOA (θ), as proposed in [8]. These models will be discussed in detail in the next sections, where values of m are calculated that will be used in Chapters 6 & 7 to evaluate the performance of the diversity combiner proposed in Chapter 5.

4.3 Exponential Fading Distribution Model

A relationship between the DOA θ and the fading parameter m, will be developed in this section based on a generalised exponential function as shown in (4.1). This is achieved by setting m in (2.2) equal to

$$m(\theta) = m_0 e^{-\delta_m(|\theta-\phi_0|)} \qquad m(\theta) > 0.5 \qquad (4.1)$$

where m_0 denotes the Nakagami parameter of the main received path and ϕ_0 the DOA of the main received signal path. δ_m is a parameter to control the increase in the severity of the fading as a function of the angular spread of the multipath signals arriving at the base station. When δ_m = 0, this model represents a standard, constant m Nakagami fading channel. The changes in m as a function of θ (that is the value of δ_m) will depend on the local scattering environment. This model however, would simulate a situation where LOS signals received exhibit less fading than signals with DOA's offset from the DOA of the mobile.

4.4 Gaussian Fading Distribution Model

Another distribution that describes fading as a result of scattering elements surrounding a mobile user is the Gaussian distribution defined in (4.2). This represents a relationship between m and θ given by

$$\mu = m(\theta) = m_0 e^{-\frac{(\theta-\phi_0)^2}{2\sigma_m^2}} \qquad m(\theta) > 0.5 \qquad (4.2)$$

The fading parameter of the multipath components in (4.2) is controlled by σ_m, the standard deviation of the fading parameter. Setting σ_m equal to ∞ will yield a constant m Nakagami fading channel. Decreasing σ_m will yield non-constant fading distribution with the fading effects becoming increasingly severe as the DOA of the multipath signal is removed from the DOA of the main signal path.

A detailed method for the calculation of δ_m and σ_m is presented in [8] and their values are summarised in Table 4.1. The Table shows values of m_0, δ_m and σ_m in LOS and NLOS for Bad urban, Typical urban and Macro cell environments. It is clear that the Gaussian model will simulate a more severe fading environment than the exponential model, although both may be used as the element of the channel model. In our system model we considered both scenarios, Gaussian model for Bad Urban environments with N-LOS propagation and exponential model for Typical and Good Urban environment.

Table 4.1: Summary of temporal fading model parameters

Environment	Temporal Fading Model	m_0	Fading Decay
Bad Urban (N-LOS)	Gaussian	1	$\sigma_m = 0.6$
Typical Urban (LOS)	Exponential	≈ 6	$\delta_m = 1$
Macro cell	Exponential	> 6	$\delta_m < 1$

4.5 Spatial/Temporal Fading Model

In the previous sections, in this Chapter we have explained the concepts and theories related to the temporal model. In order to develop a complete channel model we have to combine the results of Chapters 3 and 4 as shown in Figures 4.1, 4.2 & 4.3 to generate values for the *Channel Fading Parameter*μ, for the proposed system model as given in Table 4.2. An exponential fading for typical urban (LOS) and Gaussian fading for bad urban (NLOS) scenario is assumed as shown in Figure 4.2.

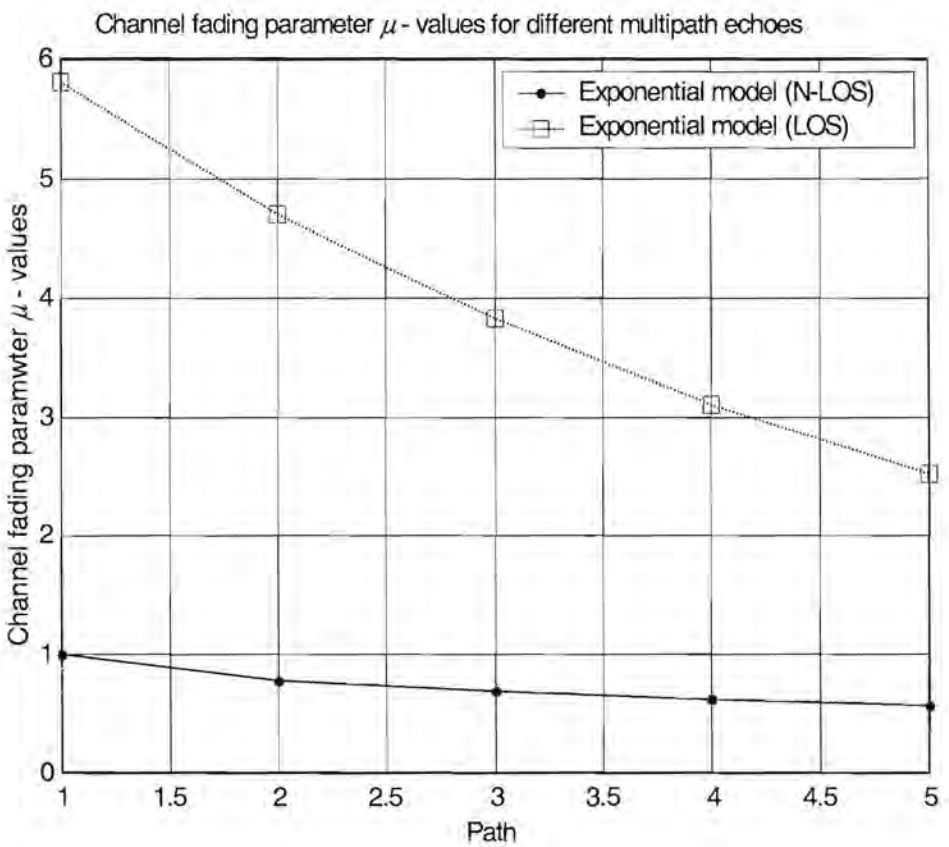

Figure 4.1: Fading parameter μ of multipath echoes at the base station using exponential model.

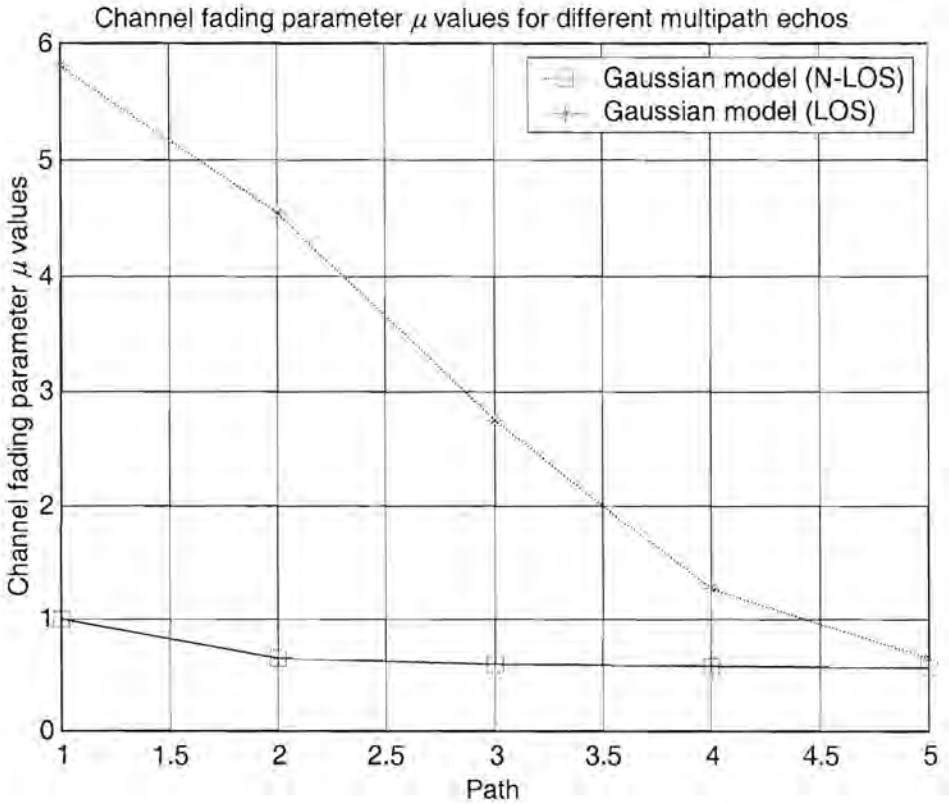

Figure 4.2: Fading parameterμ of multipath echoes at the base station using Gaussian model.

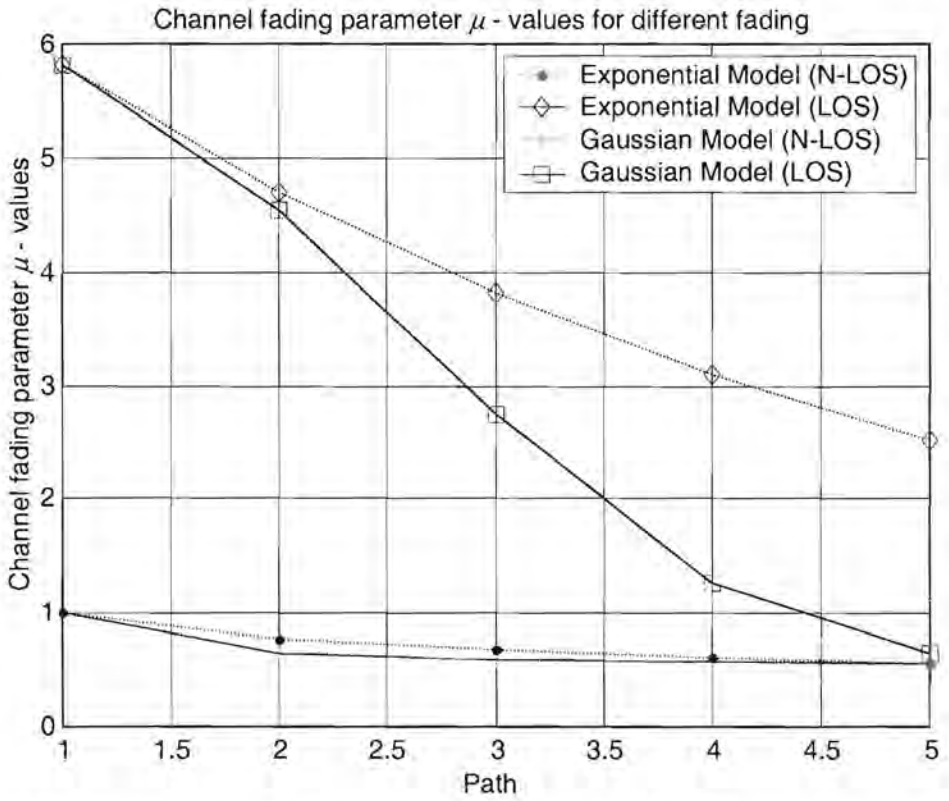

Figure 4.3: Comparison of Exponential and Gaussian Fading Models for μ values with multipath echoes.

Figure 4.1 shows values of the Channel fading parameter μ for Exponential fading model in LOS and N-LOS with 1-5 multipath components. It is important to note that in both LOS and NLOS conditions the value of the fading parameter μ reduces as the number of multipath increases from 1 to 5. It is also important to note that the value of μ in LOS reduces faster in LOS than NLOS as the number of path increase from 1 to 5.

Figure 4.2 shows values of the Channel fading parameter μ for Gaussian fading model in LOS and NLOS for the same multipath echoes as in Figure 4.1. The μ - value in the case of Gaussian fading model decreases faster than the Exponential-fading model for the same LOS conditions. This fact is illustrated in Figure 4.3.

To evaluate the performance of the system model proposed here the scope of our analysis will be restricted to Bad Urban (N-LOS) and Typical Urban (LOS) conditions with three multipath echoes. Channel fading μ values for LOS and NLOS scenarios are calculated from Figure 4.4 and are summarised in Table 4.2.

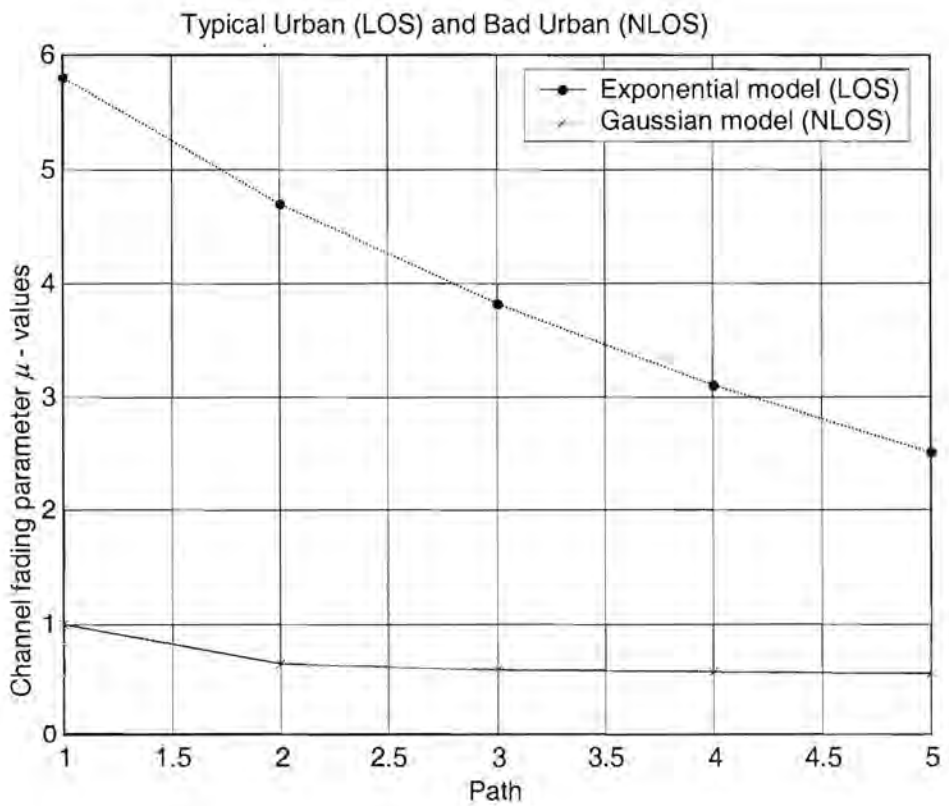

Figure 4.4: Channel fading parameter μ values with Exponential fading model for Typical Urban (LOS) and with Gaussian fading model for Bad Urban (N-LOS) scenarios.

Table 4.2: Nakagami - m values for LOS & NLOS with three multipath echoes

Environment	Temporal Fading Model	m_0	μ values for 3 multipath echoes	Fading Decay
Typical Urban (LOS)	Exponential	≈ 6	3.8	$\delta_m = 1$
Bad Urban (NLOS)	Gaussian	1	0.6	$\sigma_m = 0.5$

The complete channel model with spatial and temporal parameters is given in a flow diagram in Figure 4.5. It shows all the main blocks of the model and how they are combined to generate the channel parameter. The channel information thus calculated has the spatial information (angle of arrival) and the fading information (temporal). This channel model will help in predicting system performance close to reality. As seen in Figure 4.5, the scattering and user distribution information is calculated in parallel and is then combined by convolution. This is the AOA or the spatial parameter, which is then combined with fading parameter to calculate the Nakagami-m parameter for different number of multipaths.

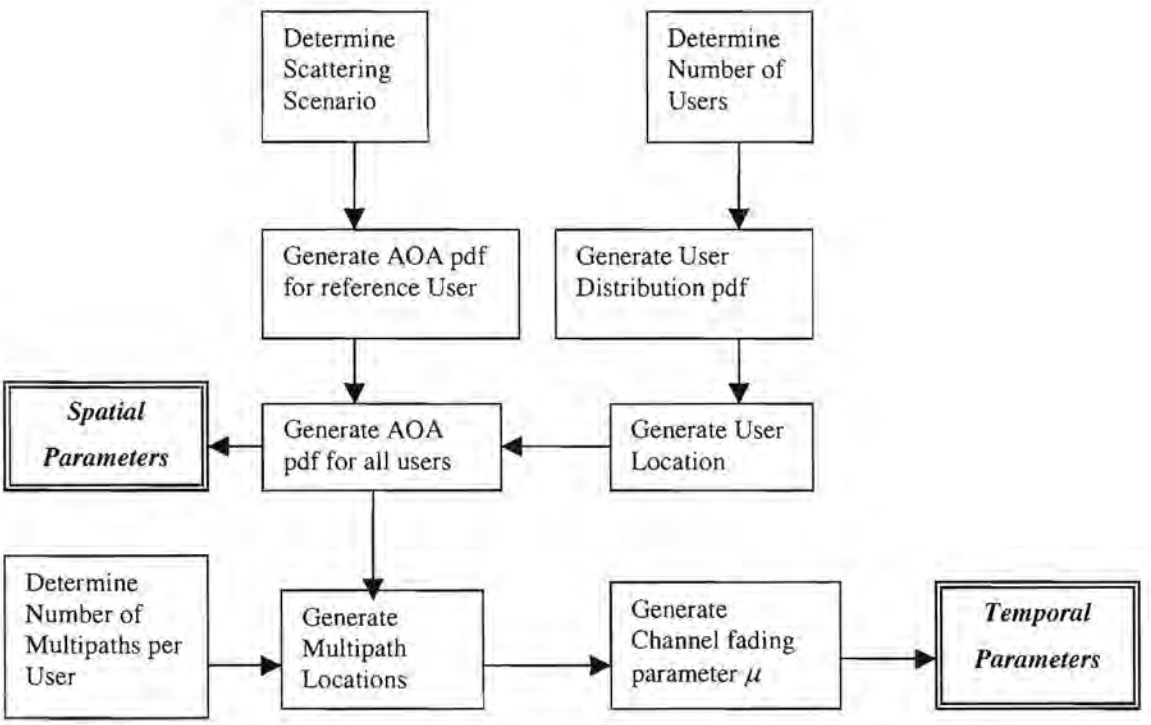

Figure 4.5: Flow diagram for the realisation of spatial/temporal channel model [8].

4.6 Conclusion

A general *special/temporal* channel model has been established in this Chapter and values of the *Channel fading parameter* μ for both LOS and NLOS conditions were calculated. The *Spatial* aspect takes into account the scattering environment around the mobile and the distribution of users based on the geographical clustering of mobiles. The *Temporal* aspect takes into account small-scale fading due to multipath. The model can easily be modified to represent any real life situation. The model combines the DOA information with the fading due to multipath echoes of the signal at the base station. The model takes into account all aspects influencing the performance of smart antenna systems. The proposed model is general in that no assumption of the transceiver is made and can be used to evaluate different CDMA, TDMA or FDMA systems.

Chapter 5

RAKE RECEIVER AND MRC

5.1 Rake Receiver

The concept of *Rake receiver* has received considerable attention in the literature due to the signal to noise ratio improvement it provides at the receiver. A Rake receiver combines the time-delayed versions of the original transmitted signal due to multipath. It collects all the time-shifted version of the original signal by providing a separate correlation receiver for each of the multipath signals. The Rake Receiver is essentially a diversity receiver designed specially for CDMA, where the diversity is provided by the fact that the multipath components are practically uncorrelated from one another when their propagation delay exceed a chip period. Figure 5.1 shows an *M*- branch (*M*-finger) Rake receiver implementation. Each correlator in the Figure detects a time-shifted version of the original CDMA transmission, and each finger of the *Rake* correlates to a portion of the signal, which is delayed by at least one chip in time from the other fingers.

In a CDMA system the spreading code is designed to provide very low correlation between successive chips. Thus, the propagation delay merely provides multiple versions of the transmitted signal at the receiver. If the multipath components of the main signal are delayed in time by more than a chip duration, they appear like uncorrelated noise at the CDMA receiver [2]. A chip rate can be selected to provide low autocorrelation properties for the CDMA spreading sequence and also assure that the multipath components are almost uncorrelate with each other.

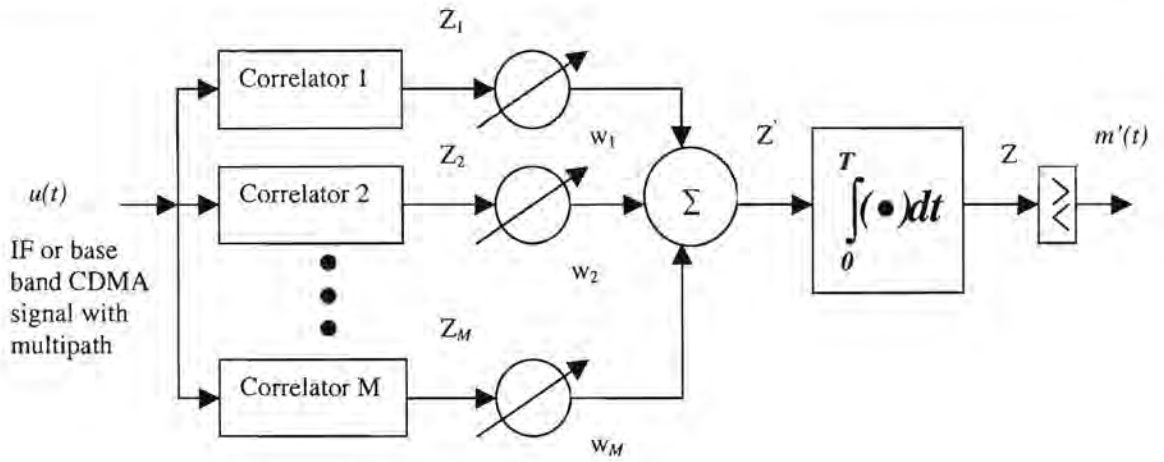

Figure 5.1: An M-branch receiver.

A *Rake* receiver utilises multiple correlators to separately detect the M strongest multipath components. The outputs of each correlator are weighted to provide a better estimate of the transmitted signal than is provided by a single component. In a CDMA Rake receiver with M-correlators used to capture the M strongest multipaths components, a weighting network is used to provide a linear combination of the correlator output for bit detection. Correlator 1 is synchronised to the strongest multipath L_1. Multipath component L_2 arrives τ_1 later than component L_1. The second correlator is synchronised to L_2. It correlates strongly with L_2 but has low correlation with L_1. If fading corrupts the output from one correlator, the others may not be, and the corrupted signal may be discounted through the weighting process. The process of weighting signals to rejecting corrupted signals and combining the remaining M signals in a Rake receiver provides a form of diversity which can overcome fading and thereby improve the performance of CDMA reception.

As shown in Figure 5.1 the M decision statistics are weighted to form an overall decision statistic. The output of the M correlators are denoted as Z_1, Z_2,...., and Z_M. They are weighted by w_1, $w_{2,....}$ and w_M, respectively. The weighting coefficients are based on the power or the SNR from each correlator output. If the power or the SNR from a particular correlator is small, it will be assigned a small weighting factor. This way of weighting signals is very similar to a *maximal ratio combining* diversity scheme and it can be concluded that maximal ratio combining is essentially a Rake receiver when applied to a CDMA system. A detailed explanation of the Rake receiver principle can be found in [2], and the performance of the Rake receiver for different modulation schemes compared in [84]. In summary, a receiver that resolves the multipaths via code correlation and then combines them is referred to as a RAKE receiver.

An important part of our system model is to develop a receiver that can effectively combat multipath fading and use the information in the multipath signals to improve system performance. The model considered here is one that can be applied to CDMA and can be used for 3G systems. A maximal ratio combiner is chosen to form part of the receiver. The combiner has received a lot of attention in the literature and has been shown to out-perform any other combining techniques for CDMA systems [37, 38, 40, 41, 42]. MRC and Nakagami distributions can be easily integrated to maximise the system gain [36]. In the next section a pdf for a receiver with MRC in a Nakagami channel is calculated.

5.2 Pdf of the signal power for M branch MRC

A *maximal ratio combiner* at the antenna of a base station is realised here by analytical analysis of the *signal*, the *correlation*, and the *fading*. The three concepts are then integrated to make up the complete channel.

5.2.1 Signal at the Diversity Antenna

The signal received at the diversity antenna forms the basis of the analysis here and needs to be explained in detail. Although the analysis considers the general case of an M-branch diversity antenna, the final system model is restricted to $M = 3$.

The signal received in the kth channel of an M-branch diversity antenna is given by Equation (5.1).

$$r_k(t) = X_{ck}(t)\cos\omega_c t + X_{sk}(t)\sin\omega_c t + n(t) \qquad (5.1)$$

where $k = 1, 2 \ldots\ldots M.$, $X_{ck}(t)$ & $X_{sk}(t)$ are zero mean stationary Gaussian random processes and $n(t)$ is the white Gaussian noise with received fading amplitude $\{\beta^{(k)}\}$. If the instantaneous signal power in the kth channel is defined as

$$S_k = \frac{1}{2}\left(X_{ck}^2 + X_{sk}^2\right) \qquad (5.2)$$

the sum of the received powers is given by

$$S = \sum_{k=1}^{M} \beta_k^2 = \sum_{k=1}^{M} \{ X_{ck}^2 + X_{sk}^2 \} = \sum_{k=1}^{M} S_k \qquad (5.3a)$$

with S_k the instantaneous power of the kth channel. We note that

$$E\{\beta_k^2\} = E\{S_k\} = \Omega_k \qquad (5.3b)$$

the random vector X in (5.2) is defined as $X = [x_1, x_2, x_3, \ldots\ldots, x_{2M}]$, which consists of the ordered sequence of in-phase and quadrature amplitudes of the signal on the diversity branches, i.e., x_{2k-1} and x_{2k} are the in-phase and quadrature signals on the kth branch, respectively.

The joint probability density function of X is given by

$$p(X) = (2\pi)^{-M}|\zeta|^{-1/2} exp\left(-\frac{1}{2}X\zeta^{-1}X'\right) \qquad (5.4)$$

where ς in (5.4) is a $(2M \times 2M)$ covariance matrix defined by

$$\zeta = [E(x_i x_j)], \qquad i, j = 1,2,,.....,2M \qquad (5.5)$$

where $E(\cdot)$ denotes expectation and ς is a positive definite matrix defined in (5.6) (from [36]):

$$\zeta = \sigma^2 \begin{bmatrix} \wedge & 0 \\ 0 & \wedge \end{bmatrix} \qquad (5.6)$$

and $E(x_i^2) = \sigma^2$ and $\wedge$ is a $M \times M$ square symmetric matrix. Equation (5.3a) can be rewritten as:

$$S = \frac{1}{2}XIX' \qquad (5.7)$$

where I is the $2M \times 2M$ density matrix and X' is the transpose of X. the characteristic function of the probability density function of S is obtained from [36] and is given in (5.8)

$$\Psi_S(t_1, t_2, \ldots\ldots, t_M) = E\left(exp\left\{i\sum_{k=1}^{M} t_k S_k\right\}\right)$$
$$= \left|I - 2i\sigma^2 T \wedge\right|^{-\lambda} \qquad (5.8)$$

where T is the diagonal matrix whose elements are $(t_1, t_2, \ldots\ldots, t_M)$, i is the symbol interval index and λ is a constant. The probability density function of S can be obtained from (5.8). If $\upsilon = 2\sigma^2$, and $\lambda > 0$ are real numbers, then the distribution of S is a multivariate Gamma distribution, each variable of which has an identical marginal probability density function given by (5.9) [36].

$$P_{S_1}(s_1) = \frac{S_1^{\lambda-1} exp(-s_1/\upsilon)}{\upsilon\Gamma(\lambda)}, \qquad s_1 > 0 \qquad (5.9)$$

where Γ is Gamma function. If $K = [k_{ij}]$ is the normalised covariance matrix of an M-variate Gamma distribution and $\wedge = [\rho_{ij}]$ is that of the "accompanying" Gaussian distribution, then

$$k_{ij} = \rho_{ij}^2 \qquad (i,j = 1,2,.....,M). \qquad (5.10)$$

5.2.2 Correlation Model

Correlation between fading signals is an important parameter when calculating the response of a diversity antenna. Diversity is an efficient way of combating multipath fading but it is only really effective if the correlation coefficient ρ is below 0.5. The effect of ρ will be studied in detail later in the Chapter where we will see the improvement as ρ approaches zero. This effect of ρ makes it important to develop accurate correlation models. Experimental data on correlation of the fading signal are usually given in terms of envelope correlation because of the ease of measurement. Given the envelope correlation, however, the power correlation can be found, and vice versa. Two correlation models, *Constant Correlation* and *Exponential Correlation* models, are presented below.

5.2.2.1 Constant Correlation Model

In this model it is assumed that the correlation between any two branches of an M-branch diversity channel is the same as shown in Equation (5.11). It can also be assumed to be a special case of the *Exponential Correlation Model.*

$$\rho_{ij} = \rho, \qquad where \qquad i,j = 1,2,.....,M \quad and \quad 0 < \rho < 1 \qquad (5.11)$$

This model is a good approximation for closely spaced diversity antennas. For our analysis we consider a three-element circular symmetric antenna array that gives rise to constant correlation. The probability density function for S with constant correlation model is given

in (5.12), where ${}_1F_1()$ is the confluent hypergeometric function given in Appendix (E-1). For $\rho = 0$, (5.12) reduces to the probability density of the sum of M independent random variables, each of which have pdf given by (5.9).

$$P_S(s) = \frac{\left(\frac{s}{\upsilon}\right)^{Mm-1} exp\left(\frac{-s}{\upsilon(1-\rho)}\right) {}_1F_1\left(m, Mm; \frac{M\rho s}{\upsilon(1-\rho)(1-\rho+M\rho)}\right)}{\upsilon(1-\rho)^{m(M-1)}(1-\rho+M\rho)^m \Gamma(Mm)} \qquad (5.12)$$

5.2.2.2 Exponential Correlation Model

The Exponential model assumes that the correlation coefficient ρ_{ij}, between branches i and j is ρ to the exponent of the modulus of the difference between i and j as given in (5.13)

$$\rho_{ij} = \rho^{|i-j|} \qquad 0 < \rho < 1 \qquad (5.13)$$

It is assumed that the diversity signals are taken from a configuration which, in some physical sense, are equispaced (either in space, frequency, time, etc.). Given the stationary nature of the overall process, and assuming that all the signals are statistically equivalent, it would be expected that the correlation between a pair of signals will decrease as the separation between them increases. In this case the probability density function of S can be very closely approximated by

$$P_S(s) = \frac{s^{\lambda_M - 1} exp(-s/\upsilon_M)}{\upsilon_M \Gamma(\lambda_M)}, \qquad s > 0 \qquad (5.14a)$$

where

$$\lambda_M = \frac{M^2\lambda}{r}, \quad \upsilon_M = \frac{r\upsilon}{M} \qquad (5.14b)$$

and

$$r = M + \frac{2\rho}{1-\rho}\left(M - \frac{1-\rho^M}{1-\rho}\right) \qquad (5.14c)$$

The approximate distribution in (5.14a) is unique, since the two moments completely determine the Gamma distribution. A numerical comparison of the approximate and exact distribution of the sum of identically distributed exponentially correlated Gamma-variates shows that the relative errors between them are very small and may be considered insignificant, even for values of M as small as 5.

5.3 MRC reception

In this section a probability density function for maximal ratio combining is calculated, that incorporates the Nakagami's fading parameter m. Nakagami m values with DOA information were calculated in Chapter 4. The pdf calculated here will provide an accurate prediction of the received signal with accuracy very close to the actual signal. MR has the best performance of in comparison to other combining techniques [34, 43]. This was pointed out in the literature study in Chapter 2. Maximal-ratio combining is the most often used to evaluate the performance of a diversity antenna system especially with CDMA techniques [37, 42]. This combining method has been widely used to evaluate correlated Nakagami fading channels [36, 38, 41].

It is important at this point to point out the characteristics of *Nakagami fading*. In a Nakagami fading environment the magnitude of the received field (in volts per meter), also referred to as signal envelope, is characterised by the Nakagami distribution. However, it is more convenient to use the square of the envelope, which is proportional to the signal power. The desired signal power S (in watts per meter) is then Gamma distributed with probability density given by:

$$P_S(s) = \left(\frac{m}{\overline{\Omega}}\right)^m \frac{s^{m-1}}{\Gamma(m)} exp\left(-\frac{ms}{\overline{\Omega}}\right), \qquad s > 0 \qquad (5.15)$$

where $m \geq ½$, $\overline{\Omega}$ is the average signal power and $\Gamma(m)$ is the gamma function of the fading parameter m. The constant m is called the fading parameter.

It is assumed that the average signal power and the fading parameter in each of the M channels of a maximal ratio diversity system are identical. This assumption is reasonable if the diversity channels are closely spaced and the gain of each channel is such that all the noise power is equal.

The SNR at the output of a Maximal-ratio combiner is given by [36]:

$$\gamma = \sum_{k=1}^{M} \gamma_k \qquad (5.16)$$

where γ_k ($k = 1,2,\ldots\ldots, M$) is the SNR which is proportional to the short- term power of the kth channel with the probability density function in (5.15) and with equal noise power in the individual branches. When the branch fading is assumed to be statistically independent, then γ is also a Gamma distribution as given in (5.17) [36].

$$P_\gamma(\gamma) = \left(\frac{m}{\overline{\Omega}}\right)^{Mm} \frac{\gamma^{Mm-1}}{\Gamma(Mm)} exp\left(-\frac{m}{\overline{\Omega}}\gamma\right), \qquad \gamma > 0. \qquad (5.17)$$

However, when the diversity branches are so closely spaced that the branch signal powers are no longer independent, the distribution of γ must be written to take the correlation between the branches into consideration. Therefore, for the equal correlation model in (5.11), the probability density function (pdf) is obtained as given in (5.18) by substituting $\upsilon = \overline{\Omega}/m$ in (5.12). Similarly, for the exponential correlation model in (5.13) the pdf of γ is obtained from (5.14) and is given by (5.19).

$$P_\gamma(\gamma) = \frac{\left(\frac{\gamma m}{\overline{\Omega}}\right)^{Mm-1} exp\left(\frac{-\gamma m}{\overline{\Omega}(1-\rho)}\right) {}_1F_1\left(m, Mm; \frac{Mm\rho\gamma}{\overline{\Omega}(1-\rho)(1-\rho+M\rho)}\right)}{\left(\frac{\overline{\Omega}}{m}\right)(1-\rho)^{m(M-1)}(1-\rho+M\rho)^m \Gamma(Mm)}, \qquad \gamma > 0 \qquad (5.18)$$

$$P_\gamma(\gamma) = \frac{\gamma^{\frac{mM^2}{r}-1} exp\left(\frac{-Mm\gamma}{r\overline{\Omega}}\right)}{\Gamma\left(\frac{mM^2}{r}\right)\left(\frac{r\overline{\Omega}}{Mm}\right)^{\frac{mM^2}{r}}}, \qquad \gamma > 0 \qquad (5.19)$$

r in (5.19) is defined in (5.14C).

In our system model we considered the constant correlation model for analysis with a three element circular symmetric antenna array ($M = 3$). Of course, any suitable value for M can be chosen. The system considered here is very general and any values for the parameters assumed can be chosen to suit a particular case.

5.4 Extension of the MRC pdf in section 5.3 for negatively correlated signals

This section deals with one of the important part of this dissertation. In this section we extend the pdf calculated in section 5.3 for negative values of the correlation coefficient. Equation (5.18) represents the pdf of the signal power over a correlated Nakagami fading channel with MRC. The pdf is only valid for correlation coefficient ρ between zero and one ($0< \rho <1$). The aim here is to develop a base and extend the pdf in (5.18) for negative values of ρ. To achieve this certain assumptions have to be made to satisfy the necessary conditions as discussed below. It is important here to note that by extending (5.18) to incorporate negatively correlated signals there may not always be a very large improvement in the performance. However it is significant enough to justify the effort, as this improvement is achieved at no extra cost.

5.4.1 Condition for negative ρ for M-branch Diversity with Gaussian Signal

In this section we develop and analyse the required condition for which ρ between the diversity branches will have negative values. Using (5.1) we can rewrite (5.2) for random signal power S with Gaussian random process, N $(0, \sigma^2)$, $E\{X_{ck}^2\} = E\{X_{sk}^2\} = \sigma^2/2$ and $n(t)$ white Gaussian noise as

$$S_k = X_{ck}^2 + X_{sk}^2 \qquad (5.20)$$

where N $(0, \sigma^2)$ is a zero mean with σ^2 the variance of the Gaussian random Process. The total power in the M branches is the same as given in (5.3). Note that $E\{S_k\} = \sigma^2$, $E\{S\} = M \cdot \sigma^2$.

The column-vector X is defined as:

$$X = \begin{pmatrix} X_c \\ X_s \end{pmatrix}, \quad X_c = \begin{pmatrix} X_{c1} \\ X_{c2} \\ \cdots \\ X_{cM} \end{pmatrix}, \qquad X_s = \begin{pmatrix} X_{s1} \\ X_{s2} \\ \cdots \\ X_{sM} \end{pmatrix}. \qquad (5.21)$$

It is also assumed that

$$E\{X_c X_c^T\} = \frac{\sigma^2}{2} R, \quad E\{X_s X_s^T\} = \frac{\sigma^2}{2} R,$$
$$E\{X_c X_s^T\} = 0 \qquad (5.22)$$

The joint pdf of X is given in (5.4), where ς is a $2M \times 2M$ correlation matrix of the form

$$\varsigma = \begin{pmatrix} R \cdot \sigma^2 / 2 & 0 \\ 0 & R \cdot \sigma^2 / 2 \end{pmatrix} \qquad (5.23)$$

where R is an arbitrary correlation matrix defined as

$$R = \begin{pmatrix} 1 & \rho_{1,2} & \rho_{1,3} & \cdots & \rho_{1,k} \\ \rho_{2,1} & 1 & \rho_{2,3} & \cdots & \rho_{2,k} \\ \rho_{3,1} & \rho_{3,2} & 1 & \cdots & \rho_{3,k} \\ \cdots & \cdots & \cdots & \cdots & \cdots \\ \rho_{k,1} & \rho_{k,2} & \rho_{k,3} & \cdots & \rho_{k,k} \end{pmatrix} \qquad (5.24)$$

According to (5.8), the multivariate characteristic function of

$$Y = (X_{c1}^2, \ldots\ldots, X_{cM}^2, X_{s1}^2, \ldots\ldots, X_{sM}^2)$$

is given by (5.25) where $\lambda = -1/2$

$$\Psi_Y(t) = E\{exp(i\left(\sum_{s=1}^{2M} t_s Y_s\right))\} = (det(I_{2M \times 2M} - 2iD_t\varsigma))^{-1/2}$$
$$and$$
$$D_t = diag(t_1, \ldots., t_{2M}) \qquad (5.25)$$

$I_{2M \times 2M}$ in (5.25) is a $2M \times 2M$ identity matrix, and i is symbol interval index.

Let

$$t_1 = t_2 = \ldots. = t_{2M} = t, \; D_t = t \cdot I_{M \times M}$$

then

$$\sum_{s=1}^{2M} t_s Y_s = t \sum_{s=1}^{2M} Y_s = t(X_{c1}^2 + \ldots + X_{cM}^2 + X_{s1}^2 + X_{sM}^2) = tS \qquad (5.26)$$

(5.25) can be written to give the characteristic function of S as

$$\Psi_s(t) = E\{exp(itS)\} = (det(I_{M\times M} - it \cdot \sigma^2 R))^{-1} \qquad (5.27)$$

where R is the arbitrary correlation matrix for $R > 0$ and is given as

$$R = \begin{pmatrix} 1 & \rho & \cdots & \rho \\ \rho & 1 & \cdots & \rho \\ \cdots & \cdots & \cdots & \cdots \\ \rho & \rho & \cdots & 1 \end{pmatrix}_{M\times M} \qquad (5.28)$$

The pdf corresponding to (5.27) is obtained by taking the inverse Fourier Transform of Ψ_s(t):

$$Ps(S) = \frac{1}{2\pi}\int_{-\infty}^{\infty}\Psi_s(t)e^{-itS}dt \qquad (5.29)$$

For a constant correlation matrix , (5.27) can be rewritten as

$$\Psi_S(t) = \left[det\begin{pmatrix} 1-it\sigma^2 & -it\sigma^2 & \cdots & -it\sigma^2 \\ -it\sigma^2 & 1-it\sigma^2 & \cdots & -it\sigma^2 \\ \cdots & \cdots & \cdots & \cdots \\ -it\sigma^2 & -it\sigma^2 & \cdots & 1-it\sigma^2 \end{pmatrix}\right]^{-1} \qquad (5.30)$$

Using (D1 & D2) to solve (5.30), the characteristic function in (5.27) can be written as

$$\Psi_S(t) = \left[1-it\sigma^2(1-\rho)\right]^{-(M-1)} \cdot \left[1-it\sigma^2(1-\rho+\rho M)\right]^{-1} \qquad (5.31)$$

The characteristic function $\Psi s(t)$ in (5.31) can be written in terms of the Laplace transform by substituting (-it) with the argument p as

$$\Psi_s(p) = \left[1+p\sigma^2(1-\rho)\right]^{-(M-1)} \cdot \left[1+p\sigma^2(1-\rho+\rho M)\right]^{-1} \qquad (5.32)$$

The probability function $p_X(S)$ as the inverse Laplace transform of $\Psi s(t)$ has value zero for $S < 0$ if and only if all of the poles of the corresponding Laplace transform $\Psi_s(p)$ have negative real parts. The function $\Psi_S(p)$ in (5.32) has two real-valued poles:

$$p_1 = -\frac{1}{\sigma^2(1-\rho)}, p_2 = -\frac{1}{\sigma^2(1-\rho+\rho M)} \qquad (5.33)$$

Then these poles are negative, provided ρ is

$$-\frac{1}{M-1} < \rho < 1 \qquad (5.34)$$

The range of values for ρ presented in the inequality (5.34) is a very important result as this is the condition for which the characteristic function $\Psi_s(t)$ has the probability density function $P_X(S)$. This result shows how to extend the range of ρ from 0 to –1, by choosing $M = 2$.

5.4.2 Pdf of SNR for M-branch Diversity combining with negatively correlated Nakagami fading

In this section we calculate the pdf of the SNR at the output of an M-branch Diversity system with arbitrary Nakagami fading, arbitrary correlation and arbitrary signal powers on each branch of the MRC receiver. Let us consider the diversity receiver in Figure 5.2 with the following assumptions:

- arbitrary signal power, Ω_l, on branch l,
- arbitrary correlation, ρ_{kl}, between branches k and l, and
- arbitrary Nakagami fading, m_l, on each branch.

The total power in the M branches of a diversity receiver, for signals given in (5.1), is given by (5.3a). Then we can write the instantaneous SNR per bit in terms of received SNR as

$$\gamma_b = \sum_{k=1}^{M} \gamma_k \qquad (5.35)$$

and the average SNR of the kth diversity branch as

$$\bar{\gamma}_k = \frac{E_b}{N_0} \Omega_k \qquad (5.36)$$

The general characteristic function for an M-branch MRC diversity system given in [26 pp 238] is given by

$$\Psi s(t) = \Pi_{k=1}^{M} \left| I_{M_k \times M_k} - itD_{M_k}(\overline{m}^{-1}) D_{M_k}(\Omega_k) J_{M_k \times M_k} \right|^{-(m_k - m_{k+1})} \qquad (5.37)$$

where $m_M + 1 = 0$, and

$$D_{M_k}(\Omega) = diag\{\Omega_1, \Omega_2, \ldots\ldots \Omega_{M_k}\}, and$$
$$D_{M_k}(\overline{m}^{-1}) = diag\{m_1^{-1}, m_2^{-1}, \ldots\ldots, m_M^{-1}\} \qquad (5.38)$$

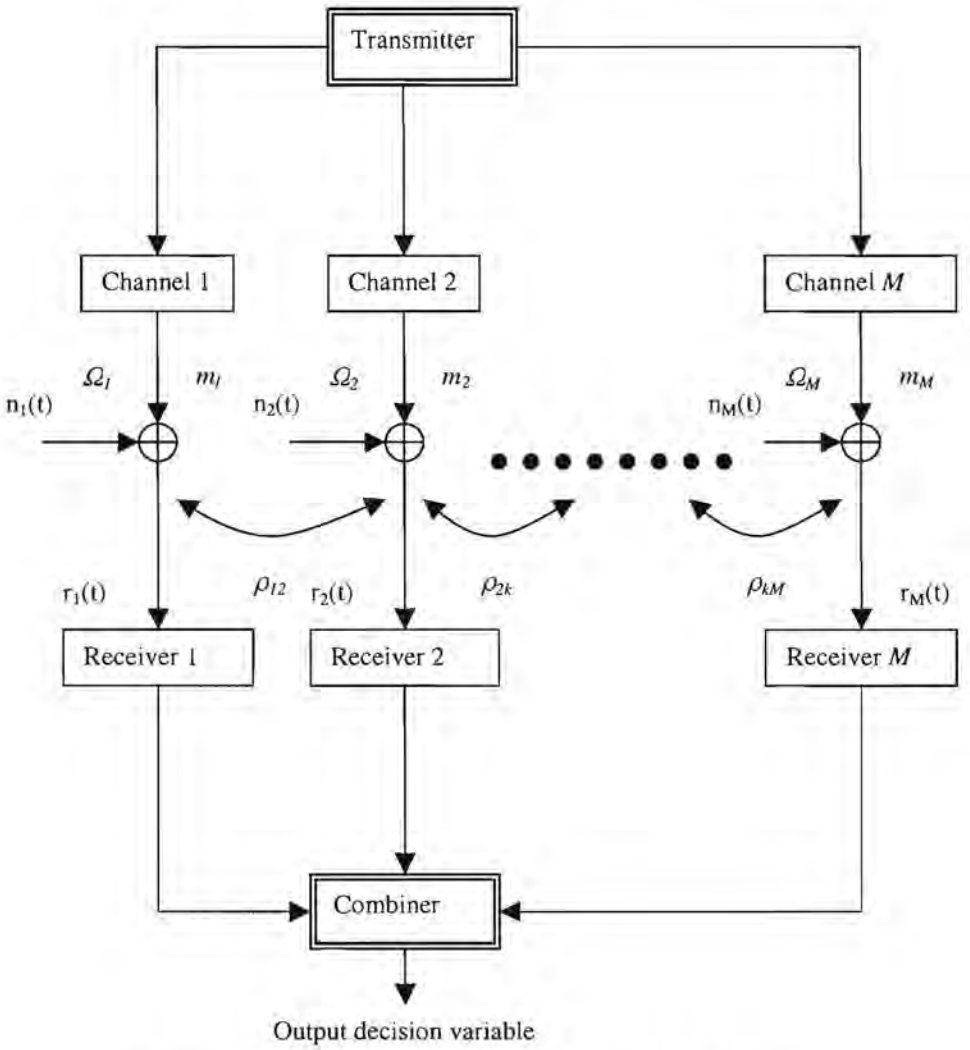

Figure 5.2: Basic Structure of a diversity combiner [26].

and $\mathbf{J}_{M \times M}$ is an $M_k \times M_k$ correlation matrix, given by

$$J_{k,l} = \rho_{kl} \sqrt{\frac{m_l}{m_k}}, k \geq l,$$
$$k = 1,2,\ldots\ldots, M. \qquad (5.39)$$

with restriction

$$m_1 \geq m_2 \geq \cdots \geq m_M \qquad (5.40)$$

and the correlation matrix $\mathbf{J}$ is valid for ρ in the range defined in (5.34).

The multivariate Gamma distribution is obtained by taking the inverse Fourier transform, of $\Psi_s(t)$ in (5.37) as shown in (5.41).

$$Ps(s) = \frac{1}{2\pi}\int_{-\infty}^{\infty}\Psi_s(t)e^{-its}\,dt \tag{5.41}$$

Finally the pdf is obtained by numerically calculating the inverse Fourier transform of (5.37) and substituting the Nakagami's m parameter with the channel fading parameter μ produces (5.42). Equation (5.42) exactly coincides with (5.18) [36]. By the same argument Equation (5.40) is also true for μ.

$$P_S(s) = \frac{\mu}{\Omega\Gamma(M\mu)}\left(\frac{s\mu}{\Omega}\right)^{M\mu-1} \times \frac{exp\left(-\frac{s\mu}{(1-\rho)\Omega}\right)\cdot {}_1F_1\left(\mu, M\mu, \frac{\rho M\mu s}{(1-\rho)(1-\rho+\rho M)\Omega}\right)}{(1-\rho)^{(M-1)\mu}(1-\rho+\rho M)^{\mu}} \tag{5.42}$$

Where ${}_1F_1(\cdot)$ is the confluent hyper geometric function (defined in Appendix E-1).

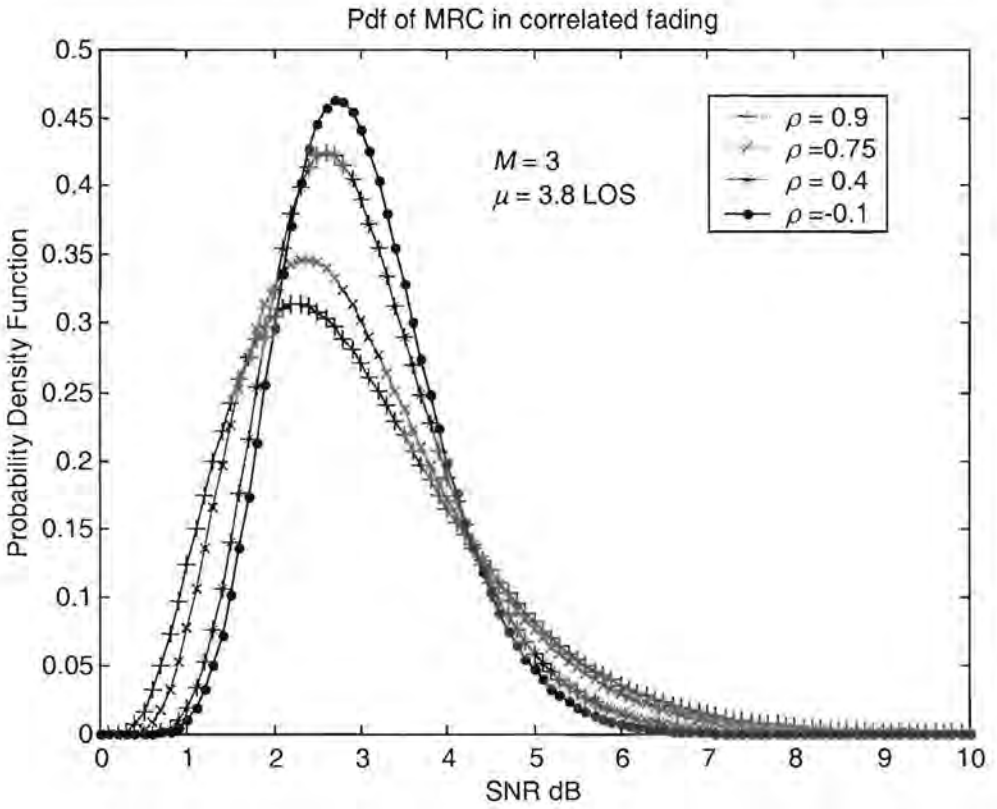

Figure 5.3: Probability density function of MRC for $M = 3$, channel fading parameter $\mu =$ 3.8, and $\rho = 0.9, 0.75, 0.4, \&-0.1$.

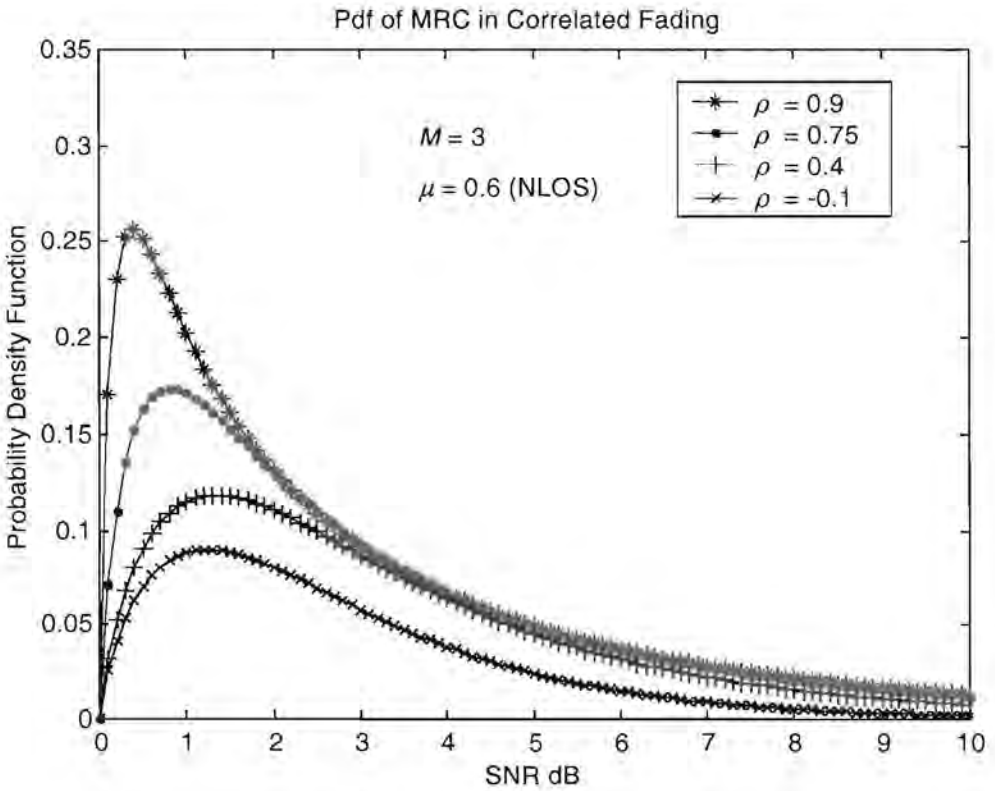

Figure 5.4: Probability density function of MRC for $M = 3$, channel fading parameter $\mu = 0.6$ and $\rho = 0.9, 0.75, 0.4, \&-0.1$

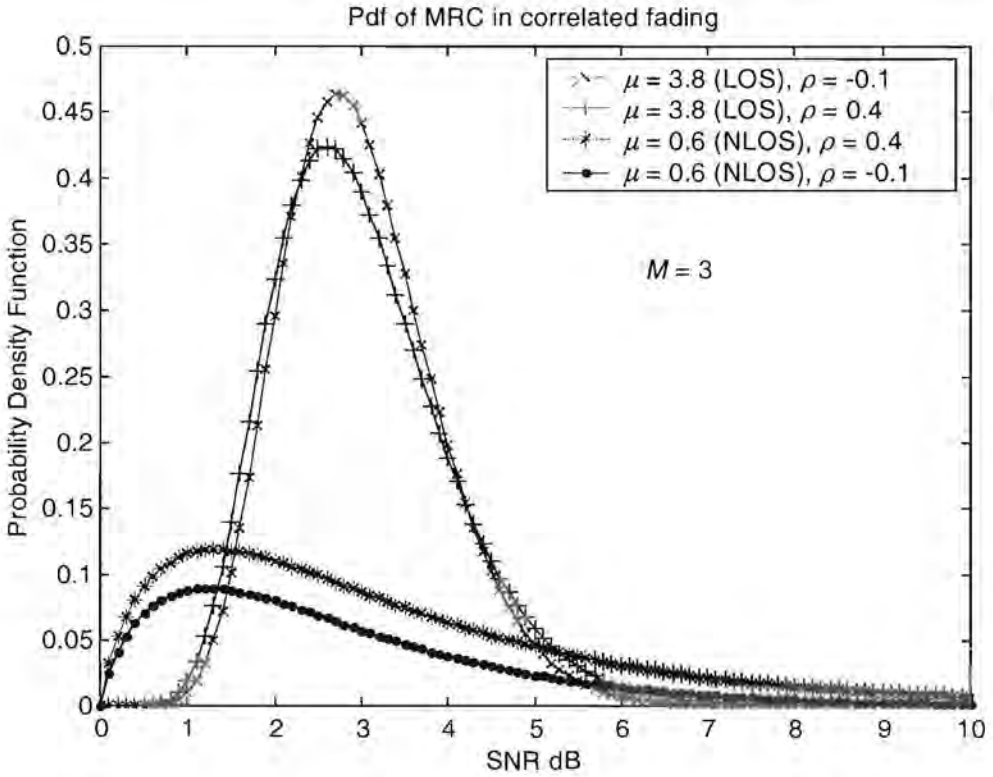

Figure 5.5: Probability density function of MRC for $M = 3$, channel fading parameter $\mu = 0.6$ & 3.8 and $\rho = 0.4$ & -0.1

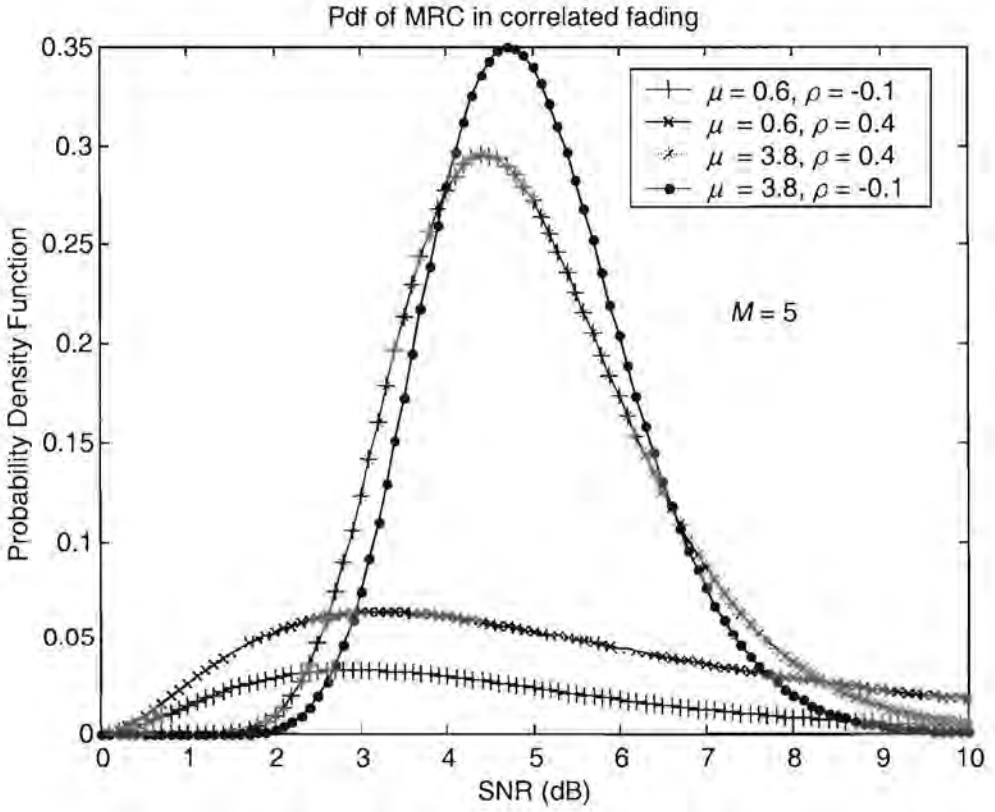

Figure 5.6: Probability density function of MRC for $M = 5$, channel fading parameter μ = 0.6 & 3.8 and $\rho = 0.4$ & -0.1

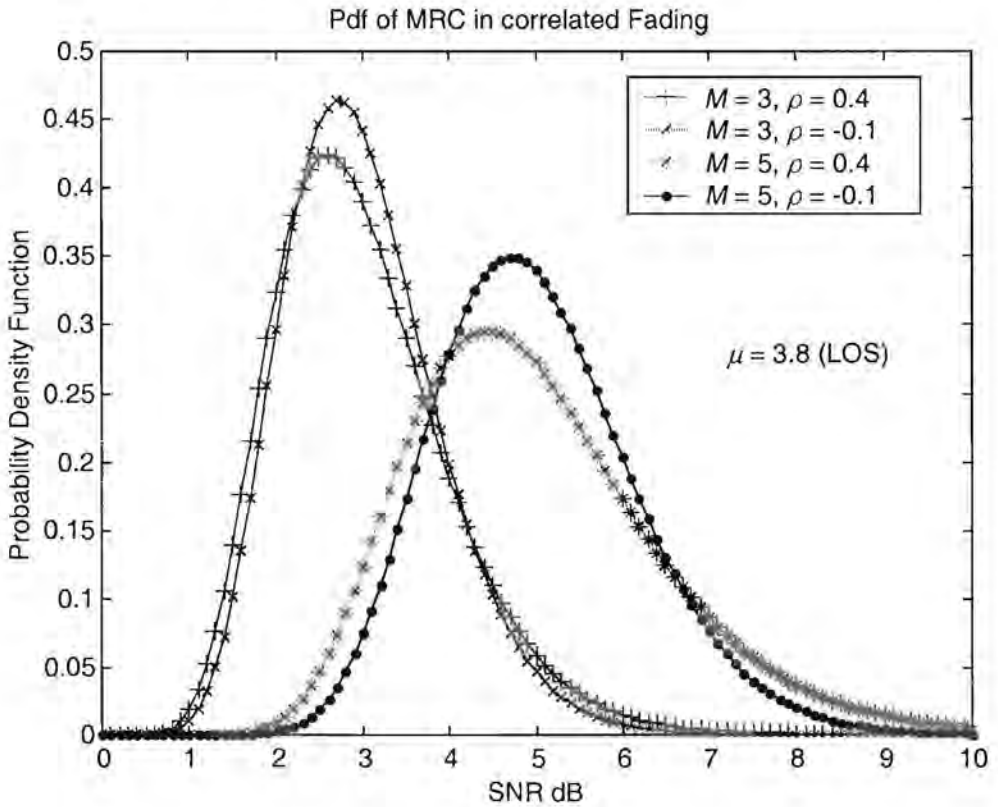

Figure 5.7: Probability density function of MRC for $M = 5$ & 3, channel fading parameter μ = 3.8 and $\rho = 0.4$ & -0.1

Equation (5.42) has the same form as (5.18); hence we can say that Equation (5.18) is also valid for signals with negative correlation coefficient within the constraints (5.40) and (5.34). The pdf in (5.18) is plotted for different values of M, μ, ρ and the average signal power is assumed to be constant ($\Omega = 1$) as shown in the Figures 5.3 – 5.7.

Figure 5.3 shows the pdf of MRC reception for $M = 3$, $\mu = 3.8$ and for$\rho = 0.9$ to – 0.1. It can be noted from the plot that as ρ reduces to zero the probability of reception of the signal increases. And finally the best probability is achieved for ρ = - 0.1. It is also important to note that the probability is high for signals with higher SNR.

In Figure 5.4 we see an interesting result where lower values of ρ do not necessarily results in higher signal probability. In fact the correlation coefficient of 0.9 (highly correlated) produces the best probability. This however suggests that other alternative methods should be used in the case of NLOS signals.

Figure 5.5 shows a comparison between $\mu = 0.6$ (NLOS) and $\mu = 3.8$ (LOS) for $\rho = 0.4$ and –0.1. It can be deduced from the plot that the MRC pdf calculated in (5.42) performs better in LOS conditions with $\mu = 3.8$ for negatively correlated signals than for signals with $\rho >$ 0. The performance in case of severe fading with $\mu = 0.6$ for negatively correlated signals is in fact worse than for signal with $\rho > 0$.

Figure 5.6 shows the probability density function for $M = 5$, $\mu = 0.6$ & 3.8, and $\rho = 0.4$ & - 0.1. The result is similar to Figure 5.5. If we compare the results of Figure 5.5 where $M = 3$ with Figure 5.6 where M = 5, we see that the pdf in Figure 5.6 caters for signals with higher SNR and for a wider range of signals. We also notice that there is an overall improvement in the probability for $M=3$.

A comparison between MRC with M = 5 and M = 3 for μ = 3 and ρ = 0.2 & -0.1 is presented in Figure 5.7. We notice that as we increase the number of diversity branches M to 5 the graph shifts to the right. This shift covers signals with a wider range of SNR although the probability is reduced in comparison to M = 3. Another point to note here is that the model with M = 5 requires a higher SNR. This means more output power from the mobile. In the final design of the system the designer has to make a choice based on his requirement.

5.5 Conclusion

In this Chapter a model of MRC presented in [36] is analysed and extended for signals with negative correlation coefficients as in [26]. By incorporating the negative correlation in our model we see an improvement in probability of reception of signals at the MRC. The final MRC model calculated is based on Equation (5.18) and is given by (5.42) with M = 3.This model, together with the DOA model calculated in Chapter 3 and the Channel fading parameter μ, calculated in Chapter 4, is used to calculate the overall system performance in Chapter 7.

Chapter 6

PROPOSED SYSTEM MODEL: ANALYSIS AND SIMULATIONS

6.1 Introduction

There is an ever-pressing demand in the field of mobile communication from vendors to provide better and cheaper services to their customers. This demand is passed on to the telecommunication industry. The industry is required to refine the existing technology and also develop new technology to meet the requirements of the service providers. The industry is also expected to be able to predict future requirements of mobile users and advise service providers around the globe about the available technologies. This will help service providers to properly plan the implementation of the new technologies in their network. The final responsibility is on the researchers to provide a solution to the above requirements of the industry.

In the constant race for developing new ways to provide solutions for future needs, researchers have to constantly come up with new ideas to improve the existing technology. The success of GSM technology has brought about the need for GPRS and UMTS technology. One important aspect of the UMTS technology is the intelligent or smart antenna systems. The smart antenna concept is an attempt to provide an efficient mechanism at the air interface of the mobile communication network. Smart antenna techniques provide considerable gain at nominal cost. An attempt is made in this

dissertation to provide a model for the air interface that takes into account the DOA information, multipath fading in the channel, and finally combines the received signal at the antenna using a Maximal Ratio combiner.

6.2 System Overview

A model for UMTS at the air interface is proposed in this report. The technique is proposed with a view to considerably reducing the level of interference between signals due to multipath. The model further improves the system performance by incorporating DOA information into the model. The smart antenna part of the model, which is the most important result here, is the proposed intelligent MRC model. Figure 6.1 summarises the proposed system model. The proposed model consists of three main parts, namely the

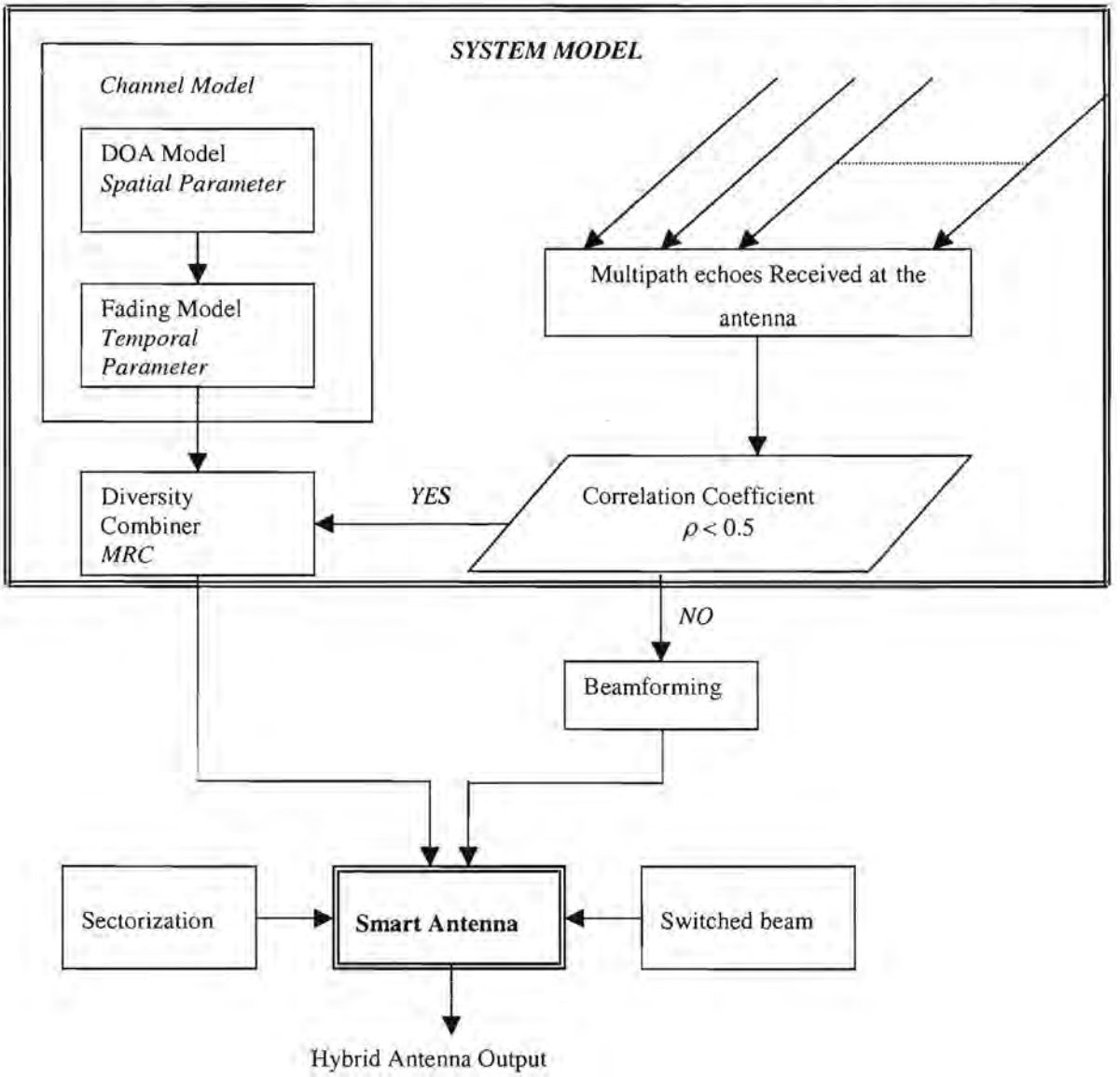

Figure 6.1: Main features of the system model with smart antenna components.

DOA model, the channel model, and the diversity combiner. It is important to note that an optimum solution to the smart antenna concept can only be realised by incorporating all the components highlighted in Figure 2.1.

6.2.1 Direction of Arrival Model

The first part of the channel model in the proposed system model is the DOA model, as shown in Figure 6.1. An accurate estimation of the Direction of Arrival of signals at the base station is of vital importance in the design of the channel model. As discussed in Chapter 2, a number of DOA models exist in the literature and can be used for the *spatial model*. It is a complicated and intense process to optimise a DOA model with all possible parameters. The DOA model proposed in [65] is chosen here as the model for the proposed system. The model was modified in Chapter 3 to make it more general by assuming a uniform user distribution. However the model can be modified to suit any user distribution scenario.

The DOA model calculated in Chapter 3 assumes a Gaussian bell shaped distribution for the scattering elements around the base station and a uniform user distribution. This model can be further improved by including estimates of the distance of the mobile from the base station or an estimate of the TOA (time of arrival) [58 pp196]. It is clear from previous discussions that the spatial parameter is affected by the geography of the cell. As will be seen in the next section the characteristics of the received signals are greatly influenced by the topography and the morphographic class of the cell.

6.2.2 Temporal Fading Model

The second part of the channel model is the *temporal model*. The model is discussed extensively in Chapter 2 and is calculated in Chapter 4. Signal attenuation caused by fading can be attributed to two types of fading as discussed in Chapter 2. Our analysis here is restricted to the short-term fading as a result of rapid fluctuation in the signal power due to multipath caused by the scattering environments in urban areas. The Nakagami-m distribution is an effective way of modelling multipath echoes as shown in Chapter 2 and can be approximated to *Rayleigh*, *Rician*, and *One-sided exponential* distribution by setting correct values for m.

Temporal fading is also dependent on the terrain of an area and can be modelled by a *Log-normal distribution* (large-scale fading). This fading is not included in our fading channel model, due to the fact that at low SNR the overall fading can be approximated to short term fading and can be modelled with sufficient accuracy, using the *Nakagami-m distribution*. However this approximation leaves room for further improvement when designing a more accurate fading channel model, to combat fading, due to the terrain over large distances with higher SNR. An optimum channel model will require a more detailed analysis to be able to propose a system that actually provides additional improvement.

The channel model considered here combines DOA information with Nakagami fading m to provide values of the channel fading parameter μ, for both LOS and NLOS. The proposed channel model provides a simple solution to be able to predict the effect of real life channels with sufficient accuracy. This was achieved by introducing two *fading* distributions as discussed in Chapter 4 [26]. The two fading distribution models are *the Exponential fading distribution* used to model typical urban (LOS) and macro-cell, and *the Gaussian fading distribution* for bad urban scenario (NLOS).

6.2.3 Diversity Combining

In telecommunication systems particularly in mobile communication, antenna types, antenna size, antenna geometry etc. have been used to achieve considerable gains. This has received considerable attention in the literature. After successful deployment of diversity combining at the antenna in GSM networks, an effective improvement of 3 dB was obtained. This brought about the need to develop simple, robust and efficient antenna systems to cater for the needs of the third generation of mobile communications. Smart antenna concept offers a simple, accurate and efficient solution to meet the requirements of the third generation UMTS systems. Diversity combining is one of the main components of smart antenna techniques as shown in Figure 2.1.

In the development of the system model in this report we looked at diversity combining in detail, as discussed in Appendix A-2, to be able to propose a combining method that offers the best result. The proposed model is based on the correlation coefficient among the received signals at the diversity antenna. The model also exploits the possibility of extra gain obtained by incorporating negatively correlated signals received at the antenna. Although negatively correlated signals are not highly likely but signals with negative

correlation have been reported in the literature [44], an attempt is made in this dissertation to use this information to improve the overall system gain at no extra cost.

A maximal ratio combiner is chosen for the system model, as this method of combining signals, received at a diversity antenna, has been shown in the literature to offer the best gain. The MR combiner considered here defined by (5.42) combines the *Channel fading parameter* μ values calculated in Chapter 4 with negatively correlated signals as shown in Chapter 5. A slight improvement in the probability of receiving signals with negative correlation coefficient was noticed, and was demonstrated in Figure 5.3, by plotting the pdf calculated in (5.42).

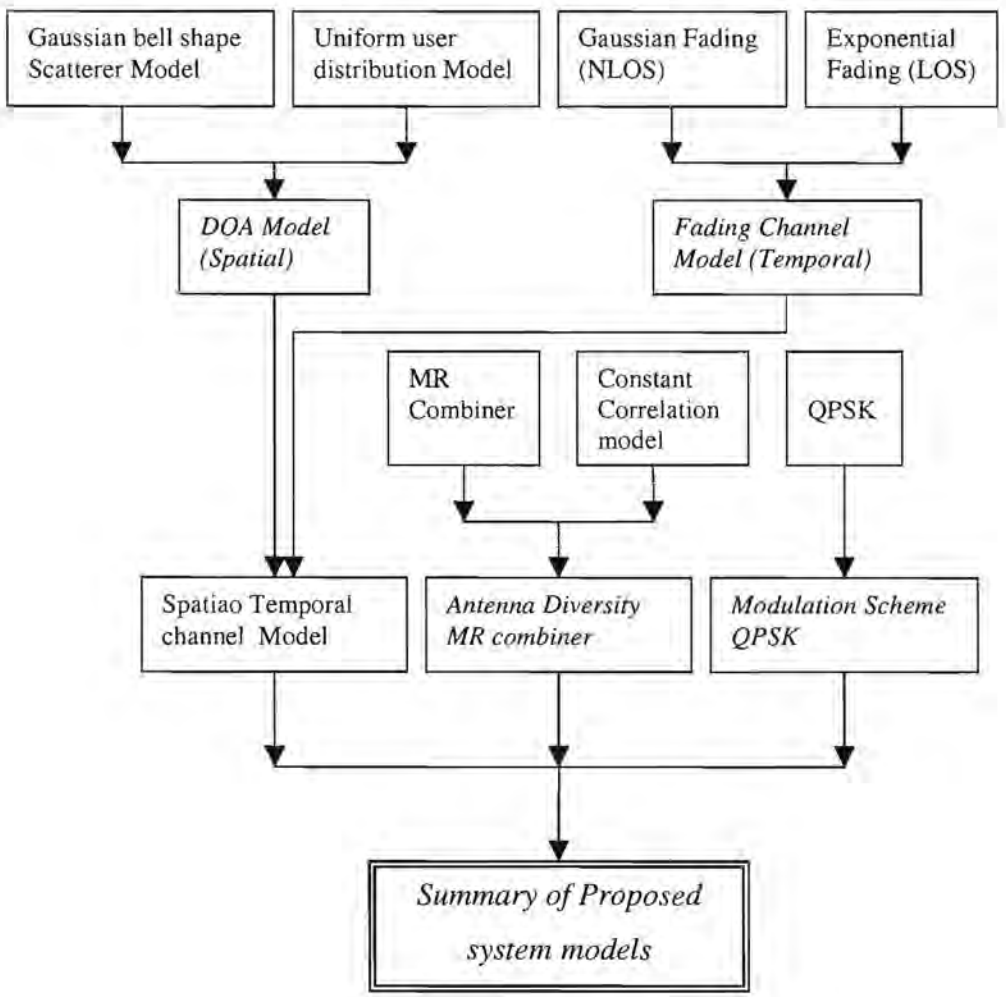

Figure 6.2: Summary of proposed system model.

6.3 System Model Analysis

The proposed system model, as discussed in the previous Chapters, can be effectively divided into four parts, namely the DOA model, the fading channel model, the diversity combiner and the modulator as shown in Figure 6.2. The DOA model is made up of two models, namely the scatterer model and the user distribution model. The fading channel model is also made up of two models, viz. the Gaussian fading model for NLOS signals and the Exponential-fading model for LOS signals.

Table 6. 1: Summary of proposed system parameters.

Model		Parameter	Value
DOA (Scattering + user distribution)	LOS	θ	126^0
	NLOS	θ	200^0
Channel	Gaussian (NLOS)	μ	0.6
	Exponential (LOS)	μ	3.8
Antenna Diversity	MRC	M	3
	Constant Correlation	ρ	0.1, -0.1, - 0.4
Modulation: NCFSK, DCPSK, CFSK & CPSK		BER & Probability of Outage (Calculated in Chapter 7)	

A system base was established in Chapter 2, and subsequently the system models are chosen, modified and calculated in Chapter 3, 4 and 5 for the unique scenario considered here. Table 6.1 summarises the main system parameters and their values. As can be seen, these values represent just one scenario. However the proposed model is very general and can be used for the entire range of values.

The DOA model calculated in Equation (3.9) is obtained by convolving the scatterer model Equation (3.4) and the user model Equation (3.1). The distribution of DOA of signals around the base station is 126^0 for LOS and 200^0 for NLOS as shown in Table 6.1. The angular distribution of the DOA of signal can easily be customised to suit individual scenarios by properly choosing the value of N_{peak} in Equation (3.1). $N_{peak} = 0$ denotes a uniform user distribution, $N_{peak} = 2$ denotes a straight road with base station on the side of the road, $N_{peak} = 4$ denotes a crossing and $N_{peak} = 6$ will denote a circle with six intersections in the heart of the city. The bell shaped Gaussian distribution model chosen in the DOA model best describes the scattering scenario, as it assumes that the density of scattering elements reduces as you go away from the centre of the bell.

The second part of the system model, the fading model, is an important part of the system as this model combines the DOA information with the fading to give the channel parameter. Two fading models are considered here as shown in Figure 6.2, to model the complete range of signals, both LOS and NLOS. The Exponential fading distribution (EFD) given in Equation (4.3) is used to model the typical urban LOS condition with the assumption that the LOS signals received exhibit less fading compared to the signals with DOA component. The Gaussian fading distribution (GFD) given in Equation (4.4) is used to model the bad urban LOS condition with the fading effect becoming increasingly severe for signals with no DOA information. In effect the two fading models considered are used to reduce the effect of fading in both LOS and NLOS conditions by exploiting the DOA information contained in the received signal. The fading parameter μ as seen in Equations (4.3) & (4.4) depends on the DOA information and also on the number of multipaths considered in the design of the model. In our system model three multipath echoes are considered.

The third system model is the antenna diversity. A Maximal Ratio Combiner is used to further improve the system performance. An MRC with constant correlation model for three-element circular symmetric antenna is calculated in Equation (5.18). The combiner is extended for negatively correlated signals in (5.42) with condition (5.34) and restriction (5.40). The extension of the MR combiner in (5.18) to incorporate negatively correlated signals that result in significant system performance gains. The combiner considered offers an improvement in the probability of received signals as can be seen in Figures 5.5, 5.6, and 5.7.

Table 6. 2: Main system model parameter and values.

Parameter	Symbol	LOS Value	NLOS Value
DOA	θ	126^0	200^0
Fading parameter	μ	3.8	0.6
Correlation Coefficient	ρ	0.1,-0.1,- 0.4	0.1,-0.1,- 0.4
Number of MRC branches	M	3	3
Antenna geometry	-	Circular	Circular

Chosen system parameters and their values are summarised in Table 6.2. These values are used to plot the output of the proposed system as shown in Figure 6.3. In Figure 4.4 it can be seen that the fading parameter stays between 5.8 and 2.5 for LOS, and between 1 and 0.5 for NLOS. The MRC proposed in the system model is based on constant correlation model, however another correlation model described in [36], namely the exponential correlation model, can also be used.

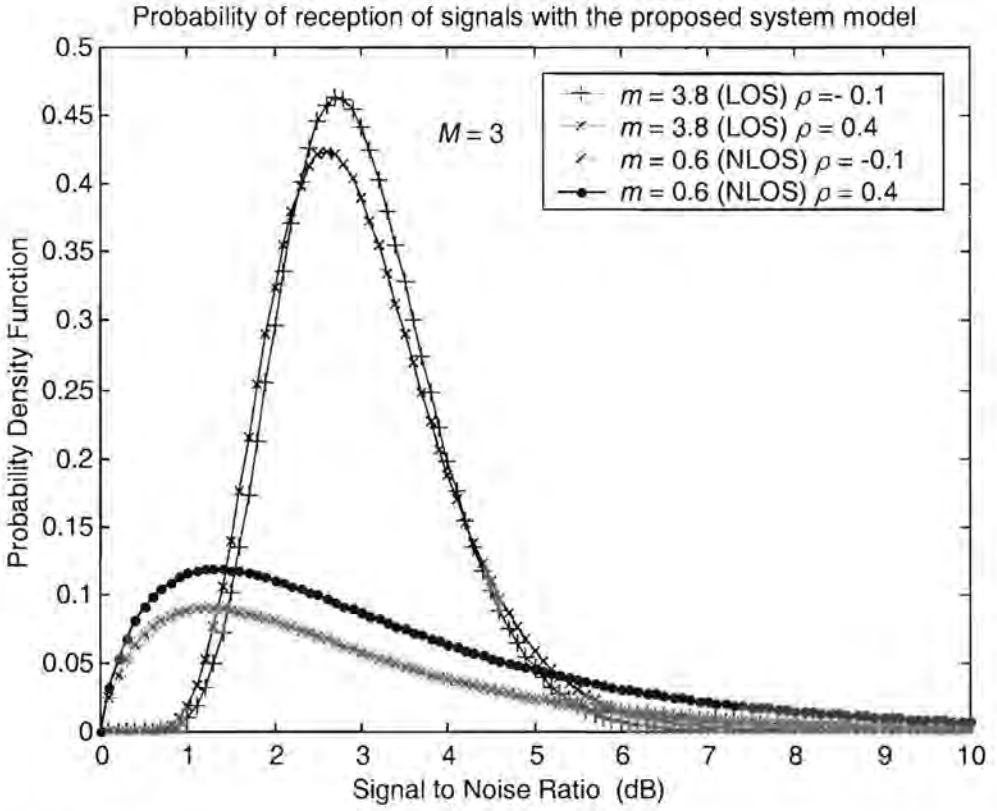

Figure 6.3: Probability density function of received signals in LOS and NLOS for the proposed system model.

In Figure 6.3 we see that the probability of receiving signals with a LOS component is higher than the NLOS and also that the negatively correlated signals have higher probability than signals with correlation coefficient $\rho > 0$. The peak of the probability density function graph for the LOS and NLOS cases are obtained at different SNR. We notice that the range of the signal power covered in the two cases is different with NLOS having low probability covering a wider range of signal power and LOS signals with higher probability spread over lower range of signal power as seen in Figure 6.3.

The last part of the system model is the modulation scheme. Modulation techniques are described in detail in Chapter 2. The proposed model is simulated in Chapter 7 to compare the performance of different modulation schemes, namely non-coherent frequency shift keying (NCFSK), differentially coherent frequency shift keying (DCFSK), coherent frequency shift keying (CFSK), and coherent phase shift keying. Our interest will be focused on the BPSK and QPSK modulation schemes, the difference between the two being that for the same bandwidth QPSK transmits double the amount of data than BPSK. Thus QPSK with double the throughput of BPSK is the preferred modulation scheme.

6.4 Conclusion

This Chapter provided a detailed description and analysis of the proposed system model. A pdf was generated and plotted in Figure 6.3 to summarise the output of the system model. A system of this nature has a definite potential for improvement due to a number of reasons, which have been identified in Chapter 8. The bit error rate performance of the system model is analysed in Chapter 7, where we can see the overall improvement in system performance due to negatively correlated signals.

Chapter 7

SYSTEM PERFORMANCE EVALUATION

7.1 Introduction

The system model developed in the previous Chapters is evaluated in this Chapter and the results obtained are analysed. Two evaluation methods, namely the BER and the probability of outage, which have been already discussed in Chapter 2, will be used to evaluate the system performance.

7.2 BER Performance

The probability of bit error for coherent and noncoherent frequency shift keying (FSK) and phase shift keying (PSK) systems with optimum matched filter receiver are considered here. The respective probabilities of error, P_e is given as [36]:

$$P_e(\gamma) = \frac{1}{2}exp(-\alpha\gamma), \begin{cases} \alpha = \frac{1}{2} & for \quad NCFSK \\ \alpha = 1 & for \quad DCPSK \end{cases} \qquad (7.1)$$

and

$$P_e(\gamma) = Q(\sqrt{2\alpha\gamma}), \begin{cases} \alpha = \frac{1}{2} & for \quad CFSK \\ \alpha = 1 & for \quad CPSK \end{cases} \qquad (7.2)$$

Q in (7.2) is the Q function defined in Appendix (C-1).

The average bit error rate is obtained by averaging the probability of error $P_e(\gamma)$ over the distribution of the SNR .

$$\overline{P_e} = \int_0^\infty P_e(\gamma)P(\gamma)d\gamma \qquad (7.3)$$

Two correlation models have been discussed in Chapter 5 that can be used to calculate the correlation coefficient ρ. Correlation coefficient is an important parameter that provides information about the relationship between replicas of the main signal arriving at the receiver, as a result of multipath. Our analysis will be restricted to the *constant correlation* model only. However the exponential model can be easily integrated into the proposed system model.

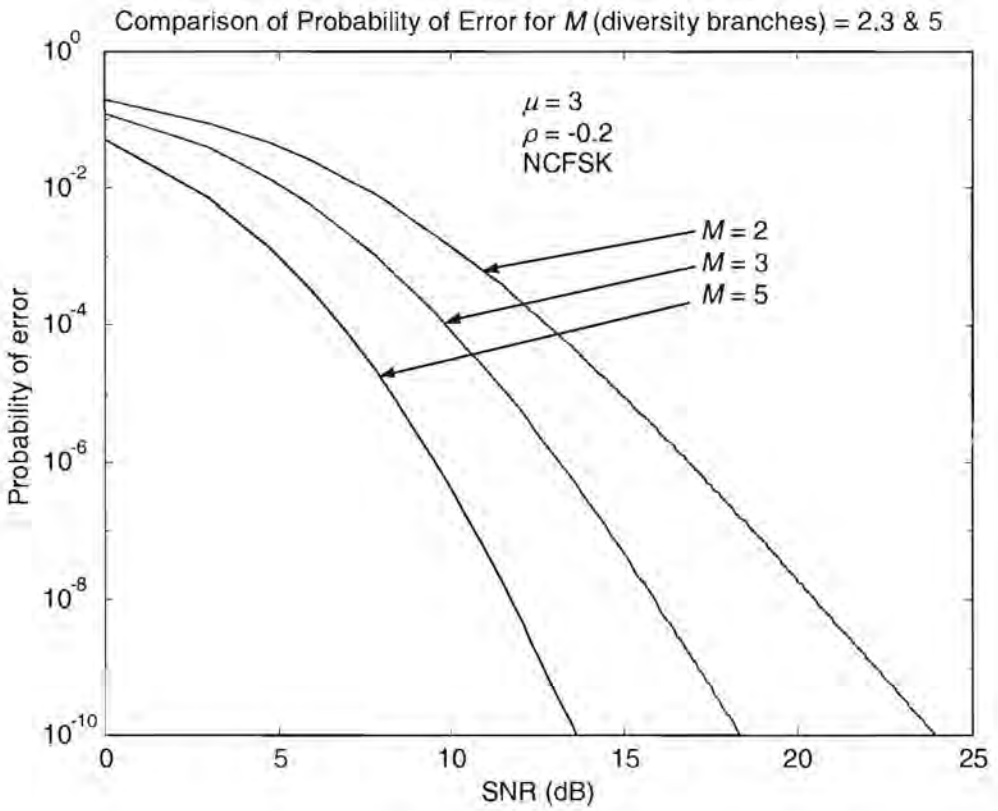

Figure 7.1: Probability of Error plot for NCFSK , for M = 2, 3 & 5.

Figures 7.1, 7.2, 7.3 and 7.4 show probability of error for NCFSK, DCPSK, CPSK and CFSK respectively, for M = 2, 3, 5. We notice that as M increases from 2 to 5, the system performance improves with CPSK being the best modulation scheme.

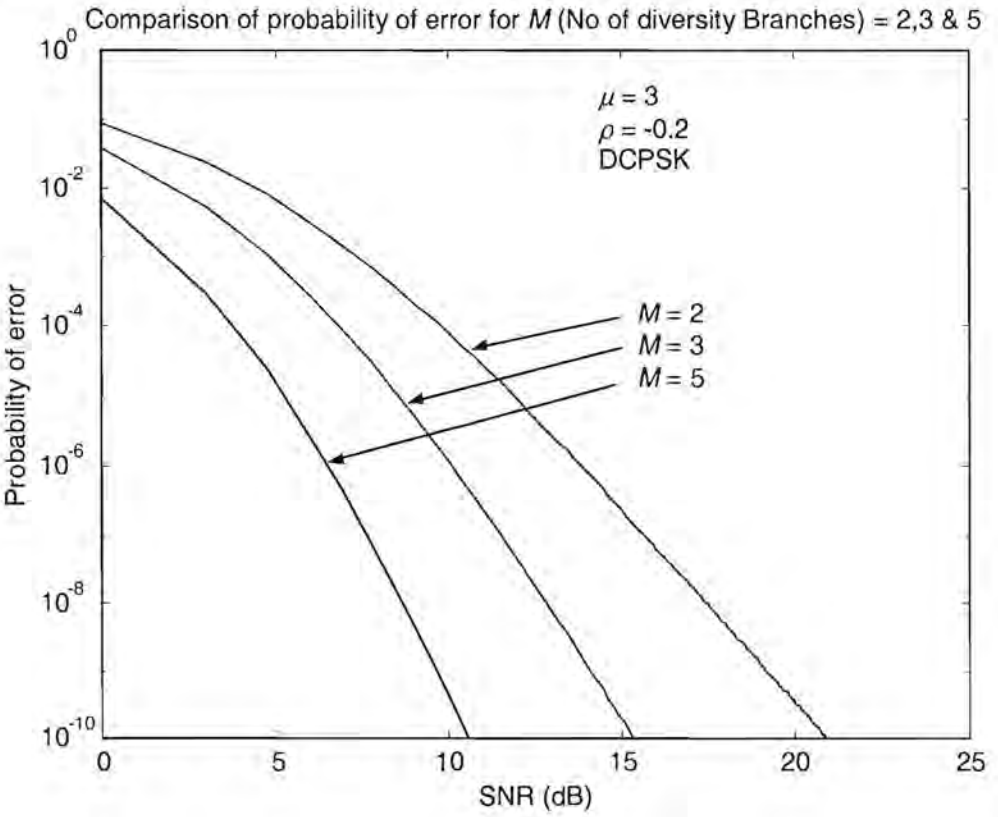

Figure 7.2: Probability of Error plot for DCPSK, for $M = 2, 3 \& 5$.

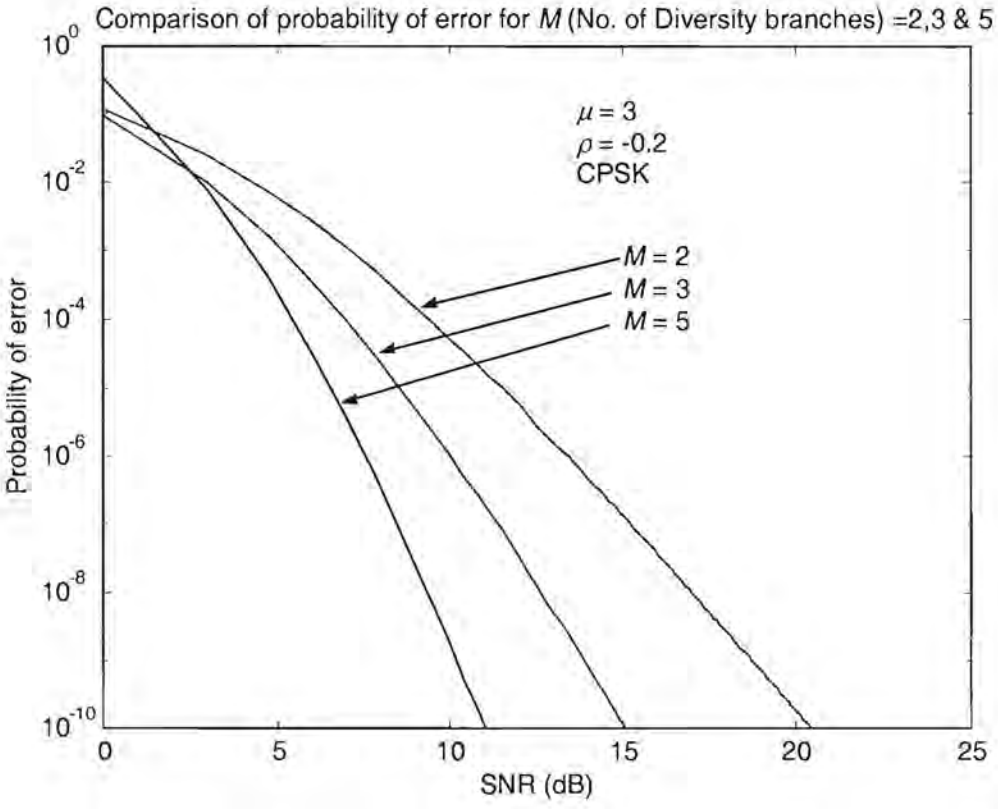

Figure 7.3: Probability of Error plot for CPSK, for $M = 2, 3 \& 5$.

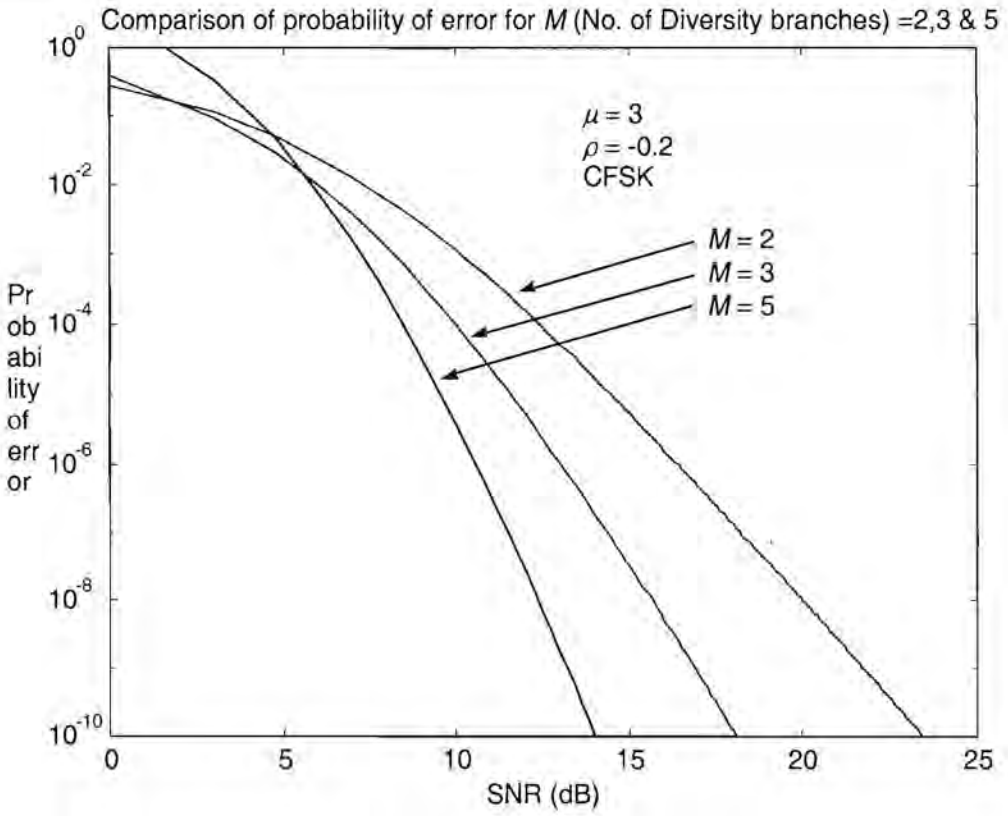

Figure 7.4: Probability of Error plot for CFSK, for $M = 2, 3 \& 5$.

7.2.1 BER Performance for (NCFSK and DCPSK)

The average bit error rate for noncoherent or differentially coherent (NCFSK or DCPSK) detection is calculated by substituting (5.18) and (7.1) in (7.3), which yields (7.4):

$$\overline{P}_{eN} = \int_0^\infty \frac{\frac{1}{2} e^{-\alpha\gamma} \gamma^{Mm-1} \exp\left(\frac{-\gamma m}{\overline{\Omega}(1-\rho)}\right) {}_1F_1\left(m, Mm; \frac{Mm\rho\gamma}{\overline{\Omega}(1-\rho)(1-\rho+M\rho)}\right)}{\left(\frac{\overline{\Omega}}{m}\right)^{Mm} (1-\rho)^{m(M-1)}(1-\rho+M\rho)^m \Gamma(Mm)} d\gamma \qquad (7.4)$$

Equation (7.4) can be simplified using (E-6) to give

$$\overline{P}_{eN} = \frac{{}_2F_1\left(m, Mm; Mm; \frac{Mm\rho}{\overline{\Omega}(1-\rho)(1-\rho+M\rho)\left(\alpha + \frac{m}{s(1-\rho)}\right)}\right)}{2\left[\frac{\overline{\Omega}\alpha}{m} + \frac{1}{1-\rho}\right]^{Mm} (1-\rho)^{m(M-1)}(1-\rho+M\rho)^m} \qquad (7.5)$$

where ${}_2F_1$ () is the Gaussian hypergeometric function whose series representation is given in (E-3). Equation (7.5) can be further simplified using (E-5) to give (7.6).

$$\overline{P}_{eN} = \frac{1}{2}\left(\frac{m^M}{\left[\overline{\Omega}\alpha(1-\rho+M\rho)+m\right]\left[\overline{\Omega}\alpha(1-\rho)+m\right]^{M-1}} \right)^m \quad for \quad \rho \geq 0 \qquad (7.6a)$$

and

$$\overline{P}_{eN} = \frac{1}{2}\left(\frac{m^M}{\left[\overline{\Omega}\alpha(1-\rho+|M\rho|)+m\right]\left[\overline{\Omega}\alpha(1-\rho)+m\right]^{M-1}} \right)^m \quad for \quad \rho < 0 \qquad (7.6b)$$

Equation (7.6) can be solved for the special cases of $\rho = 0$ and $\rho = 1$ and is given by (7.7) and (7.8) respectively.

$$\overline{P}_{eN}|_{\rho=0} = \frac{1}{2}\left(\frac{m}{\overline{\Omega}\alpha+m} \right)^{Mm} \qquad (7.7)$$

and

$$\overline{P}_{eN}|_{\rho=0} = \frac{1}{2}\left(\frac{m}{M\overline{\Omega}\alpha+m} \right)^{m} \qquad (7.8)$$

Equation (7.6) is the final probability of error Equation used for the proposed system model to calculate BER. Equation (7.6) is simulated in accordance with Table 7.1 to plot BER graphs for NCFSK and DCPSK as shown in Figures 7.5 and 7.6.

Table 7.1: Simulation Table of BER for NCFSK and DCPSK.

$M = 3$, $\Omega = 1$ to 1000 w						
Modulation Scheme	$\alpha = ½$ for NCFSK and $\alpha = 1$ for DCPSK					
Fading environment	LOS, $\mu = 3.8$			NLOS, $\mu = 0.6$		
Correlation Coefficient ρ	0.1	-0.1	-0.4	0.1	-0.1	-0.4

We notice that as a general trend LOS signals perform better than NLOS signals, as expected. We also notice that signals with negative correlation coefficient (ρ) have a lower BER value as compared to $\rho = 0$ or $\rho > 0$. Finally, it is also clear from the plot that DCPSK modulation performs better that NCFSK as shown in Figures 7.5 and 7.6.

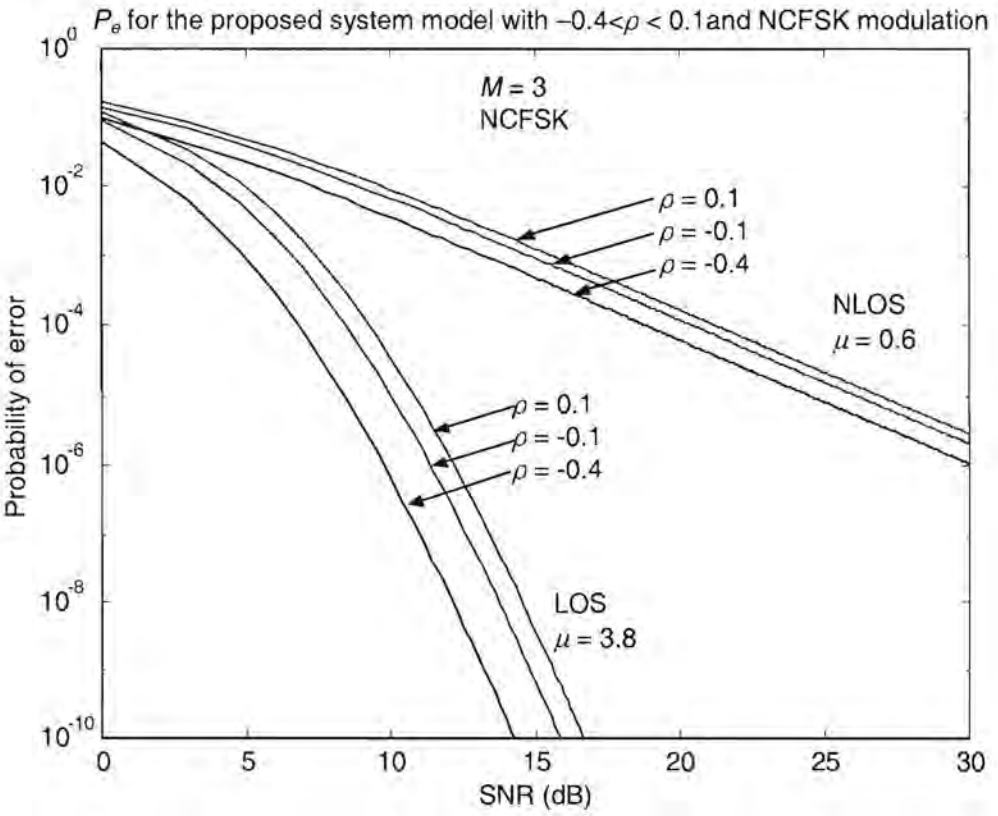

Figure 7.5: Probability of error for the proposed system model with negative ρ, LOS & NLOS, and NCFSK modulation.

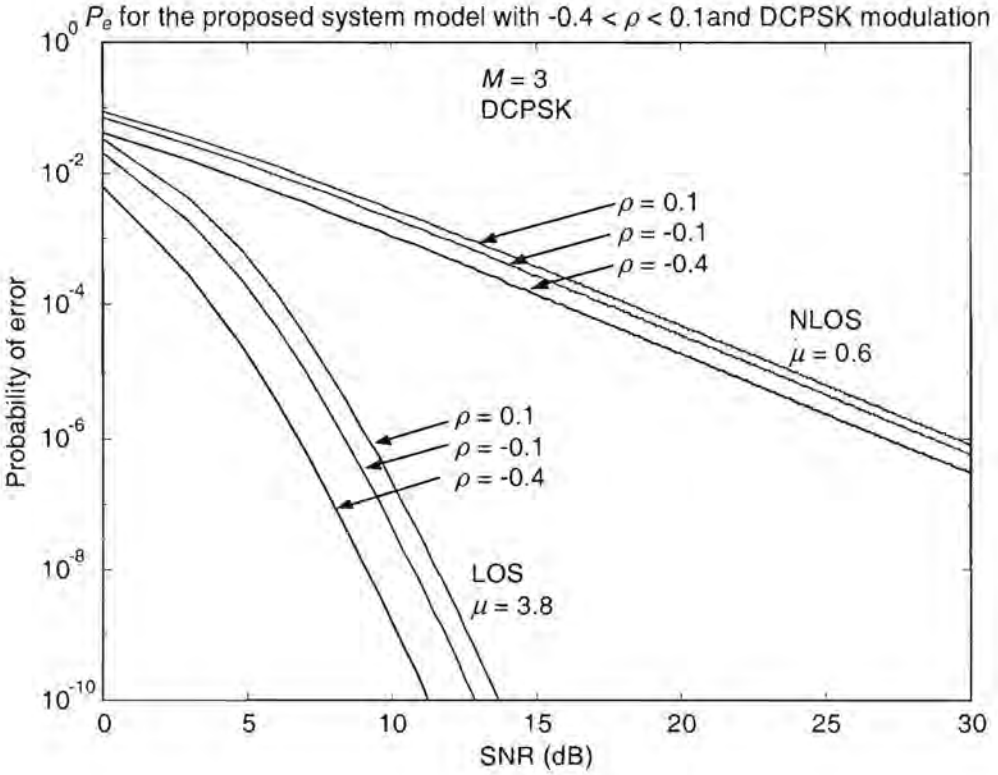

Figure 7.6: Probability of error for the proposed system model with negative ρ, LOS & NLOS, and DCPSK modulation.

7.2.2 BER Performance for (CFSK and CPSK)

The average bit error rate for coherent coherent CFSK or CPSK detection is calculated by substituting (5.18) and (7.2) in (7.3), which gives (7.9)

$$\overline{P}_{eC} = \int_0^\infty \frac{Q(\sqrt{2\alpha\gamma})\gamma^{Mm-1}\exp\left(\frac{-\gamma m}{\overline{\Omega}(1-\rho)}\right) {}_1F_1\left(m, Mm; \frac{Mm\rho\gamma}{\overline{\Omega}(1-\rho)(1-\rho+M\rho)}\right)}{\left(\frac{\overline{\Omega}}{m}\right)^{Mm}(1-\rho)^{m(M-1)}(1-\rho+M\rho)^m\Gamma(Mm)}d\gamma \tag{7.9}$$

For $\rho = 0$, (E-6) and (E-7) is used in (7.29) to obtain

$$\overline{P}_{eC}|_{\rho=0} = \frac{\Gamma(2Mm)}{\Gamma(Mm)\Gamma(Mm+1)}\left(\frac{m/4}{m+\overline{\Omega}\alpha}\right)^{Mm}\left(\frac{\overline{\Omega}\alpha}{m+\overline{\Omega}\alpha}\right)^{1/2} \cdot {}_2F_1\left(1, Mm+\frac{1}{2}; Mm+1; \frac{m}{m+\overline{\Omega}\alpha}\right) \tag{7.10}$$

For $\rho > 0$, (7.9) can be rewritten using (E-8) as (7.11)

$$\overline{P}_{eC} = \left(\int_0^\infty \frac{\gamma^{Mm-1}\exp\left(\frac{-m\gamma}{\overline{\Omega}(1-\rho)}\right) \cdot {}_1F_1\left(m; Mm; \frac{Mm\rho\gamma}{\overline{\Omega}(1-\rho)(1-\rho+M\rho)}\right)}{2\left(\frac{\overline{\Omega}}{m}\right)^{Mm}(1-\rho)^{m(M-1)}(1-\rho+M\rho)^m\Gamma(Mm)}d\gamma\right) \cdot \left(\gamma^{Mm-\frac{1}{2}}\exp\left[-\left(\alpha+\frac{m}{\overline{\Omega}(1-\rho)}\right)\gamma\right] \cdot {}_1F_1\left(1; \frac{3}{2}; -\alpha\gamma\right) \cdot {}_1F_1\left(m; Mm; \frac{Mm\rho\gamma}{\overline{\Omega}(1-\rho)(1-\rho+M\rho)}\right)\right) - \sqrt{\frac{\alpha}{\pi}}\int_0^\infty \frac{}{\left(\frac{\overline{\Omega}}{m}\right)^{Mm}(1-\rho)^{m(M-1)}(1-\rho+M\rho)^m\Gamma(Mm)}d\gamma \tag{7.11}$$

The first integral in (7.11) can be shown to be equal to ½ [36], while the second integral, after a change in variable, can be written in terms of Appell's hypergeometric function F_2 () [36] given in (E-13). Using (E-12) and after further simplification, the bit error rate of CFSK and CPSK is given by (7.12)

$$\overline{P}_{eC} = \frac{1}{2} - \sqrt{\frac{\alpha}{\pi}} \frac{\Gamma\left(Mm + \frac{1}{2}\right)}{\Gamma(Mm)} \left(\frac{\overline{\Omega}(1-\rho)}{\overline{\Omega}\alpha(1-\rho)+m}\right)^{1/2} \left[\left(\frac{m}{\overline{\Omega}\alpha(1-\rho)+m}\right)^{M} \left(\frac{1-\rho}{1-\rho+|M\rho|}\right)\right]^{m}$$
$$\cdot F_2\left(Mm + \frac{1}{2}; 1, m; \frac{3}{2}, Mm; \frac{-\overline{\Omega}\alpha(1-\rho)}{\overline{\Omega}\alpha(1-\rho)+m}\right) \left(\frac{Mm\rho}{\left[\overline{\Omega}\alpha(1-\rho)+m\right]\left[1-\rho+M\rho\right]}\right) \quad (7.12)$$

Table 7.2: Simulation Table of BER for CFSK and CPSK.

$M = 3$, $\Omega = 1$ to 1000 w						
Modulation Scheme	$\alpha = ½$ for CFSK and $\alpha = 1$ for CPSK					
Fading environment	LOS, $\mu = 3.8$			NLOS, $\mu = 0.6$		
Correlation Coefficient ρ	0.1	-0.1	-0.4	0.1	-0.1	-0.4

Equation (7.12) is used in accordance with Table 7.2 to plot BER graphs for CFSK and CPSK modulation schemes as shown in Figures 7.7 and 7.8. It is clear from the plots in Figures 7.7 and 7.8 that CPSK out performs CFSK in both LOS and NLOS conditions. Figure 7.9 is a comparison between all the modulation schemes considered and again CPSK is shown to perform better than all other modulation schemes considered.

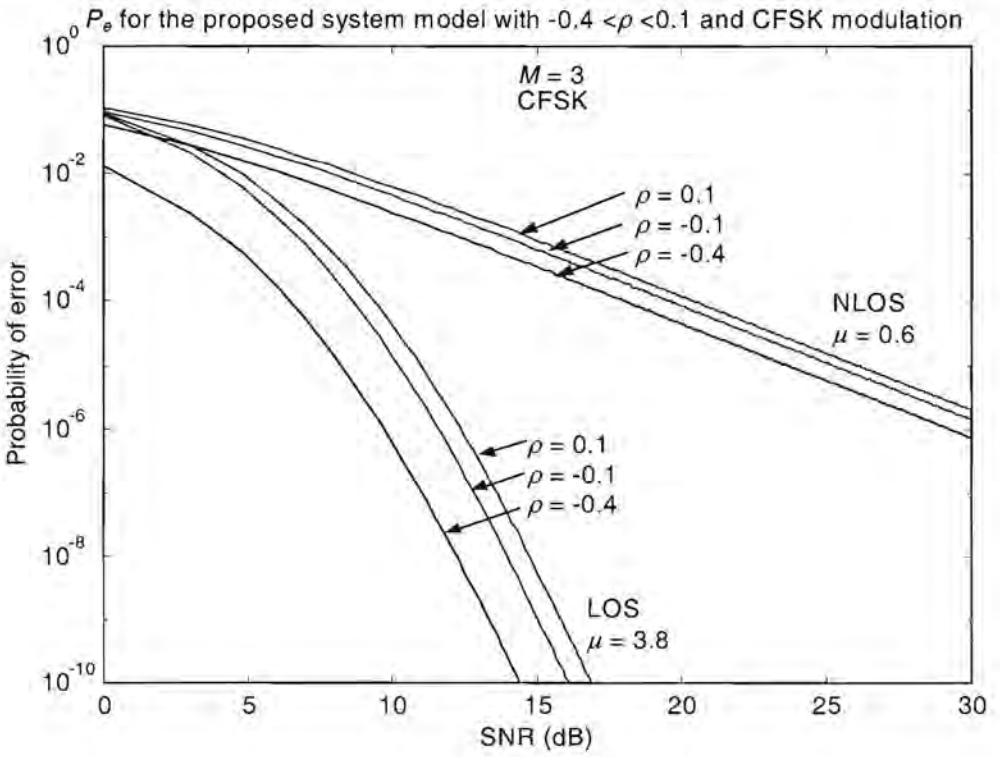

Figure 7.7: Probability of error for the proposed system model with negative ρ, LOS & NLOS, and CFSK modulation.

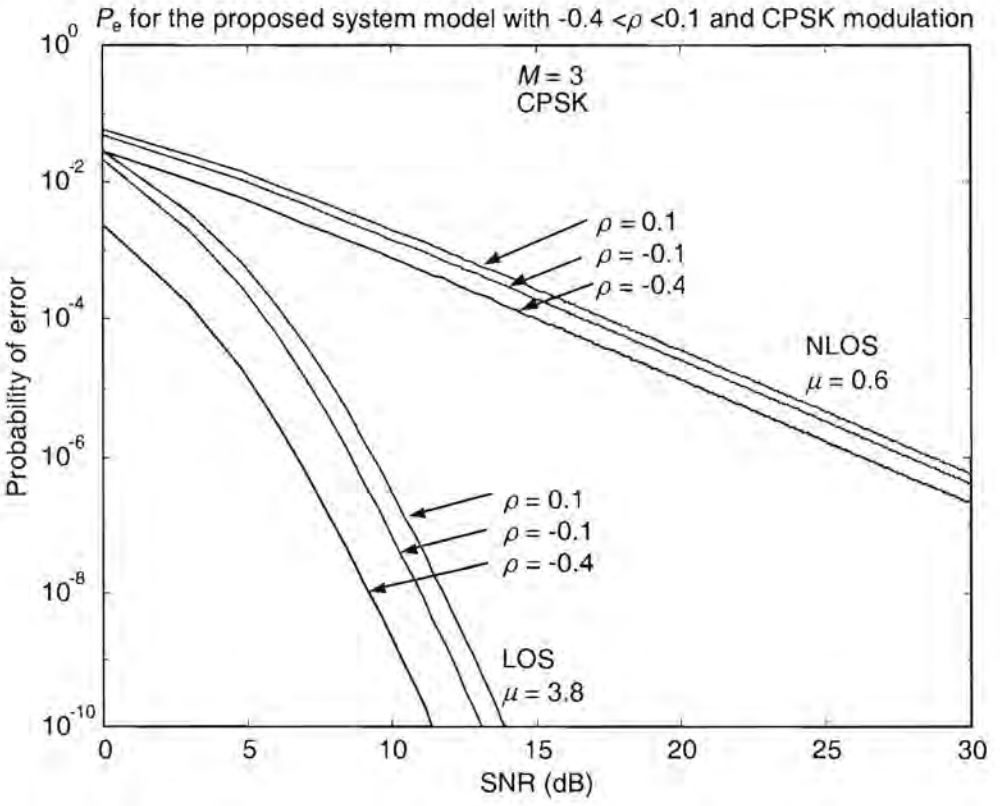

Figure 7 8: Probability of error for the proposed system model with negative ρ, LOS & NLOS, and CPSK modulation

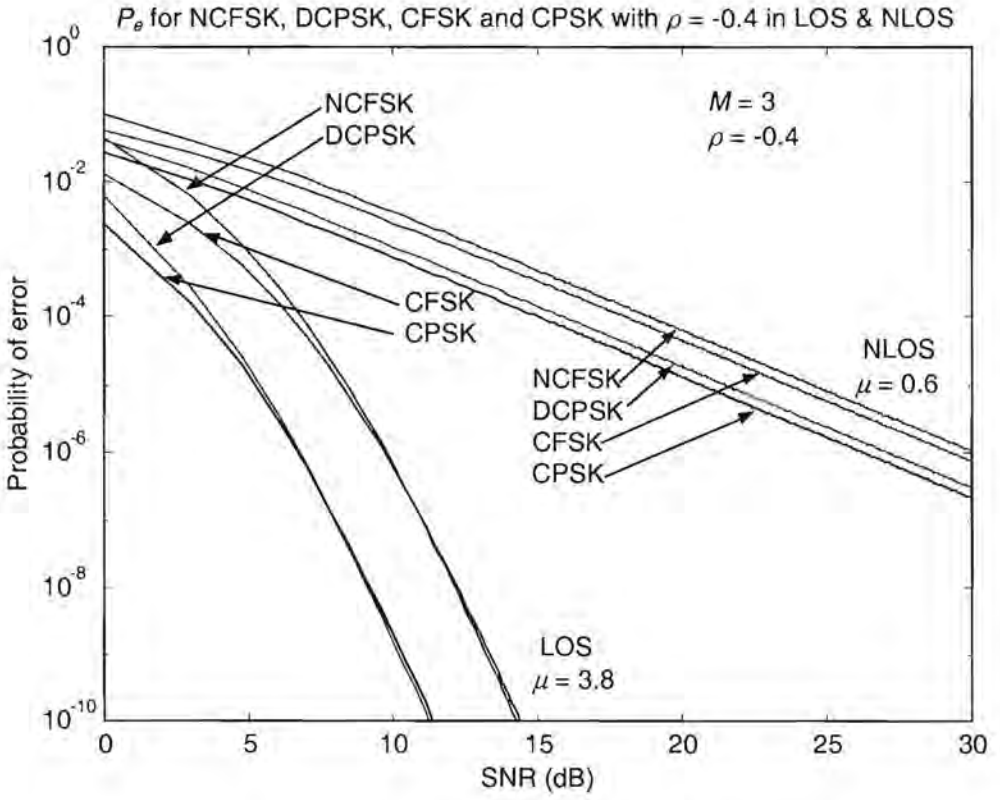

Figure 7.9: Comparison of probability of error for NCFSK, DCPSK, CFSK & CPSK with ρ = -0.4 in LOS & NLOS.

7.3 Probability of Outage

The proposed system model is also evaluated for its *Probability of Outage*, another criteria to be able to predict the performance of any given system. Probability of outage P_o is the probability that the instantaneous bit error probability of the system exceeds a specified value P^*_e and is given by (7.13) [36].

$$P_o = \int_0^{\gamma^*} P_\gamma(\gamma)d\gamma \tag{7.13}$$

where

$$P_e(\gamma^*) = P_e^* \tag{7.14}$$

γ^* in (7.14) is obtained from (7.1) and (7.2) as:

$$\gamma^* = \begin{cases} \frac{1}{\alpha} ln\left(\frac{1}{2P_e^*}\right) & for \begin{cases} NCFSK \\ DCPSK \end{cases} \\ \frac{1}{2\alpha}\left[Q^{-1}(P_e^*)\right]^2 & for \begin{cases} CFSK \\ CPSK \end{cases} \end{cases} \tag{7.15}$$

$Q^{-1}(z)$ in (7.15) is the inverse of $Q(z)$ function defined in appendix C.

Probability of outage P_0 for an equal correlation model is obtained by substituting (5.18) in (7.13) and using (*E-1b*) as described in [36]

$$P_o = A\int_0^{c\gamma^*}\int_0^1 x^{M\mu-1}t^{\mu-1}(1-t)^{\vartheta-1}.exp(-(b-t)x)dtdx \tag{7.16}$$

where

$$A = \frac{1}{\Gamma(\mu)\Gamma(\vartheta)}\left(\frac{1-\rho}{M\rho}\right)^{\mu} b^{\vartheta}, \qquad b = \frac{1-\rho+M\rho}{M\rho};$$

$$c = \frac{\mu}{\Omega b(1-\rho)}, \text{ and} \qquad \vartheta = \mu(M-1).$$

The function under the integral in (7.16) is continuous in both x and t, therefore; the order of integration can be changed and (7.16) can be rewritten as;

$$P_o = A\int_0^1 (b-1)^{-M\mu} t^{\mu-1}(1-t)^{\vartheta-1} \cdot P(M\mu, c(b-1)\gamma^*)dt \qquad (7.17)$$

where

$$P(a,x) = \int_0^x t^{a-1}e^{-t}dt \qquad (7.18)$$

P_o is obtained by numerically evaluating the integral in (7.17) where γ^* is given in (7.15) for the different modulation schemes considered. The fading parameter μ ($\geq$ 1/2) may take on either integer or noninteger values. For integer values of μ, using (*E-9*) – (*E-11*) in (7.17) the outage probability is given by;

$$P_o = A\left\{\Phi_1\left(\mu, M\mu, M\mu, \frac{1}{b}, 0\right) - e^{-b\gamma^*}\sum_{n=0}^{b-1}\frac{[\gamma^*]^n}{n!}\cdot\Phi_1\left(\mu, M\mu - n, M\mu, \frac{1}{b}, c\gamma^*\right)\right\} \qquad (7.19)$$

where Φ_1 ( ) is the generalised hypergeometric function defined in Appendix (*E-11*).

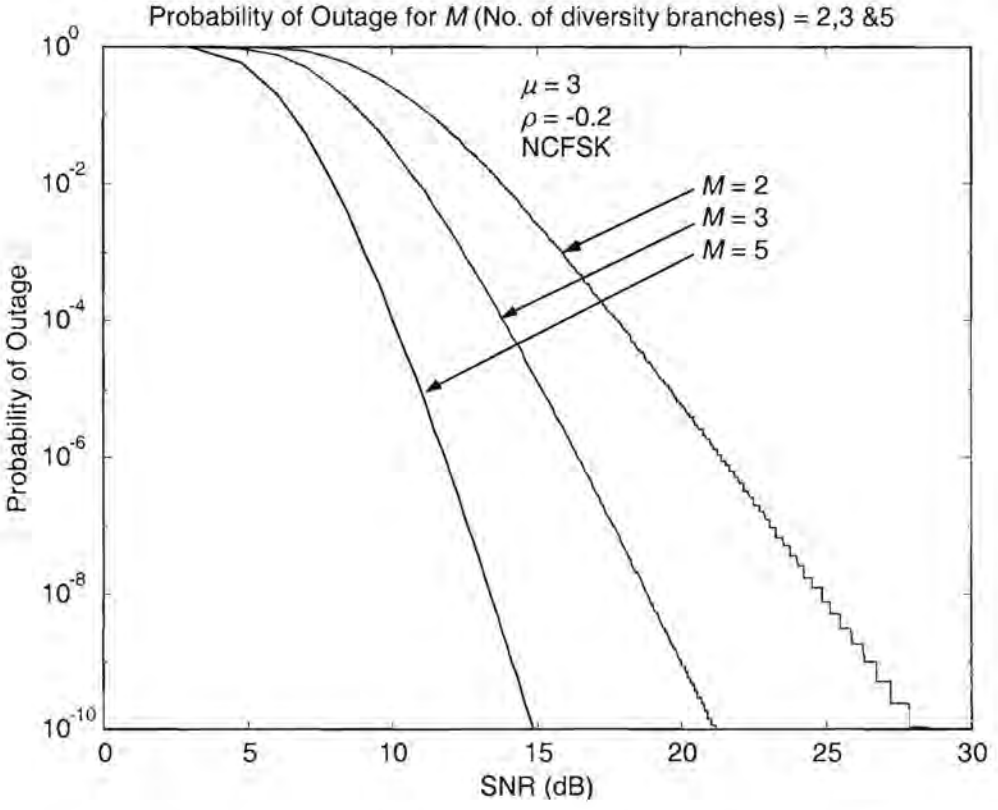

Figure 7.10: Probability of Outage plot for NCFSK with M = 2, 3 & 5

The channel fading parameter μ calculated in Chapter 4 does not always have an integer value. It is therefore more appropriate to use (7.17) to calculate the probability of outage for the proposed system model in our analysis.

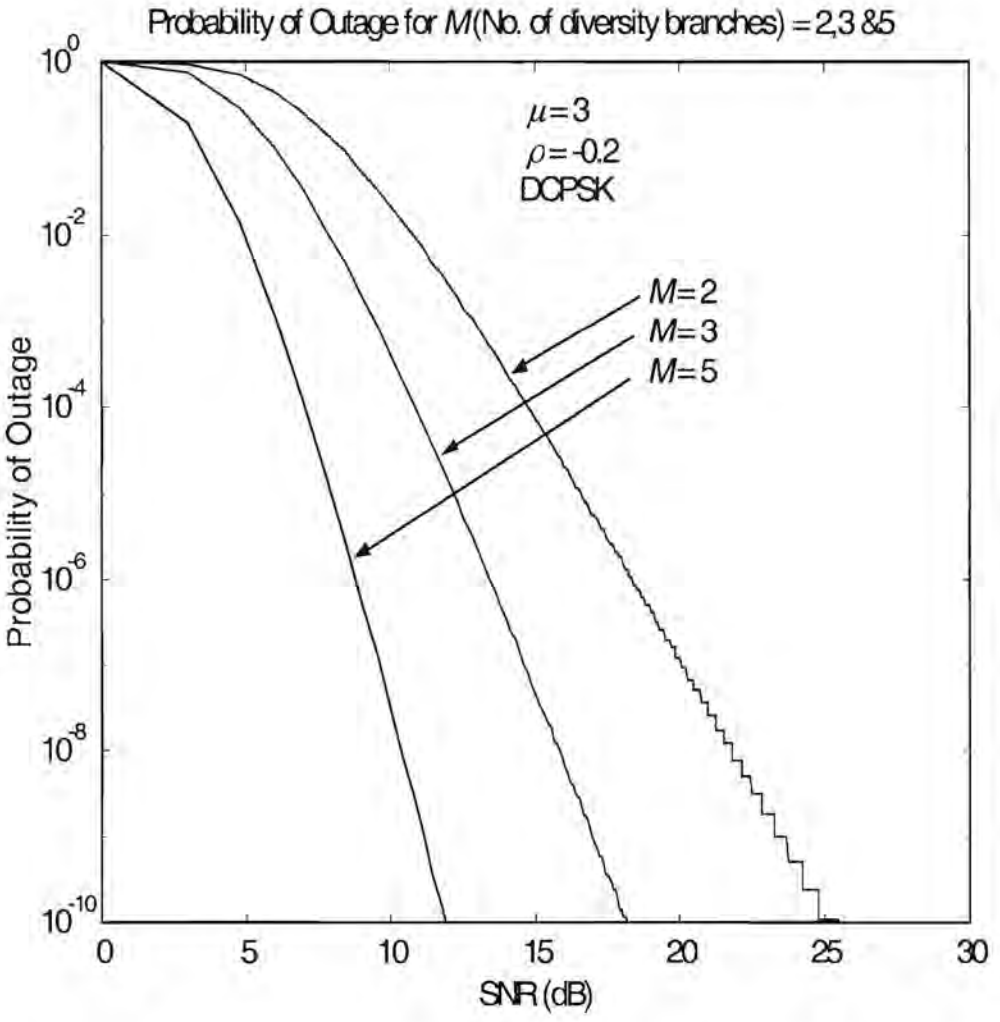

Figure 7.11: Probability of Outage plot for DCPSK with M = 2, 3 & 5

The final expression for *probability of outage* is given by (7.17). Equation (7.17) is valid for all the modulation schemes considered. In (7.17) the value of γ^* which is calculated from (7.15) determines the type of modulation scheme used. Figures 7.10, 7.11, 7.12 and 7.13 show the performance of NCFSK, DCPSK, CFSK and CPSK respectively for different values of M.

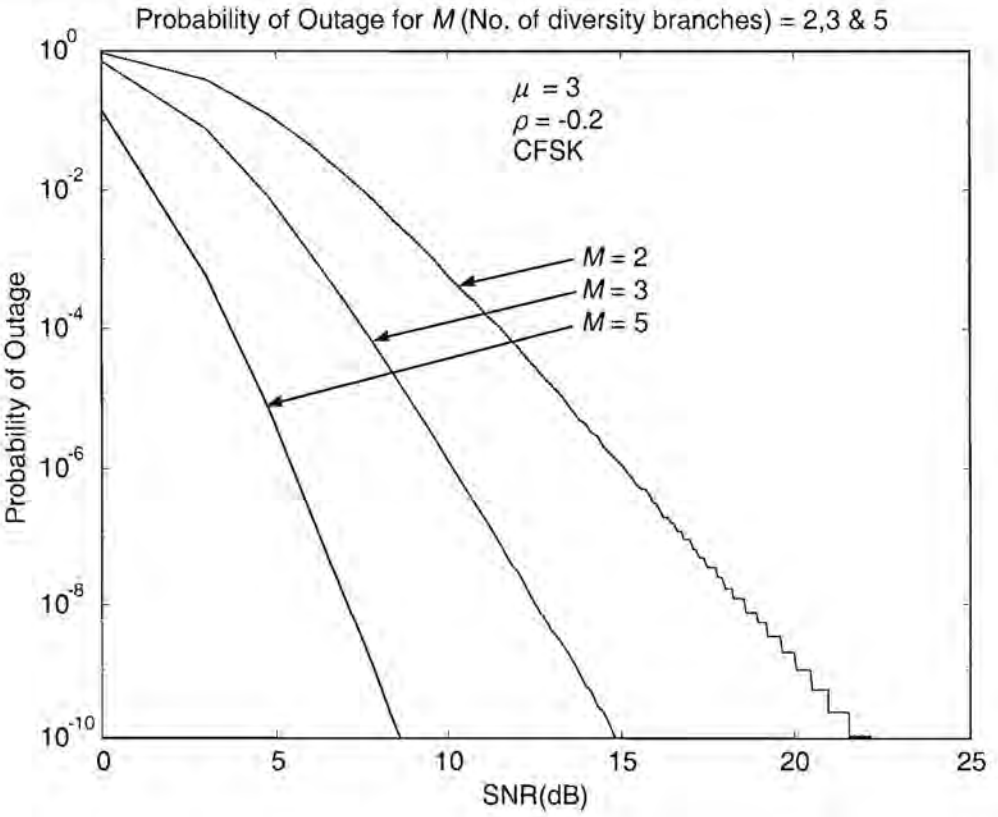

Figure 7.12: Probability of Outage plot for CFSK with $M = 2, 3 \& 5$

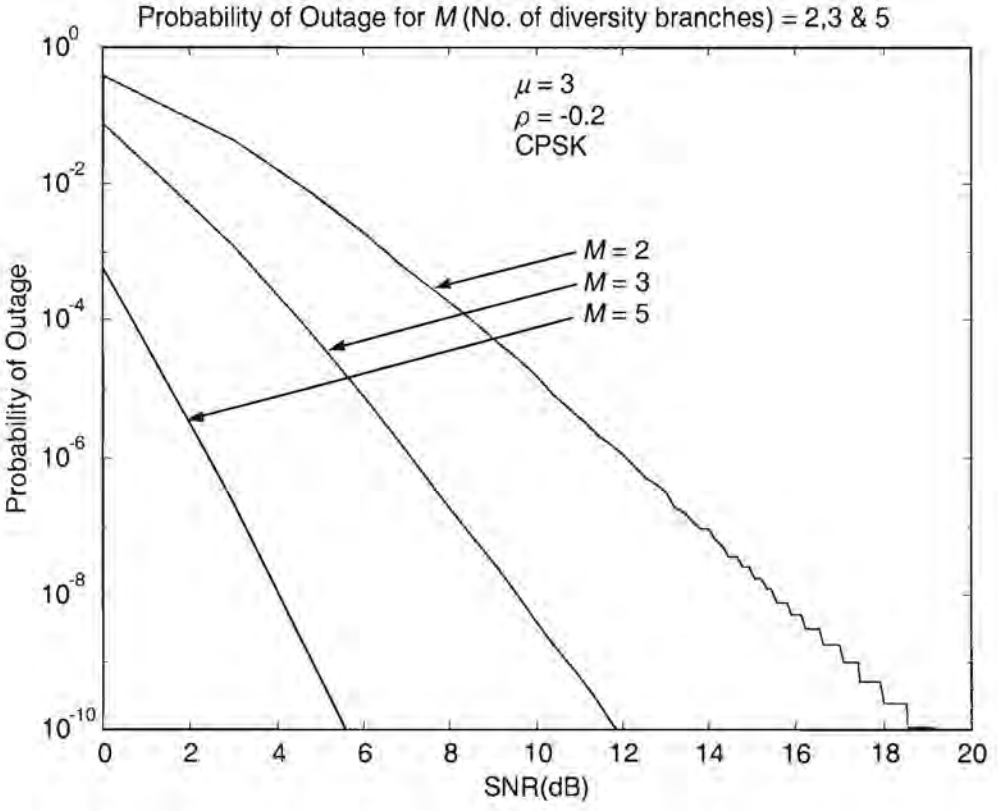

Figure 7.13: Probability of Outage plot for CPSK with M = 2, 3 & 5

Table 7.3: Simulation Table of probability of outage for NCFSK and DCPSK.

$M = 3, \quad \Omega = 1$ to 1000 w, $\gamma^* = \frac{1}{\alpha} ln\left(\frac{1}{2P_e^*}\right)$, $P_e^* = 10^{-4}$						
Modulation Scheme	$\alpha = ½$ for NCFSK and $\alpha = 1$ for DCPSK					
Fading environment	LOS, $\mu = 3.8$			NLOS, $\mu = 0.6$		
Correlation Coefficient ρ	0.1	-0.1	-0.4	0.1	-0.1	-0.4

Tables 7.3 summarise the simulation conditions for NCFSK & DCPSK as shown in Figures 7.14 & 7.15 respectively and Table 7.4 summarises the simulation conditions for CFSK & CPSK as shown in Figures 7.16 & 7.17 respectively.

Table 7.4: Simulation Table of probability of outage for CFSK and CPSK.

$M = 3, \quad \Omega = 1$ to 1000 w, $\gamma^* = \frac{1}{2\alpha}\left[Q^{-1}\left(P_e^*\right)\right]^2$, $P_e^* = 10^{-4}$						
Modulation Scheme	$\alpha = ½$ for CFSK and $\alpha = 1$ for CPSK					
Fading environment	LOS, $\mu = 3.8$			NLOS, $\mu = 0.6$		
Correlation Coefficient ρ	0.1	-0.1	-0.4	0.1	-0.1	-0.4

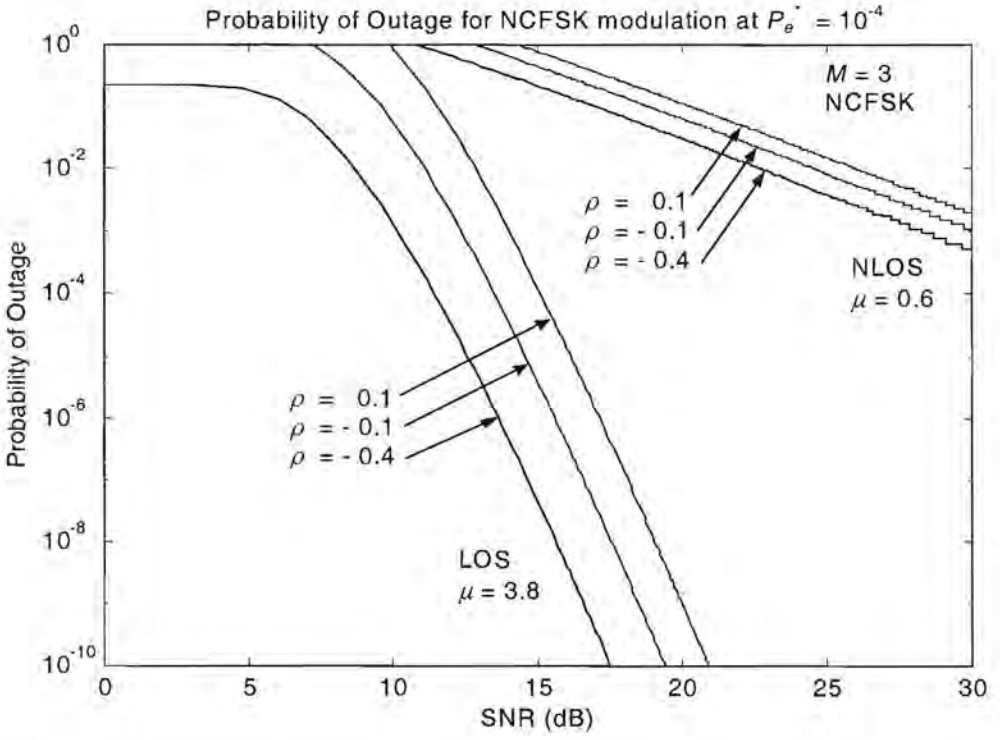

Figure 7.14: Probability of Outage for NCFSK with $P_e^* = 10^{-4}$ and $\rho = 0.1, -0.1, -0.4$.

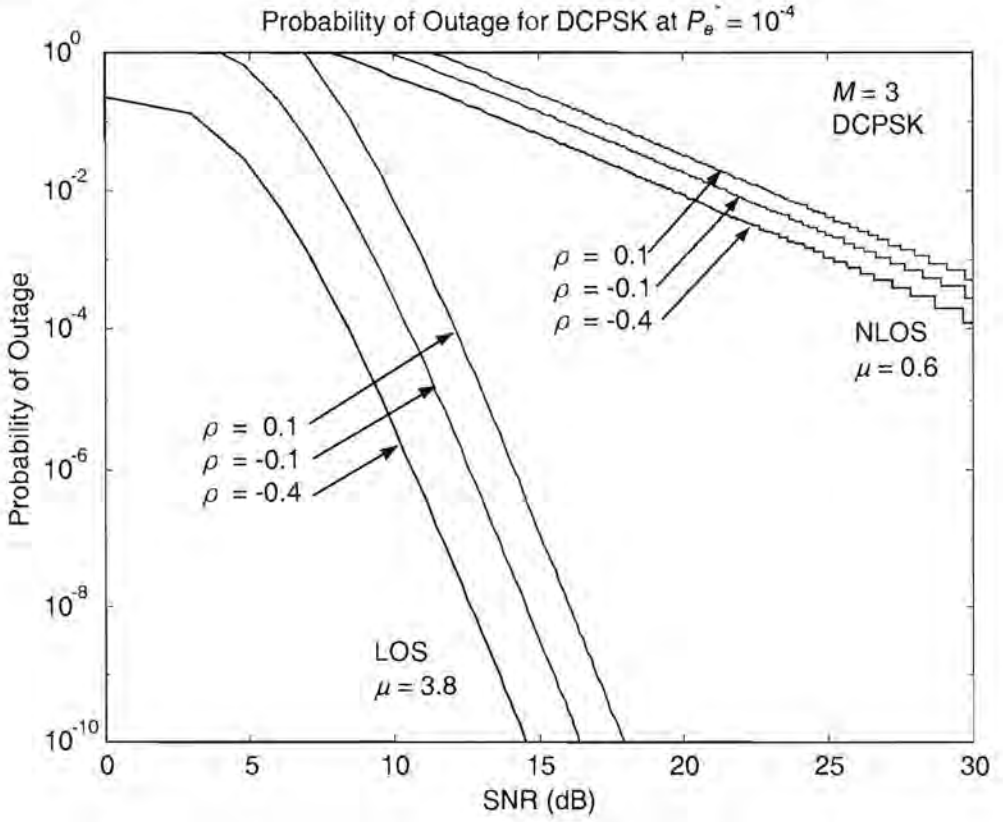

Figure 7.15: Probability of Outage for DCPSK with $P_e^* = 10^{-4}$ and $\rho = 0.1, -0.1, -0.4$

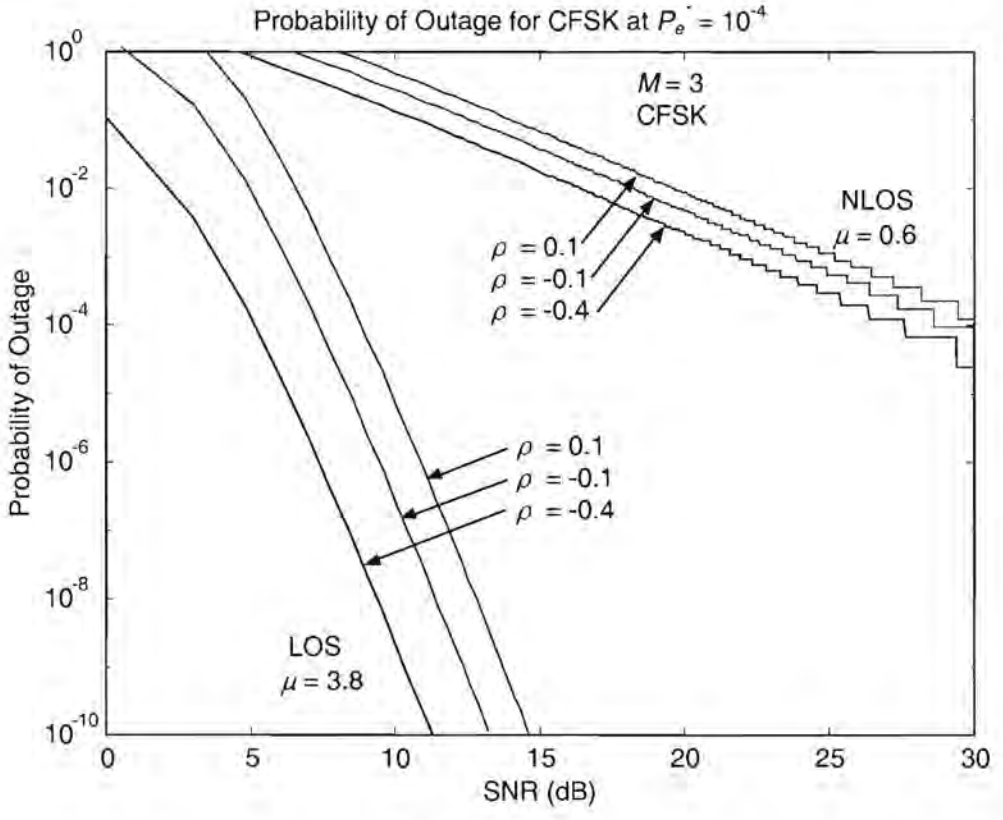

Figure 7.16: Probability of Outage for CFSK with $P_e^* = 10^{-4}$ and $\rho = 0.1, -0.1, -0.4$

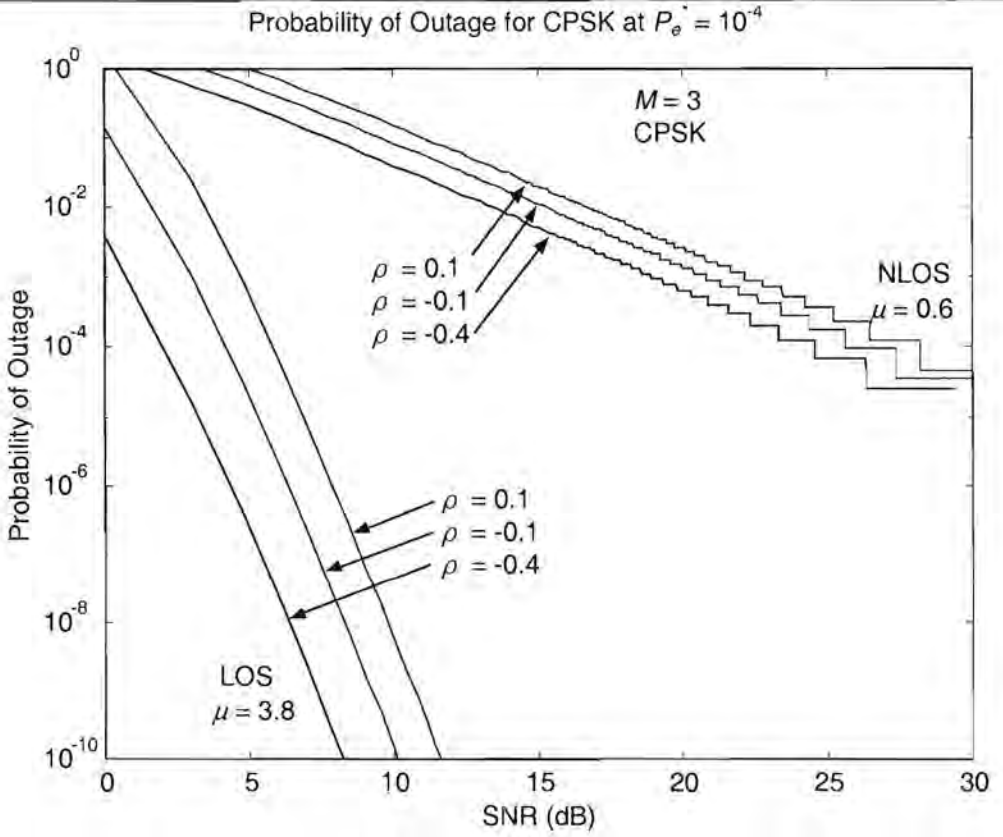

Figure 7.17: Probability of Outage for CPSK with $P_e^* = 10^{-4}$ and $\rho = 0.1, -0.1, -0.4$

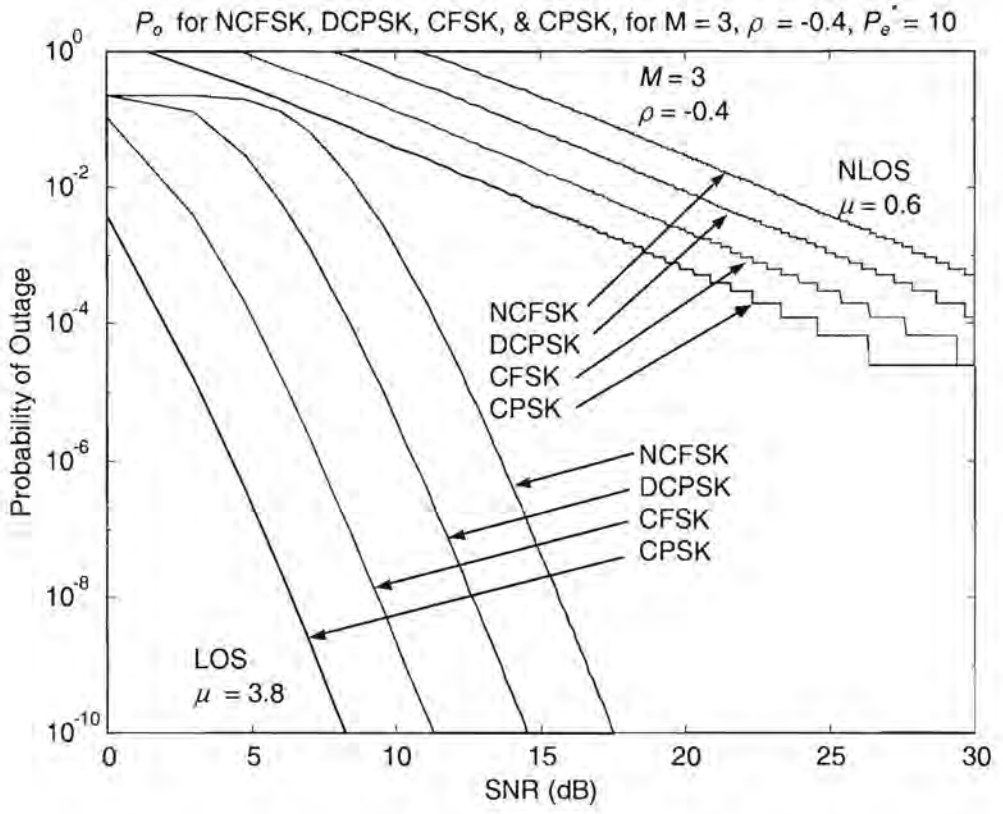

Figure 7.18: Comparison of Probability of Outage for NCFSK, DCPSK, CFSK & CPSK, with $M = 3$, $\rho = -0.4$ and $P_e^* = 10^{-4}$

7.4 Results

In this Chapter we used *probability of error* and *probability of outage* to evaluated the performance of the proposed system model. The following observations are noted:

Probability of Error

- Equation (7.6) is used to plot Figures 7.1 & 7.2 and Equation (7.12) is used to plot Figures 7.3 & 7.4, mainly to study the effect of correlated signals.
- Figures 7.1, 7.2, 7.3 & 7.4 present a comparison of the performance of the system for $M = 2, 3$ & 5. It is noticed that as the number of diversity branches increase from 2 to 5 the performance of the system is significantly improved. It is also noticed that *Coherent Phase Shift Keying* (CPSK) modulation performs the best.
- To produce results that provide tangible conclusions the simulation environment for NCFSK and DCPSK are summarised in Table 7.1, where $M = 3$ (diversity branches) was chosen during the system design discussed in Chapter 5, section 5.3.
- The conditions defined in Table 7.1 for NCFSK and DCPSK are used to plot Figures 7.5 & 7.6. The values for α are obtained from (7.1), values of μ are obtained from Table 4.2, and values for ρ are obtained from the condition given in (5.34). It is noticed that for both NCFSK and DCPSK modulation ρ = -0.4 (highly negatively correlated signals) perform the best, offering a gain of up to 3dB, in both LOS and NLOS conditions. It is also noticed that the system gain is better in LOS conditions than NLOS, as expected.
- Equation (7.12) is used in accordance with the simulation conditions for CFSK & CPSK in Table 7.2 to plot Figures 7.8, & 7.9. It is noticed that CPSK performs better than CFSK in all conditions with best results when ρ = -0.4 and μ = 3.8 (LOS).
- Figure 7.9 shows a comparison between all the modulation schemes considered for $M = 3$, ρ = -0.4 and μ = 3.8 (LOS) & 0.6 (NLOS).

Probability of Outage

- The probability of outage is calculated to be able to predict coverage for the proposed system. An instantaneous bit error probability $P_e^* = 10^{-4}$ is used in (7.17) for the calculation. The value of γ^* in (7.15) determines the type of modulation scheme used.

- Figures 7.10, 7.11, 7.12 & 7.13 illustrate the probability of outage for M (No. of diversity branches) = 2, 3 & 5, for the different modulation schemes. It was noted that $M = 5$ gives the lowest outage in all cases.
- The simulation conditions summarised in Table 7.3 are used in (7.17) to plot Figures 7.14 for NCFSK and 7.15 for DCPSK. It is clear from the plots that signals with $\rho = -0.4$ have the lowest outage as compared to signals with $\rho > 0$ in both LOS and NLOS conditions.
- Simulation conditions that are mentioned in Table 7.4 are used to plot Figures 7.16 & 7.17 for CFSK and CPSK modulations, respectively. Again we notice that conditions with $\rho = -0.4$ result in lower outage as compared to $\rho > 0$ for both modulation schemes in LOS and NLOS scenarios.
- A final comparison of all modulation schemes with $\rho = -0.4$ is presented in Figure 7.18. It is noticed that CPSK with $\mu = 3.8$ (LOS) provides the lowest outage.

7.5 Conclusion

In this Chapter results on the performance of the proposed system model are presented. Two techniques namely *Probability of error* and *Probability of outage* are used to predict the performance and coverage respectively. From the observation listed above we can conclude the following.

- An increase in the number of diversity branches used at the MRC proposed receiver results into significant gain in the system performance. This improvement is achieved by employing additional antenna elements, which is an additional cost to hardware. A trade off therefore has to be reached between increasing the number of antenna elements and employing other means to provide further gain. An antenna with three elements is proposed in this dissertation.
- Coherent Phase Shift Keying (CPSK) has been seen to out perform all other modulation schemes considered. CPSK is identical to BPSK and therefore we can say that BPSK modulation performs the best. Extending the theory further we can safely say that QPSK will also perform the best with the proposed system as BER for QPSK is identical to that of BPSK, the only difference being that with QPSK twice as much data can be sent as compared to BPSK.

- The system performs better in LOS conditions as compared to NLOS, as should normally be the case.
- An optimum model, therefore will be with QPSK modulation, three diversity branches ($M = 3$) and one that employs negative correlation ($-0.4 < \rho < 1$).
- The proposed model provides low outage for CPSK, hence low outage for QPSK and better or improved coverage.

Chapter 8

CONCLUSIONS

8.1 Introduction

This Chapter briefly discusses the goals of the dissertation, the different components of the proposed system model and how well these goals were met. We also discuss the findings during the development of the proposed system model and draw conclusions from these findings. The work presented here deals with *spatial/temporal* modelling of an *MRC* receiver with unique consideration to negatively correlated signals. It provides a new dimension for further research and refinement of the technology associated with *smart antennas*.

8.2 Overview

The goal of this dissertation was to develop a smart antenna model that uses multipath echoes to mitigate the effect of fading and provide significant improvement to 3G mobile technology based on UMTS systems. The dissertation was divided into eight chapters as shown in Figure 1.7 and the contents of each chapter are summarised in Figure 1.8. However, the goals outlined were achieved in three main parts as listed below.

1) The *spatial/temporal* channel model was developed in Chapters 3 & 4. The channel model developed is obtained by combining the spatial aspect discussed in Chapter 3 and temporal aspects discussed in Chapter 4.

- The *spatial* model was made up of two models, namely a user distribution model and a scatterer distribution model. A Gaussian bell shape distribution of scatterers and a Uniform distribution for the users were assumed. The two components of the spatial aspect together produced a general spatial model that can be adapted to any user and scatterer environment by selecting the correct parameters.
- The *temporal* part modelled the instantaneous fading of signals in a Nakagami fading channel. Nakagami fading was used mainly because it can be closely approximated to other fading channels as discussed in Chapter 2, by the correct choice of the fading parameter m. Two models, namely exponential for LOS and Gaussian for NLOS were used to model the spatial/temporal channel.

Finally the spatial part θ (DOA) was combined with the temporal part m (Nakagami fading) to produce the channel fading parameter μ used for modelling the MRC receiver in Chapter 5.

2) The second important part is the *MRC* receiver, which was developed in Chapter 5. An MRC receiver with spatial/temporal fading for negatively correlated signals was developed. A constant correlation model is considered, defined by (5.11). The pdf calculated is thus valid for negatively correlated signals where the correlation coefficient ρ is defined by (5.34) with restrictions given by (5.40).

3) Finally the proposed system model was evaluated and analysed in Chapter 7. The following conclusions are made:

- It is absolutely vital to use an accurate and flexible channel model as was chosen here to produce the required degree of accuracy for the proposed system model.
- By exploiting the negative correlation concept inherent to the arriving signals at the MRC receiver, we have successfully obtained considerable improvement in system performance providing gains of up to 3dB.
- CPSK modulation is shown to have the best performance with the highest gains for all simulation conditions that were considered.
- The proposed model is also valid for QPSK modulation and will produce the same gain and improvement in system performance as CPSK. This is due to the fact that the probability of error for CPSK is identical to the Probability of error for QPSK.

- An improvement in outage was also noted for signals with negative correlation coefficient resulting in lower probability of outage. This implies better or improved coverage. We can therefore conclude that by extending our model to employ techniques that exploit negative correlation between signals at the receiver, we have obtained significant improvement in coverage.

8.3 Main Contributions

The main contributions of this dissertation are as listed below:

- A spatial/temporal channel model proposed in [8] was modified to suit more general scenarios and can adapt to any changes with simple modifications.
- The conditions and the theory established in [26] to be able to extend the MRC pdf presented in [36] for negative values of ρ were verified.
- The new MRC receiver, valid for correlation coefficient $\rho < 0$, was used to calculate the probability of error for different modulation schemes and to propose the best modulation technique based on performance.
- The receiver was also analysed for different values of M (number of diversity branches) and $M = 3$ is proposed for the best results.
- Finally, the probability of outage analysis was done to predict coverage.

8.4 Future research

The proposed system model is very general and can be easily modified to suit any scenario. It is designed with a view to accommodate most variations in system parameters and also to be able to integrate with other models. It is designed to suit the need of the third generation UMTS systems based on WCDMA technology. However, there is a need and possibility to further improve the proposed model. The following are possible areas for future research:

- The Direction of Arrival (DOA) algorithm can be further improved by incorporating Time of Arrival (TOA) information and also by comparing the different DOA models available. The user distribution model (3.1) can be modified to depend on the distance by using the variable transformation in (3.3).

- The channel model should be further improved to provide more accurate values of the fading parameter (Nakagami's m value) in LOS and NLOS conditions for all possible forms of population areas (morpho classes).
- The effect of antenna geometry on the reception of the signal should be analysed. This implies that all possible antenna structures and the number of branches on each antenna type should be considered.
- The MRC considered here is based on constant correlation model and can be assumed to be a good approximation of real time models. However, this model needs to be compared with other correlation models to choose the best model or may be propose a hybrid correlation model. One such model is the Exponential correlation model presented in [36] that should be compared with the constant correlation model.
- Finally the signal power in the MR combiner on each branch is assumed identical. It is a reasonable assumption but is not always met in practice. Therefore there is a need for an improved model to model the signal power.

8.5 Conclusion

The aim of this dissertation was to develop an MRC receiver employing negative correlation and to integrated it with a spatial /temporal channel model. The proposed system model was evaluated using evaluation techniques mentioned in Chapter 7 to verify the goals of this dissertation. The proposed spatial/temporal MRC receiver with negative correlation produced significant improvement in system performance with gains of up to 3dB and more. The proposed model also provides considerable improvement in coverage by providing low outage. In view of the above facts we can say that the goals of the dissertation were successfully achieved.

Finally the diversity antenna proposed here was designed to be integrated with a beamforming algorithm to provide a complete solution to the smart antenna concept. Diversity reception is recommended for ρ (correlation coefficient) less than 0.5 and for ρ greater than 0.5, beamforming is recommended. The optimum smart antenna will be a hybrid antenna that combines both diversity and beam forming.